UC Irvine

UC Irvine Electronic Theses and Dissertations

Title

Development and characterization of novel transgenic strains to track neurodegeneration and test mTOR-mediated neuroprotection in 5xFAD mice

Permalink

https://escholarship.org/uc/item/0b80b3nx

ISBN

9798171647971

Author

Gallardo, Daisy

Publication Date

2026-10-27

Peer reviewed|Thesis/dissertation

eScholarship.org Powered by the California Digital Library
University of California

UNIVERSITY OF CALIFORNIA,
IRVINE

Development and characterization of novel transgenic strains to track neurodegeneration and test mTOR-mediated neuroprotection in 5xFAD mice

DISSERTATION

submitted in partial satisfaction of the requirements
for the degree of

DOCTOR OF PHILOSOPHY

in Biomedical Sciences

by

Daisy Nallely Gallardo

Dissertation Committee:
Professor Oswald Steward, Chair
Professor Christine Gall
Professor Javier Diaz-Alonso
Professor Marcelo Wood
Professor Andrea Tenner
Professor Kim Green
Professor Melanie Cocco

2026

Chapter 2 © 2026 Experimental Neurology
© 2026 Daisy Nallely Gallardo

DEDICATION

To

My mom, dad, sister and my two lovely nephews. Thank you for your support.

TABLE OF CONTENTS

Page

DEDICATION ii

TABLE OF CONTENTS iii

LIST OF FIGURES v

LIST OF TABLES vii

ACKNOWLEDGMENTS viii

VITA ix

ABSTRACT OF THE DISSERTATION xiii

Chapter 1 - Introduction 1

References 15

Chapter 2 - Conditional genetic labeling of neurons that degenerate in 5xFAD mice reveals previously un-described features of age-related neurodegeneration 23

Graphical abstract 23

Abstract 23

Introduction 24

Methods 27

Results 41

Discussion 62

References 87

Chapter 3 - Progression of neurodegeneration in 5xFAD Alzheimer's disease mouse model following mTOR activation 92

Abstract 92

Introduction 92

Methods 95

Results 107

Discussion 118

References 131

Chapter 4 - Motor behavior in 5xFAD Alzheimer's disease mouse model following mTOR activation 134

Abstract 134

Introduction 135

Methods 137

Results 142

Discussion 152

References 161

Chapter 5 - Summary and Conclusions 164

LIST OF FIGURES

Page

Figure 2.1 Immunofluorescence (IF) for hAPP in the cortex, hippocampus and entorhinal cortex of young 5xFAD$^{+/-}$/Rosa^{tdT} and Rosa^{tdT} mice. 71

Figure 2.2 Expression of hAPP in subcortical regions in young 5xFAD$^{+/-}$/Rosa^{tdT} mice. 72

Figure 2.3 Expression of hAPP in the brainstem and spinal cord of young 5xFAD$^{+/-}$/Rosa^{tdT} mice 73

Figure 2.4 1D1-positive granules in older 5xFAD$^{+/-}$/Rosa^{tdT} mouse. 75

Figure 2.5 Staining pattern of 1D1 and 6E10 in a 12-month-old male 5xFAD$^{+/-}$/Rosa^{tdT} mouse. 76

Figure 2.6 Retrograde transduction and induction of tdT expression in CSNs via AAV-rg/Cre injections at C5. 78

Figure 2.7 Neurodegenerative changes can be tracked by tdT fluorescence. 80

Figure 2.8 Neurodegenerative changes tracked by tdT fluorescence. 82

Figure 2.9 Characterization of tdT-positive granules in older 5xFAD$^{+/-}$/Rosa^{tdT} mice. 86

Figure 3.1. PTEN is deleted in corticospinal neurons of 5xFAD$^{+/-}$/ PTEN$^{f/f}$/Rosa^{tdT} and PTEN$^{f/f}$/Rosa^{tdT} mice. 122

Figure 3.2. PTEN deletion maintains hAPP transgene expression as the 5xFAD$^{+/-}$/ PTEN$^{f/f}$/Rosa^{tdT} mice age. 124

Figure 3.3. Successful activation of the mTOR pathway persists 4 months post-PTEN deletion. 126

Figure 3.4. Quantifications of tdT-labeled neurons decline as accumulations increase with age. 129

Figure 3.5. Longitudinal bioluminescent labeling of CSNs in brain and spinal cord declines... 130

Figure 4.1 PTEN deletion ameliorated motor deficits in 5xFAD$^{+/-}$/PTEN$^{f/f}$/Rosa^{tdT} mice on the rotarod task..... 158

Figure 4.2 Forelimb grip strength declines with age independently of genotype..... 159

Figure 4.3 PTEN deletion decreases foot slips without affecting speed on balance beam task. 160

LIST OF TABLES

Page

Table 2.1. Mice injected with AAV-rg/Cre 30

Table 3.1 Mice used for immunohistology 97

Table 3.2. Primary antibody list 104

Table 4.1 Experimental animals 139

ACKNOWLEDGMENTS

I would like to express my gratitude to my advisor and committee chair, Dr. Oswald Steward. Thank you for the years of support during my graduate training. I appreciate the time you've taken to help me with writing, advise me on experiments, help me prepare for presentations and provide guidance on my career. Your mentorship has had a profound impact on my career and life.

I'd also like to thank my committee members Dr. Christine Gall, Dr. Javier Diaz-Alonso, Dr. Kim Green, Dr. Andrea Tenner, Dr. Melanie Cocco and Dr. Marcelo Wood. I greatly appreciate your invaluable input and support throughout my graduate training.

This work was supported in part by a T32 Aging and Alzheimer's Disease NIA Training Grant (T32 AG00096), Graduate Dean's Dissertation Fellowship and RO1 to O. Steward (NIH-NS108189).

Conflict of interest disclosure: O. Steward is Co-founder and has economic interests in the company Axonis Inc. which is seeking to develop new therapies for spinal cord injury and other neurological disorders.

VITA

Daisy Nallely Gallardo

EDUCATION

2026	Doctor of Philosophy in Biomedical Sciences, University of California, Irvine
2020	Bachelor of Science in Neuroscience, University of California, Santa Cruz

FIELD OF STUDY

Neuroscience

POSITIONS, SCIENTIFIC APPOINTMENTS AND HONORS

2025 –2026	Graduate Dean's Dissertation Fellowship, UC Irvine
2025 – 2025	Mentor, Research Discovery Program, Undergraduate Research Opportunity Program
2024 – 2026	Co-chair, Research and Education in Memory Impairments and Neurological Disorders (REMIND)
2024 – 2026	T32 Neurobiology of Aging and Alzheimer's Disease training grant appointment
2024 – 2025	Member, Center for the Neurobiology of Learning and Memory Irvine Brain Bee committee
2024 – 2024	Judge, Minority Science Program symposium 2024
2024 – 2024	Trainee Professional Development Award, Society for Neuroscience
2023 – 2023	Teaching Assistant – Genetics course, UC Irvine

2023 – 2025	Neuronline Community Leader, Society for Neuroscience
2023 – 2023	Katherine and Robert Phalen Endowment – honorable mention award
2022 – 2024	Member of leadership committee, Association for Women in Science
2022 – 2023	Member, Reach Out to Teach Out – Science outreach
2021 – 2026	Graduate Student Researcher, UC Irvine
2021 – 2023, 2024 – 2025	Member, Center for the Neurobiology of Learning and Memory Adult outreach committee
2021 – 2021	National Institutes of Health – Initiative for Maximizing Student Development Scholar (NIH – IMSD), UC Irvine
2020 – 2021	Laboratory Assistant, UC Irvine
2019 – 2020	Dean's Honor List – Spring 2019 and Spring 2020
2019 – 2020	National Institutes of Health – Initiative for Maximizing Student Development Scholar (NIH – IMSD), UC Santa Cruz
2019 – 2020	Public Relations Director, Women in Science Society
2018 – 2020	Undergraduate Laboratory Assistant, UC Santa Cruz

PUBLICATIONS

1. **Gallardo, D.** & Steward, O. Development and characterization of a novel transgenic strain to selectively label neurons that degenerate in 5xFAD mice. Experimental Neurology 405, 115914 (2026).

2. Metcalfe, M., Steward, O. & **Gallardo, D.** Widespread AAV-mediated CSPG digestion impairs functional recovery after cervical spinal cord injury. Preprint at https://doi.org/10.64898/2026.05.22.727165 (2026).
3. Tsyporin, J., Tastad, D., Ma, X., Nehme, A., Finn, T., Huebner, L., Liu, G., **Gallardo, D.,** Makhamreh, A., Roberts, J., Katzman, S., Sestan, N., McConnell, S., Yang, Z., Qiu., S., Chen, B., Transcriptional repression by FEZF2 restricts alternative identities of cortical projection neurons. Cell Reports 35, 109269 (2021).

PRESENTATIONS

1. **Gallardo, D.**, Steward, O. (2026) Novel Approaches to Track Neurodegeneration in Murine Models of Alzheimer's Disease Reveal Previously Unknown Aspects of Extracellular Aggregate Deposition. Poster presentation at the 2026 UCI REMIND Emerging Scientists Symposium, University of California, Irvine, Irvine, CA.
2. **Gallardo, D.**, Steward, O. (2025) Novel Approaches to Track Neurodegeneration in Murine Models of Alzheimer's Disease Reveal Previously Unknown Aspects of Extracellular Aggregate Deposition. Poster presentation at the 2025 Southern California Alzheimer’s Disease Centers Collaborative Research Symposium, University of California, Irvine, Irvine, CA.
3. **Gallardo, D.**, Steward, O. (2025) A new platform and paradigm to track age-dependent neurodegeneration in a murine model of Alzheimer's Disease (5xFAD mice). Poster presentation at the 2025 UCI REMIND Emerging Scientists Symposium, University of California, Irvine, Irvine, CA.

4. **Gallardo, D.**, Steward, O. (2024) A new platform and paradigm to track age-dependent neurodegeneration in a murine model of Alzheimer's Disease (5xFAD mice). Poster presentation at the School of Medicine Grad Day at the University of California, Irvine, Irvine, CA.
5. **Gallardo, D.**, Steward, O. (2024) Interventions targeting neurodegeneration in a mouse model of AD. Oral presentation at the University of California, Irvine, Progress in Neuroscience seminar.
6. **Gallardo, D.**, Steward, O. (2024) Provisional evidence that selective activation of mTOR in neurons that degenerate in 5xFAD mice delays age-related neurodegeneration. Poster presentation at the 2024 Society for Neuroscience conference, Chicago, IL.
7. **Gallardo, D.**, Steward, O. (2023) The impact of PTEN deletion in a 5xFAD mouse model. Poster presentation at the 2023 Southern California Alzheimer's disease research symposium, University of California, Irvine, Irvine, CA.
8. **Gallardo, D.**, Steward, O. (2023) A new platform and paradigm to track age-dependent neurodegeneration in a murine model of Alzheimer's Disease (5xFAD mice). Poster presentation at the 2023 Society for Neuroscience conference, Washington, DC.
9. **Gallardo, D.** (2022) Exploring the localization of DAGL-α in the hippocampus. Oral presentation at the University of California, Irvine Interdepartmental Neuroscience Program Symposium, Irvine, CA.

ABSTRACT OF THE DISSERTATION

Development and characterization of novel transgenic strains to track neurodegeneration and test mTOR-mediated neuroprotection in 5xFAD mice

by
Daisy Nallely Gallardo
Doctor of Philosophy in Biomedical Sciences
University of California, Irvine, 2026
Professor Oswald Steward, Chair

Alzheimer's Disease (AD) is one of the most prevalent neurodegenerative diseases. It's estimated that by 2060 there will be 13.8 million people aged 65 and older with AD (Alzheimer's Association, 2025). Neurodegeneration is a primary pathological feature of late-stage Alzheimer's Disease (AD), including dendritic atrophy, axonal destabilization and neuronal death yet mechanisms are not well understood. Early in disease onset, AD is primarily characterized by the accumulation of extracellular amyloid beta (Aß) plaques and intracellular neurofibrillary tangles in neurons. The prevailing hypothesis, "amyloid hypothesis," driving the field has been that neuronal dysfunction and degeneration are driven by extracellular Aß in one form or another. New antibody treatments that target Aß have been approved by the FDA, but so far, these result in only mild delays in cognitive impairment, have potentially serious side effects, and may not delay neurodegeneration. Accordingly, there is a major un-met need to identify mechanisms underlying neurodegeneration and identify potential interventions to slow down its rate and progression. In chapter 2, we validate a method for labeling and tracking neurodegeneration in a mouse model of AD. In chapter 3, we test whether Adeno-associated Virus (AAV)-based interventions that activate the AKT/Mechanistic target of Rapamycin (mTOR) pathway are a potential therapeutic target for promoting neuronal survival. In chapter 4, we assess whether mTOR activation, via PTEN deletion, in corticospinal neurons (CSNs) delays motor deficits in AD.

Chapter 1 - Introduction

"Many neurons, especially the ones in the upper layer, have completely disappeared." – Alzheimer, 1907, as translated in Stelzmann et al., 1995

1.1 History of AD

The first to discover histological alterations in a brain of Alzheimer's disease (AD) was Alois Alzheimer, as he reported in 1906. He found what are now known as Aß plaques, neurofibrillary tangles and neurodegeneration in the post-mortem brain of Auguste Deter. Auguste showed signs of dementia and severe memory impairment at only 50 years old (Alzheimer, 1907). Alzheimer used silver staining methods to visualize histological changes in the brain and found neurofibrils and senile plaques. To my knowledge, there aren't reports of follow-up work until Dr. Terry and Dr. Kidd published electron microscopy images of AD neuropathology in 1963 (Terry, 1963; Kidd, 1963). After their publications, there were many papers identifying components of AD pathology. One was the isolation of amyloid protein, from brains of AD patients, and characterization by Glenner and Wong in 1984 at the University of California, San Diego (Glenner and Wong, 1984). Shortly after, Tau was found to be the main component of neurofibrillary tangles (Brion, et al., 1985). Throughout this, several hypotheses were formed, the first hypothesis to be proposed was the cholinergic hypothesis. The hypothesis was formed due to reports on the loss of cholinergic neurons, and thus reduction of choline acetyltransferase, in postmortem AD brains (Davies and Maloney, 1976). The next major hypotheses that prevailed was the amyloid hypothesis proposed in 1991. The hypothesis proposed ß-amyloid as the driving

factor of neuropathology in AD and has been one of the major prevailing hypotheses since then (Selkoe, 1991; Hardy and Allsop, 1991; Hardy and Selkoe, 2002).

1.2 Alzheimer's Disease - clinical

The clinical progression of AD starts with the preclinical AD stage where patients have AD pathological markers but remain cognitively unimpaired (Dubois, et al., 2016). The mild stage of AD is defined when cognitive symptoms begin to interfere with daily life. Patients are diagnosed with mild cognitive impairment (MCI) due to AD during the mild stage. During the moderate stage, patients are diagnosed with dementia as their memory and cognition begin to decline. In the severe stage, the patients display severe dementia, have motor deficits such as difficulty with motor coordination, and trouble swallowing. Throughout all the clinical stages of AD, there is a progressive accumulation of Aß plaques and neurofibrillary tangles, but the timeline of neurodegeneration remains undefined.

1.3 Amyloid precursor protein (APP) processing

The dysfunctional processing of APP is a key mechanism in driving disease pathology. APP is a transmembrane protein that in normal conditions is cleaved by an α-secretase (such as ADAM 10/17) in the Aβ domain. The cleavage of the Aβ domain, results in soluble-APPα (sAPPα) and a C83 fragment that remains within the membrane. C83 is then cleaved by γ-secretase and produces p3 and AICD fragments that play a role in synaptic signaling. However, in an amyloidogenic state, a β-secretase (BACE1) cleaves in a region of APP that results in soluble-

APPβ (sAPPβ) and C99 fragments. Then, γ-secretase cleavage results in Aβ40 and Aβ42 fragments. Aβ42 fragments lead to aggregation and become a barrier to synaptic communication. In the normal state, Aβ domain cleavage prevents formation of the Aβ40 and Aβ42.

1.4 Tau and neurofibrillary tangles

Neurofibrillary tangles (NFTs) are one of the defining neuropathological features of AD. The neurofibrillary tangles were first described by Alzheimer in 1906 (Alzheimer, 1906) and later isolated from brains of AD patients by Iqbal and colleagues in 1974 (Iqbal et al., 1974). Electron microscopy images showed that the tangles were pairs of 10 nm fibrils twisted around one another, known as paired helical filaments (Wisniewski et al., 1978). It wasn't known that they were composed of tau until 1985 when Brion and colleagues used a tau antiserum and found that it bound to the neurofibrillary tangles (Brion et al., 1985). These findings were later confirmed the following year (Ihara et al., 1986; Grundke-Iqbal et al., 1986; Kosik et al., 1986).

Tau is a soluble microtubule-associated protein prominently present in neurons. Tau supports axonal transport by binding and stabilizing microtubules. Alternative splicing of tau produces six isoforms in the adult central nervous system. In normal human brains, tau isoforms with three or four microtubule-binding repeat domains (3R and 4R tau) are found in a ratio of 1:1 (Noble et al., 2013).

The binding of tau to microtubules is regulated by phosphorylation. Under normal conditions, tau is phosphorylated by a large number of kinases including glycogen synthase kinase-3 (GSK-

3) and casein kinase 1 (CK1). In addition, Tau is dephosphorylated by many phosphatases, including protein phosphatase-1 (PP1) and 2A (PP2A) (Liu et al., 2005). In AD, tau becomes hyperphosphorylated, reducing its affinity for microtubules. This dissociated tau accumulates within the neuronal soma and its processes, where it self-assembles into paired helical filaments that aggregate into what are referred to as neurofibrillary tangles (Chohan et al., 2005).

1.5 Neurodegeneration

The first site of neurodegeneration in human AD is the entorhinal cortex (Hyman et al., 1984; Gomez-Isla et al., 1996). Importantly, the report by Hyman and colleagues showed that neuronal loss occurred in layer II of the entorhinal cortex (Hyman et al., 1984). Layer II of the entorhinal cortex is the origin of the perforant path which connects the entorhinal cortex to the rest of the hippocampus. Hyman and colleagues also reported neuronal loss in layer IV of the entorhinal cortex, the subiculum and CA1 (Hyman et al., 1984). In the Gomez-Isla report (1996), profound loss of layer II entorhinal cortex was found even in patients who were categorized to be in the clinically mild stage of AD (Gomez-Isla et al., 1996).

The most common methods of cell death are necrosis and apoptosis. The presence of these cell death mechanisms in AD has been debated for decades. In recent years, a form of cell death, necroptosis, was suggested to occur in AD (Caccamo et al., 2017; Balusu et al., 2023). Necroptosis was first described in 1988 (Laster et al., 1988) but wasn't named until 2005 in a landmark study (Degterev et al., 2005). In most of the papers that suggest necrosis, apoptosis and

necroptosis as forms of cell death in AD, they have identified immunohistological markers that show activation of the pathway. The problem is that, in vivo, these markers can't be directly correlated to neurodegeneration. The presence of markers can't be directly linked to subsequent neurodegeneration because the timeline of neurodegeneration has not been defined. If we knew at which timepoint many cells were going to degenerate, we could look at the markers of cell death right before that occurred. If the markers of a certain type of cell death were upregulated shortly before neurodegeneration occurred, this would identify the mechanism. To prevent cell death, we need to define the cell death mechanism by which they degenerate.

1.6 Methods for detecting neurodegeneration (Humans and mouse models of AD)

Neurodegeneration is measured differently in living human patients than in post-mortem tissue or animal models. Each approach for measuring or detecting neurodegeneration carries distinct limitations. In human patients, atrophy of the brain can be seen by magnetic resonance imaging (MRI) and/or computerized tomography (CT). Size and structure of the brain is compared to previous scans or to those of a person of the same size and age, where shrinkage may indicate neurodegeneration. Fluorodeoxyglucose-positron emission tomography (FDG-PET) is used to identify areas of the brain where there is synaptic dysfunction, shown by the reduction in fluorodeoxyglucose uptake (Jack et al., 2010). Sustained elevated levels of total-tau (t-tau) in cerebrospinal fluid (CSF) is also considered a biomarker of synaptic degeneration (Soares et al., 2025), while elevated levels of neurofilament light chain (NfL) in CSF are a biomarker for axonal damage and neuronal cell death. Neurofilaments (Nf) are scaffolding proteins that compose the axonal cytoskeleton and are composed of four subunits: neurofilament heavy

(NfH), median (NfM), light (NfL) and α-internexin (Int). NfL is the most abundant and soluble of these four subunits. Therefore, high amounts of NfLs in the CSF indicate neuroaxonal damage (Bridel et al., 2019). However, with fluid biomarkers, there's an inability to determine what population of neurons are degenerating.

In post-mortem tissue, Nissl, cresyl violet and NeuN immunostaining is done to visualize cells. Neurodegeneration in cortical layers can be implied by a low density of neurons within the observed layer. Cell death markers are also used to detect cells in the process of degenerating. Widely used markers for the programmed cell death, apoptosis, are caspase-3 and the terminal deoxynucleotidyl transferase dUTP nick end labeling assay (TUNEL assay). Fluro-Jade-C (FJC) is used to identify neurodegeneration, regardless of which form of the specifc mechanism of cell death. The primary limitation with using cell death markers for identifying neurodegeneration are their limited temporal window. The cell death markers are only labeling actively dying cells rather than labeling the trajectory of cell loss.

1.7 motor dysfunction in AD

AD is primarily defined by a progressive loss of cognitive function, but motor dysfunction often accompanies AD pathology as well. A National Institute on Aging (NIA) review reported that pyramidal and extrapyramidal motor impairments affect a substantial amount of AD patients even at early stages of the disease (Alber et al., 2015). Motor signs in AD may include gait disturbance (Kim et al., 2025), bradykinesia (Bologna et al., 2020) and postural instability (Da Rocha Anselmo et al., 2025). It's also been reported that motor impairments progressively

worsen alongside cognitive impairment and may even precede the onset of cognitive impairment by a decade or more (Albers et al., 2015). A longitudinal cohort study of 204 healthy seniors revealed that slowing of gait speed occurred approximately 12 years before onset of mild cognitive impairment (MCI) in those that developed MCI compared to those that did not (Buracchio et al., 2010).

Despite the presence of motor deficits in AD, relatively early on in the disease, the corticospinal system has received little attention in the AD field. Motor deficits in human AD involve pyramidal and extrapyramidal systems. Thus, determining the population of neurons that are degenerating in the pyramidal system would give us insight into the motor impairments seen in AD patients.

1.8 layer V pyramidal neurons

The cerebral cortex is composed of six layers of neurons. Each layer contains neurons with specific structures appropriate for its identity and function (O'Leary and Koester, 1993). In the cortex, there are two classes of neurons. The two types are interneurons, which participate in local connections, and projection neurons, which project axons outside of their local circuit to distant targets (Molyneaux et al., 2007). Depending on the target that the neurons project to results in their classification: intracortical, subcortical and subcerebral. The projection neurons in cortical layer V are among the largest neurons in the cerebral cortex. They are distinctly characterized by their pyramidal-shaped soma, an apical tuft extending towards the pial surface and basal dendrites extending near the neuronal cell body (Spruston, 2008). The large pyramidal

neurons that are located in layer V and extend projections to the brainstem and spinal cord are known as subcerebral projection neurons (SCPNs) (Greig et al., 2013). The SCPNs are subdivided into many distinct subtypes but the primary subtypes are: corticotectal neurons that have primary projections to the superior colliculus and collateral projections to the rostral pons, corticopontine neurons that have primary projections to the pons and corticospinal neurons (CSNs) that have primary projections to the spinal cord and collateral projections to the striatum, red nucleus, caudal pons and medulla. During development, subcerebral projection neurons of layer V are transcriptionally regulated by transcription factors *FEZF2* and *CTIP2* (McKenna et al., 2011). Without *FEZF2* or *CTIP2*, the corticospinal tract is not formed in mice (Arlotta et al., 2005, Chen et al., 2005). The CSNs are the most-well studied SCPN subtype due to their clinical and developmental importance.

CSNs can be reliably identified and targeted by their projection. A way of doing this is by targeting their projections to the spinal cord (Ozdinler et al., 2014). The development of retrograde adeno-associated viruses (AAV-rg) carrying Cre (Tervo et al., 2016) combined with Cre-dependent reporter lines (Madisen et al., 2010) has made it possible. For example, an injection of AAV-rg carrying Cre (AAV-rg/Cre) into cervical level 5 (C5) of the spinal cord in reporter mice $Rosa^{tdTomato}$ results in permanent and selective tdTomato labeling of CSNs (Steward et al., 2021).

1.9 Mouse models of AD

Transgenic mouse models are widely used to study AD. The first transgenic models expressing mutant human APP were shown to recapitulate a central pathological marker of AD, amyloid plaques (Games et al., 1995; Hsiao et al., 1996). The benefits of an AD mouse model are their shorter life spans which facilitates the study of an age-related disease.

However, a limitation is that no mouse model fully recapitulates the disease. Most AD mouse models either develop amyloid plaques or neurofibrillary tangles, but not both. In addition, very few AD mouse models develop neuronal loss (Drummond and Wisniewski, 2017). Most of the commonly used AD mouse models that do exhibit neurodegeneration have tau pathology, but exhibit very minimal neurodegeneration. Few mouse models exhibiting only amyloid pathology display neuronal death. One of the mouse models that displays neuron loss is the double transgenic mouse strain, APP/PS1, that co-expresses hAPP with the Swedish mutation and hPSEN1 with the L166P mutation. The AAP/PS1 strain exhibits neuronal death in CA1 and CA2 of the hippocampus (Casas et al., 2004). 5xFAD mice are among the few mouse models that display substantial neurodegeneration and the only one that displays neurodegeneration in cortical layer V (Oakley et al., 2006).

The 5xFAD mice express mutant human APP (hAPP) and PSEN1 (hPSEN1). The mouse model carries three mutations in hAPP (Swedish, Florida and London mutations) and two in hPSEN1 (M146L and L286V). Both transgenes are inserted at a single locus and driven by neuron-specific promoter, Thy-1 (Oakley et al., 2006). Total APP expression in the 5xFAD brain is approximately 1.8-fold that of non-transgenic controls (Sadleir et al., 2018). The high expression of hAPP results in a rapid and aggressive amyloid plaque pathology. Intraneuronal Aβ appears

by 1.5 months, extracellular plaques begin to appear by 2 months, synapse loss is seen at 6 months and neuronal loss is reported to occur at 9 months (Oakley et al., 2006; Eimer and Vassar, 2013; Jawhar et al., 2012; Forner et al., 2021).

2.0 *PTEN* deletion/mTOR activation in relation to AD and aging

Neurodegeneration is a neuropathological feature of AD and an aspect of normal aging. Because neurodegeneration is age-related, it is possible that inducing intrinsic growth capacity similar to levels of that during younger developmental years, could delay or prevent neurodegeneration, cognitive or functional decline associated with aging. The focus on targeting age-related mechanisms and reverting neurons to a developmental-like state was suggested for promoting axonal regeneration (Filbin, 2006). Following that, the study by Park et al. (2008) was the first to establish the specific importance of a cell growth regulating pathway, the mTOR pathway, in promoting axonal regeneration. The Park et al. (2008) study reported conditional knock-out of various cell growth control genes (*retinoblastoma protein* (*Rb*), *P53*, *Smad4*, *dicer*, *LKB1*, *PTEN* and *TSC1*). Out of those genes, deletion of *PTEN (phosphatase and Tensin Homolog)* and *TSC1* were the ones that promoted axonal regeneration. Genetic deletion or knockdown of *PTEN*, a negative regulator of the AKT/mTOR pathway, transforms adult neurons to a growth state. Findings from our lab have shown selective AAV-mediated deletion of *PTEN* gene in cortical motoneurons results in growth of cell body size, an increase in dendritic branching, size and complexity 4 months post-deletion (Gallent and Steward, 2018). During early development, the AKT/mTOR pathway is a key signaling pathway that regulates cell growth, proliferation, survival, and metabolism. The AKT/mTOR pathway is essential for maintaining the balance

between cell growth and cell death, as well as coordinating cellular responses to environmental signals and nutrient availability. Receptor tyrosine kinases (RTK) on the cell membrane activate PI3K, which activates the mTOR pathway. *PTEN* acts as a negative regulator of this pathway by catalyzing the conversion of Phosphatidylinositol-3,4,5-triphosphate (PIP3) to Phosphatidylinositol 4,5-bisphosphate (PIP2), reversing the enzymatic action of PI3K (Switon et al., 2017; Ma and Blenis, 2009). So, deleting *PTEN* results in sustained activation of the AKT/mTOR pathway, promoting cellular growth. It's important to note that *PTEN* is a tumor suppressor gene. Seizures, autism disorder, macrocephaly and several types of cancers have been associated with *PTEN* mutations (Goffin et al., 2001; Hollander et al., 2011). A germline knockout of *PTEN* is lethal, and silencing or deleting *PTEN* during development could lead to developmental disorders, but selective deletion of *PTEN* in the central nervous system during adulthood does not have evident negative consequences, even for over a year (Gutilla and Steward, 2016).

Our lab's discovery of adult neuron growth involved conditional genetic deletion of PTEN with injections of AAV/Cre in $PTEN^{f/f}/Rosa^{tdT}$ mice (Gallent and Steward, 2018; Yonan and Steward, 2023). This transformation to a state like that in development is rejuvenation. More recent studies reveal that AAV-based delivery of shPTEN in adult rodents, rats in this case also activates mTOR and triggers growth of adult neurons (Metcalfe et al., 2022).

An additional key finding in the Park et al. (2008) study was an increased survival of retinal ganglion cells (RGCs) following a nerve crush injury in mice with Cre-mediated deletion of *PTEN* prior to injury (Park et al., 2008). Whether this pro-survival effect of mTOR activation

mediated by PTEN deletion extends to a non-injury model is unknown. The central hypothesis tested in this project is that neurodegeneration of layer V Corticospinal neurons (CSNs) can be prevented or delayed by AKT/mTOR pathway activation. If mTOR activation and the resulting growth state prevented or delayed neurodegeneration in AD, it could be harnessed as a therapeutic target for treatment of AD.

However, the consensus in the field is that activation of the mTOR pathway contributes to AD pathology (Cai et al., 2015; Scalia et al., 2023). The mTOR pathway is activated by Brain derived-neurotrophic factor (BDNF), insulin-like growth factor (IGF)-1, vascular endothelial growth factor (VEGF), insulin and cytokines binding to various kinase receptors (Scalia et al., 2023). When mTOR is activated and thus ULK1 is inhibited, autophagy is inhibited. It's thought that the decrease in autophagy which regulates removal of cellular components, is a major contributor to AD pathology (Yuan et al., 2022). Treatments of mice with rapamycin, an inhibitor of mTOR, have been shown to slow AD pathology (Spilman et al., 2010; Xu et al., 2023).

The proposed dissertation aims to track neurodegenerative changes and investigate whether PTEN deletion delays or prevents neuronal death and motor deficits in 5xFAD mice. Neurodegeneration has been established in the 5xFAD model and PTEN deletion is established as a manipulation to induce cell growth. Whether that growth delays or prevents neuronal survival and motor deficits is unknown. The field's prediction is that mTOR activation would exacerbate AD pathology. However, they are based on mTOR inhibition studies. Here, we conditionally activate the mTOR pathway.

In Chapter 2, we demonstrate that conditional genetic labeling of CSNs reveals age-related features of neurodegeneration in the 5xFAD mouse model that had not been previously described. We show that retrograde transduction of CSNs, by delivery of AAV-rg/Cre into cervical level 5 of the spinal cord results in labeling of axons, dendrites and cell bodies of CSNs. The permanent and selective labeling of CSNs allows for quantification of a vulnerable population of neurons in 5xFAD mice. Our quantifications reveal that CSNs degenerate over time. Along with degeneration of CSNs, accumulations of tdT begin to appear and progressively increase as the mouse ages. Notably, the tdT accumulations increase as the neurons degenerate which provides a second form of tracking neurodegeneration.

In chapter 3, we determine whether activating the mTOR pathway, through PTEN deletion, results in a delay or prevention of neurodegeneration in 5xFAD mice. We do this by using our method of labeling CSNs with tdT (Chapter 2) combined with PTEN deletion in those same neurons. Confirmation of PTEN deletion was done by demonstrating tdT positive neurons were PTEN negative. The activation of mTOR was confirmed by showing elevated levels of phosphorylated ribosomal S6 in tdT positive neurons. Our quantifications of tdT positive CSNs showed that PTEN deletion did not delay or prevent neurodegeneration but it didn't accelerate it either.

Finally, in Chapter 4, we investigate whether PTEN-deletion mediated activation of mTOR results in a delay or prevention of motor deficits in 5xFAD mice. Motor behavior testing across age on the rotarod, grip strength meter and balance beam revealed that 5xFAD mice with PTEN

deletion did delay motor deficits on the balance beam and rotarod task. In contrast to the 5xFAD mice without PTEN deletion that developed motor deficits revealed by Rotarod and balance beam.

Together, these results establish that PTEN deletion may not delay or prevent neurodegeneration in our model but can delay motor deficits regardless of the progressive neurodegeneration.

References

1. Oakley, H. et al. Intraneuronal beta-amyloid aggregates, neurodegeneration, and neuron loss in transgenic mice with five familial Alzheimer's disease mutations: potential factors in amyloid plaque formation. J Neurosci 26, 10129–10140 (2006).
2. Eimer, W. A. & Vassar, R. Neuron loss in the 5XFAD mouse model of Alzheimer's disease correlates with intraneuronal Aβ42 accumulation and Caspase-3 activation. Molecular Neurodegeneration 8, 2 (2013).
3. Jawhar, S., Trawicka, A., Jenneckens, C., Bayer, T. A. & Wirths, O. Motor deficits, neuron loss, and reduced anxiety coinciding with axonal degeneration and intraneuronal Aβ aggregation in the 5XFAD mouse model of Alzheimer's disease. Neurobiology of Aging 33, 196.e29-196.e40 (2012).
4. Filbin, M. T. Recapitulate development to promote axonal regeneration: good or bad approach? Phil. Trans. R. Soc. B 361, 1565–1574 (2006).
5. Hyman, B. T., Van Hoesen, G. W., Damasio, A. R. & Barnes, C. L. Alzheimer's Disease: Cell-Specific Pathology Isolates the Hippocampal Formation. Science 225, 1168–1170 (1984).
6. Terry, R. D. THE FINE STRUCTURE OF NEUROFIBRILLARY TANGLES IN ALZHEIMER'S DISEASE: Journal of Neuropathology and Experimental Neurology 22, 629–642 (1963).
7. Kidd, M. Paired Helical Filaments in Electron Microscopy of Alzheimer's Disease. Nature 197, 192–193 (1963).

8. Glenner, G. G. & Wong, C. W. Alzheimer's disease: Initial report of the purification and characterization of a novel cerebrovascular amyloid protein. Biochemical and Biophysical Research Communications 120, 885–890 (1984).
2. Brion, J. P., Couck, A. M., Passareiro, E. & Flament-Durand, J. Neurofibrillary tangles of Alzheimer's disease: an immunohistochemical study. J Submicrosc Cytol 17, 89–96 (1985).
3. Davies, P. SELECTIVE LOSS OF CENTRAL CHOLINERGIC NEURONS IN ALZHEIMER'S DISEASE. The Lancet 308, 1403 (1976).
4. Selkoe, D. J. The molecular pathology of Alzheimer's disease. Neuron 6, 487–498 (1991).
5. Selkoe, D. J. & Hardy, J. The amyloid hypothesis of Alzheimer's disease at 25 years. EMBO Mol Med 8, 595–608 (2016).
6. Hardy, J. & Selkoe, D. J. The amyloid hypothesis of Alzheimer's disease: progress and problems on the road to therapeutics. Science 297, 353–356 (2002).
7. Dubois, B. et al. Preclinical Alzheimer's disease: Definition, natural history, and diagnostic criteria. Alzheimers Dement 12, 292–323 (2016).
8. Iqbal, K. et al. Protein changes in senile dementia. Brain Res 77, 337–343 (1974).
9. Wisniewski, K., Howe, J., Williams, D. G. & Wisniewski, H. M. Precocious aging and dementia in patients with Down's syndrome. Biol Psychiatry 13, 619–627 (1978).
10. Brion, J. P., Couck, A. M., Passareiro, E. & Flament-Durand, J. Neurofibrillary tangles of Alzheimer's disease: an immunohistochemical study. J Submicrosc Cytol 17, 89–96 (1985).
11. Ihara, Y., Nukina, N., Miura, R. & Ogawara, M. Phosphorylated tau protein is integrated into paired helical filaments in Alzheimer's disease. J Biochem 99, 1807–1810 (1986).

12. Kosik, K. S., Joachim, C. L. & Selkoe, D. J. Microtubule-associated protein tau (tau) is a major antigenic component of paired helical filaments in Alzheimer disease. Proc Natl Acad Sci U S A 83, 4044–4048 (1986).
13. Noble, W., Hanger, D. P., Miller, C. C. J. & Lovestone, S. The importance of tau phosphorylation for neurodegenerative diseases. Front Neurol 4, 83 (2013).
14. Iqbal, K. et al. Tau pathology in Alzheimer disease and other tauopathies. Biochim Biophys Acta 1739, 198–210 (2005).
15. Liu, F., Iqbal, K., Grundke-Iqbal, I., Rossie, S. & Gong, C.-X. Dephosphorylation of tau by protein phosphatase 5: impairment in Alzheimer's disease. J Biol Chem 280, 1790–1796 (2005).
16. Gómez-Isla, T. et al. Profound loss of layer II entorhinal cortex neurons occurs in very mild Alzheimer's disease. J Neurosci 16, 4491–4500 (1996).
17. Caccamo, A. et al. Necroptosis activation in Alzheimer's disease. Nat Neurosci 20, 1236–1246 (2017).
18. Balusu, S. et al. MEG3 activates necroptosis in human neuron xenografts modeling Alzheimer's disease. Science 381, 1176–1182 (2023).
19. Laster, S. M., Wood, J. G. & Gooding, L. R. Tumor necrosis factor can induce both apoptic and necrotic forms of cell lysis. J Immunol 141, 2629–2634 (1988).
20. Yuan, J. & Horvitz, H. R. The Caenorhabditis elegans cell death gene ced-4 encodes a novel protein and is expressed during the period of extensive programmed cell death. Development 116, 309–320 (1992).
21. Bridel, C. et al. Diagnostic Value of Cerebrospinal Fluid Neurofilament Light Protein in Neurology: A Systematic Review and Meta-analysis. JAMA Neurol 76, 1035–1048 (2019).

22. Albers, M. W. et al. At the interface of sensory and motor dysfunctions and Alzheimer's disease. Alzheimers Dement 11, 70–98 (2015).
23. O'Leary, D. D. & Koester, S. E. Development of projection neuron types, axon pathways, and patterned connections of the mammalian cortex. Neuron 10, 991–1006 (1993).
24. Arlotta, P. et al. Neuronal subtype-specific genes that control corticospinal motor neuron development in vivo. Neuron 45, 207–221 (2005).
25. Chen, B., Schaevitz, L. R. & McConnell, S. K. Fezl regulates the differentiation and axon targeting of layer 5 subcortical projection neurons in cerebral cortex. Proc Natl Acad Sci U S A 102, 17184–17189 (2005).
26. Tervo, D. G. R. et al. A Designer AAV Variant Permits Efficient Retrograde Access to Projection Neurons. Neuron 92, 372–382 (2016).
27. Madisen, L. et al. A robust and high-throughput Cre reporting and characterization system for the whole mouse brain. Nat Neurosci 13, 133–140 (2010).
28. Steward, O. et al. Rostro-Caudal Specificity of Corticospinal Tract Projections in Mice. Cereb Cortex 31, 2322–2344 (2021).
29. Games, D. et al. Alzheimer-type neuropathology in transgenic mice overexpressing V717F beta-amyloid precursor protein. Nature 373, 523–527 (1995).
30. Hsiao, K. et al. Correlative memory deficits, Abeta elevation, and amyloid plaques in transgenic mice. Science 274, 99–102 (1996).
31. Drummond, E. & Wisniewski, T. Alzheimer's disease: experimental models and reality. Acta Neuropathol 133, 155–175 (2017).

32. Casas, C. et al. Massive CA1/2 neuronal loss with intraneuronal and N-terminal truncated Abeta42 accumulation in a novel Alzheimer transgenic model. Am J Pathol 165, 1289–1300 (2004).

33. Forner, S. et al. Systematic phenotyping and characterization of the 5xFAD mouse model of Alzheimer's disease. Sci Data 8, 270 (2021).

34. Gallent, E. A. & Steward, O. Neuronal PTEN deletion in adult cortical neurons triggers progressive growth of cell bodies, dendrites, and axons. Exp Neurol 303, 12–28 (2018).

35. Spruston, N. Pyramidal neurons: dendritic structure and synaptic integration. Nat Rev Neurosci 9, 206–221 (2008).

36. Ma, X. M. & Blenis, J. Molecular mechanisms of mTOR-mediated translational control. Nat Rev Mol Cell Biol 10, 307–318 (2009).

37. Switon, K., Kotulska, K., Janusz-Kaminska, A., Zmorzynska, J. & Jaworski, J. Molecular neurobiology of mTOR. Neuroscience 341, 112–153 (2017).

38. Gutilla, E. A. & Steward, O. Selective neuronal PTEN deletion: can we take the brakes off of growth without losing control? Neural Regen Res 11, 1201–1203 (2016).

39. Yonan, J. M. & Steward, O. Vector-mediated PTEN deletion in the adult dentate gyrus initiates new growth of granule cell bodies and dendrites and expansion of mossy fiber terminal fields that continues for months. Neurobiol Dis 184, 106190 (2023).

40. Park, K. K. et al. Promoting axon regeneration in the adult CNS by modulation of the PTEN/mTOR pathway. Science 322, 963–966 (2008).

41. Spilman, P. et al. Inhibition of mTOR by rapamycin abolishes cognitive deficits and reduces amyloid-beta levels in a mouse model of Alzheimer's disease. PLoS One 5, e9979 (2010).

42. Soares, C. et al. CSF total tau as a proxy of synaptic degeneration. Nat Commun 16, 8076 (2025).
43. Jack, C. R. et al. Hypothetical model of dynamic biomarkers of the Alzheimer's pathological cascade. Lancet Neurol 9, 119–128 (2010).
44. Jack, C. R. et al. Hypothetical model of dynamic biomarkers of the Alzheimer's pathological cascade. Lancet Neurol 9, 119–128 (2010).
45. Kim, S.-W. et al. Gait impairment associated with neuroimaging biomarkers in Alzheimer's disease. Sci Rep 15, 5539 (2025).
46. Bologna, M. et al. Bradykinesia in Alzheimer's disease and its neurophysiological substrates. Clin Neurophysiol 131, 850–858 (2020).
47. Da Rocha Anselmo, M. et al. Posturographic Evidence of Sensory Integration Deficits and Postural Instability in Alzheimer's Disease. Alzheimer's & Dementia 21, e108344 (2025).
48. Buracchio, T., Dodge, H. H., Howieson, D., Wasserman, D. & Kaye, J. The trajectory of gait speed preceding mild cognitive impairment. Arch Neurol 67, 980–986 (2010).
49. Cai, Z., Zhou, Y., Xiao, M., Yan, L.-J. & He, W. Activation of mTOR: a culprit of Alzheimer’s disease? NDT 1015 (2015) doi:10.2147/NDT.S75717.
50. Chohan, M. O. et al. Hyperphosphorylation-induced self assembly of murine tau: a comparison with human tau. J Neural Transm 112, 1035–1047 (2005).
51. Goffin, A., Hoefsloot, L. H., Bosgoed, E., Swillen, A. & Fryns, J. PTEN mutation in a family with Cowden syndrome and autism. Am. J. Med. Genet. 105, 521–524 (2001).

52. Greig, L. C., Woodworth, M. B., Galazo, M. J., Padmanabhan, H. & Macklis, J. D. Molecular logic of neocortical projection neuron specification, development and diversity. Nat Rev Neurosci 14, 755–769 (2013).

53. Iqbal, K. & Grundke-Iqbal, I. Mechanism of Alzheimer neurofibrillary degeneration and the formation of tangles. Mol Psychiatry 2, 178–180 (1997).

54. Hollander, M. C., Blumenthal, G. M. & Dennis, P. A. PTEN loss in the continuum of common cancers, rare syndromes and mouse models. Nat Rev Cancer 11, 289–301 (2011).

55. McKenna, W. L. et al. Tbr1 and Fezf2 Regulate Alternate Corticofugal Neuronal Identities during Neocortical Development. J. Neurosci. 31, 549–564 (2011).

56. Molyneaux, B. J., Arlotta, P., Menezes, J. R. L. & Macklis, J. D. Neuronal subtype specification in the cerebral cortex. Nat Rev Neurosci 8, 427–437 (2007).

57. Nukina, N. & Ihara, Y. One of the Antigenic Determinants of Paired Helical Filaments Is Related to Tau Protein1. The Journal of Biochemistry 99, 1541–1544 (1986).

58. Özdinler, P. H. et al. Corticospinal Motor Neurons and Related Subcerebral Projection Neurons Undergo Early and Specific Neurodegeneration in hSOD1G93A Transgenic ALS Mice. J. Neurosci. 31, 4166–4177 (2011).

59. Scalia, P. & Williams, S. J. Over-expression by degradation rescue of RTKs via cancer-secreted autocrine growth factors: a Phospho-degron-driven actionable layer of post-translational regulation? Front. Oncol. 13, 1278402 (2023).

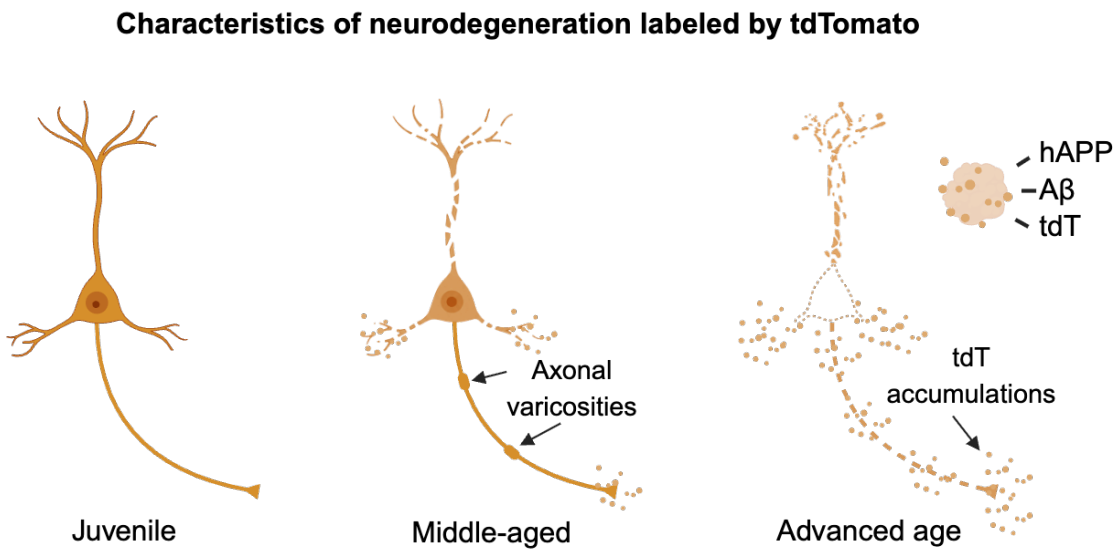
60. Xu, L. & Wang, Q. The bidirectional relationship between Alzheimer's disease (AD) and epilepsy: A Mendelian randomization study. Brain and Behavior 13, e3221 (2023).

61. Hardy, J. & Allsop, D. Amyloid deposition as the central event in the aetiology of Alzheimer's disease. Trends in Pharmacological Sciences 12, 383–388 (1991).

62. Sadleir, K. R., Popovic, J. & Vassar, R. ER stress is not elevated in the 5XFAD mouse model of Alzheimer's disease. Journal of Biological Chemistry 293, 18434–18443 (2018).
63. Degterev, A. et al. Chemical inhibitor of nonapoptotic cell death with therapeutic potential for ischemic brain injury. Nat Chem Biol 1, 112–119 (2005).

Chapter 2 - Conditional genetic labeling of neurons that degenerate in 5xFAD mice reveals previously un-described features of age-related neurodegeneration

Graphical abstract



Abstract

This paper describes a novel double transgenic-based platform developed by crossing a murine model of Alzheimer's disease (AD), 5xFAD mice with Rosa$^{tdTomato\ (tdT)}$ reporter mice, to track degeneration of specific populations of neurons. 5xFAD$^{+/-}$/Rosa^{tdT} mice received intra-spinal cord injections of AAV-retrograde (rg)/Cre at 2-3 months of age to retrogradely transduce and induce tdT expression by corticospinal neurons (CSNs) in layer V of the sensorimotor cortex as

well as neurons in the red nucleus and reticular formation that project to the spinal cord. Brains and spinal cords were collected 2-3 weeks post-injection or between 7-10 and 11-15 months of age. Immunohistochemical studies of transgene expression throughout the brain and spinal cord using an antibody selective for human APP (hAPP) revealed age-dependent accumulation of clusters of hAPP-positive granules in areas containing hAPP-labeled neuronal cell bodies. Surprisingly, there were also hAPP-positive granules in regions containing axons and synaptic terminals from hAPP expressing neurons. Moreover, tdT expressed by CSNs accumulated in the same granules as hAPP, and both tdT and hAPP were present in clusters of granules with other markers of AD pathology. Quantitative assessments confirmed age-related degeneration of layer V CSNs accompanied by progressive accumulation of clusters of tdT and hAPP-positive granules. Overall, our results indicate that accumulation of aggregated hAPP in areas containing axons and synaptic terminals from hAPP expressing neurons is a prominent feature of AD pathophysiology in 5xFAD mice and that accumulation of clusters of hAPP granules provides a secondary measure to track neurodegeneration of identified populations of genetically labeled neurons.

Introduction

Alzheimer's Disease (AD) is one of the most prevalent neurodegenerative diseases with an estimated 6.9 million Americans aged 65 and older currently affected (2024 Alzheimer's disease facts and figures). Early in disease onset, AD is characterized by the accumulation of amyloid beta (Aß) plaques and neurofibrillary tangles (Terry, 1963). In late-stage AD, neurodegeneration is a primary pathological feature. Neurodegeneration involves dendritic atrophy, spine loss,

axonal destabilization and finally neuron death (Terry et al., 1991; Thal et al., 2002). Aggregated Aß deposits are commonly surrounded by degenerating neuronal processes, and these together are termed neuritic plaques. Some of these pathological features are recapitulated in animal models of AD (Drummond and Wisniewski, 2016). Characterizing the progression of pathology in these models is crucial for the understanding of disease mechanisms and development of effective treatments.

There are several well characterized murine models of AD, but most do not exhibit actual neurodegeneration. One murine model that does exhibit neurodegeneration is the 5xFAD transgenic strain. 5xFAD mice express two mutant human genes [amyloid precursor protein (APP) and presenilin 1 (PSEN1)] with 5 familial AD mutations (3 in APP; 2 in PSEN1). During the creation of 5xFAD mice, the two transgenes are inserted into a single locus are driven by the neuron-specific elements of the mouse Thy-1 promoter (Oakley et al., 2006). The Thy-1 promoter drives expression in select neuron populations in the forebrain. Using an antibody that recognizes both mouse and human proteins, total levels of APP protein expression in the brain (endogenous mouse and transgenic human APP) have been found to be about 1.8 times that in non-transgenic control mice (Sadleir et al., 2018).

As they age, 5xFAD mice develop high $A\beta_{42}$ levels, amyloid plaques, and exhibit decreases in synaptic and neuronal markers in the brain (Oakley et al., 2006) and exhibit neurodegeneration in cortical layer V and the subiculum. Cortical layer V and the subiculum are areas where the transgenes are highly expressed based on them being driven by Thy1 (Moechars et al., 1996;

Oakley et al., 2006) and are areas that develop high amyloid plaque burden (Oakley et al., 2006; Eimer and Vassar, 2013).

Despite extensive use of 5xFAD mice, there have been limited studies of the overall pattern of transgene expression in different neuron types throughout the brain and spinal cord. Additionally, there have been limited studies on whether different neuron types that express the transgene exhibit age-dependent transgene expression and/or degenerative changes. One goal of this study is to explore this question in immunocytochemical studies using a commercially available antibody that selectively recognizes the mutant human APP (hAPP) in 5xFAD mice and not mouse APP (mAPP) (Anti-APP, clone 1D1, Millipore Cat# MABN2287, RRID:AB_3665093). The 1D1 antibody is one of two antibodies (1D1 and 7H6) developed by Hofling et al., (2016) that recognize hAPP and not mouse hAPP. Prior to the 1D1 and 7H6 antibodies, there were no available antibodies that selectively detected human APP, but not mAPP, in brains of APP-transgenic mice. Hofling et al., (2016) document that 1D1 recognizes an epitope in the N-terminus of hAPP, amino acids 40-64 of its unmodified state, and detects both membrane bound and soluble hAPP (Hofling et al., 2016). We chose to use the 1D1 antibody because it robustly labels hAPP in immunocytochemistry studies. Importantly, Hofling et al also provide strong evidence that 1D1 does not detect Aß peptides, in contrast to another widely used antibody (6E10) which recognizes Aβ in immunocytochemical preparations, enzyme linked immunosorbent assays (ELISA) and western blots from APP-transgenic mouse tissue (Herzig et al., 2004; Zheng et al., 2012; Hofling et al., 2016).

The second goal of this study was to develop a technique that selectively and permanently labels one population of neurons that degenerate in 5xFAD mice, specifically targeting layer V pyramidal neurons in the sensorimotor cortex. The purpose of the technique is to allow quantitative analyses of the time course and characteristics of neurodegeneration of this population of neurons. Previous reports of neurodegeneration in 5xFAD mice have used routine neurohistological stains such as cresyl violet to document decreases in numbers of large cells in layer V of the somatosensory cortex. To our knowledge, there have been no studies using selective markers to label specific populations of neurons. For example, although it is reasonable to speculate that some of the layer V neurons that degenerate are the neurons that give rise to the corticospinal tract, this has not been established. For this purpose, we developed a new strain of double-transgenic 5xFAD mice that allows selective and permanent retrograde labeling of layer V cortical neurons and other neuron types in the brain that project to the spinal cord. Full labeling of dendrites and axons allows tracking of features of neurodegeneration across age. This model has allowed specific identification of age dependent degeneration of layer V corticospinal neurons (CSNs) as well as other neuron types that have not previously been reported to degenerate in $5xFAD^{+/-}/Rosa^{tdT}$ mice. We also document early degenerative changes in axons and dendrites and discovered that clusters of tdT-positive granules accumulate as neurons degenerate, providing a secondary tool to track neurodegeneration from an identified population of neurons.

Methods

2.1 Experimental Animals

All procedures involving animals were approved by the Institutional Animal Care and use Committee (IACUC) at the University of California, Irvine (UCI) in accordance with the National Institute of Health (NIH) guidelines. Mice had *ad lib* access to food and water and were housed at 25°C with a 12h light/dark cycle.

Breeding strategy: To produce the transgenic mice for these studies, hemizygous 5xFAD (B6SJL-Tg (APPSwFlLon, PSEN1*M146L*L286V) 6799Vas/Mmjax; RRID:MMRRC_034840-JAX) mice were initially crossed with homozygous $Rosa^{tdT}$ mice. 5xFAD mice were obtained from Jackson Laboratory (Stock No: 34840-JAX). The $Rosa^{tdT}$ mice were originally obtained from Jackson Laboratory (Stock No: 007905) and had been maintained in our breeding colony over multiple generations before being crossed with 5xFAD mice.

All mice of the F1 generation from the $5xFAD^{+/-}$ x $Rosa^{tdT\ +/+}$ cross were hemizygous at the $Rosa^{tdT}$ locus and approximately 50% of the mice were hemizygous for 5xFAD. Genotypes were determined by real time PCR with probes designed for hAPP and hPSEN1 (Transnetyx, Cordova, TN). When sufficient numbers of $5xFAD^{+/-}/Rosa^{tdT\ +/+}$ were obtained, breeding pairs were created with $Rosa^{tdT\ +/+}/5xFAD^{+/-}$ crossed with $Rosa^{tdT\ +/+}$ to generate $Rosa^{tdT\ +/+}/\ 5xFAD^{+/-}$ and $Rosa^{tdT\ +/+}/5xFAD^{-/-}$ controls. Genotyping of progeny of these breeders was done with PCR probes designed according to the protocol provided by Jackson lab (protocol ID = 22421) with confirmation of presence, or absence of hAPP by IF against hAPP protein using the clone 1D1 primary antibody (RRID:AB_3665093). Details on the age of mice when injected with AAV-rg/Cre and age at tissue collection are in Table 1. In initial studies, mice received AAV-rg/Cre injections between 4-5 months of age. However, we discovered signs of neurodegeneration at this age and so transitioned to injecting mice with AAV-rg/Cre at 2-3 months of age to label

neurons with tdT before neurodegeneration began. Some results from mice injected between 4-5 months are illustrated in figures as noted in respective legends, but mice injected between 4-5 months are not included in the quantitative analyses of neuron numbers.

Previous studies using routine histological stains (cresyl violet) indicate the loss of most large neurons in layer V of the sensorimotor cortex as 5xFAD mice age, but the actual quantitative extent of loss of layer large V neurons is not known. Accordingly, we carried out power analysis using G*Power with different effect sizes (0.9, 0.8, 0.75, $\alpha = 0.05$ and target power of 0.80. The analysis indicated that n = 4, 6, 7 could be sufficient for adequate power with effect sizes of 0.9, 0.8 and 0.75 respectively. In practice, however, sample sizes were limited by availability of mice

from the breeding colony, variability in AAV-rg/Cre injection efficiency leading to inadequate tdT labeling in some mice (see Table 1 for explanation of N per genotype).

Table 2.1. Mice injected with AAV-rg/Cre

2-4 Months of age

Months of age	Months of age at injection	5xFAD$^{+/-}$/Rosa^{tdT}	5xFAD$^{+/-}$/Rosa^{tdT} – Fewer than 500 tdT-labeled neurons	Rosa^{tdT}	Rosa^{tdT} – Fewer than 500 tdT-labeled neurons
2	2	8 (6M, 2F)	5 (5M) – 2M had 0 tdT-labeled neurons	1 (1F)	1 (1F) - Had 0 tdT-labeled neurons
3	2	-	-	5 (5F)	-
4	2	-	-	1 (1M)	-
3	3	3 (1M, 2F)	3 (1, 2F)	3 (2F, 1M)	2 (1F, 1M) – Had 0 tdT-labeled neurons

6-10 Months of age

Months of age	Months of age at injection	5xFAD$^{+/-}$/Rosa^{tdT}	Rosa^{tdT}
10	3	2 (2M)	-
5	4	3 (1F, 2M)	-
8	4	5 (1F, 4M)	4 (2F, 2M)

11+ Months of age

Months of age	Months of age at injection	5xFAD$^{+/-}$/Rosa^{tdT}	Rosa^{tdT}
12	2	2 (2M)	-
14	2	2 (1F, 1M)	1 (1F)
15	2	-	2 (2F)
12	3	3 (3F)	-
15	3	2 (2F)	-
12	4	4 (3F, 1M)	-

2.2 Surgical procedures

At 2-3 months of age, mice received unilateral intra-spinal cord injections of AAV-retrograde(rg)/Cre (Addgene viral prep #24593-AAVrg) at cervical level 5 (C5). For surgery, mice were anesthetized with continuous Isoflurane (2-2.5%) administration, their eyes were swabbed with Vaseline to prevent drying, and the scalp was shaved and cleaned with Betadine®. A laminectomy was performed at C5 to expose the spinal cord and AAV-rg/Cre was injected 0.5 mm left of the midline and 0.5 mm deep using a Hamilton microsyringe fitted with a pulled glass micropipette. Injection volume was 0.3µL of vector stock solution with 1E10 genome copies (GC)/µL for a total dose of 3E9GC. Injections were unilateral in order to transduce neurons on the contralateral side of the brain leaving most neurons on the ipsilateral side as non-transduced control. The needle was kept in place for 1 minute after completing the injection. Following injection, the muscle layers were sutured, and the skin was closed by wound clips.

2.3 Post-operative care

After surgery, mice were immediately placed in cages with Alpha-Dri bedding with half of the cage placed on a circulating water warming pad set to 37ºC. Placing the cage partially on top of warming pads allows mice to remove themselves from the heat source, if desired. Mice were kept on the warming pad for 3 days post-surgery and received lactated Ringer's solution once a day (1ml/20g, subcutaneously), enrofloxacin once a day (Baytril® 2.5mg/kg, subcutaneously) and buprenorphine twice a day (0.01mg/kg, subcutaneously). Mice were monitored twice daily for 3 days post-surgery for general health and signs of distress. If bladders of mice were full, indicating difficulty to urinate due to surgery, the bladders were manually expressed twice daily. Bladder expression was required for a small number of animals and for a maximum of 3 days post-surgery. After 3 days, the cages were removed from the warming pads and were transferred back to the mouse housing room set at 25°C. Once in the housing room, mice were routinely monitored by vivarium staff and research staff.

2.4 Tissue collection

All mice were euthanized using Fatal Plus®, followed by transcardiac perfusion with 4% paraformaldehyde (PFA). Brains and spinal cords were removed intact and imaged at 2X using an Olympus fluorescent microscope to visualize tdT fluorescence at the spinal cord injection site and in the cortex. Brains and spinal cords were kept in 4% PFA for at least 24 hours. The tissue was then submerged in 27% sucrose for 24 hours for cryoprotection and frozen in Tissue-Tek O.C.T. embedding medium. Brains were then sectioned at 30µm in coronal or horizontal planes

(*see Results*), using a cryostat. Sections were stored free-floating in phosphate-buffered saline (1xPBS, 20mM, pH7.4) with 0.1% sodium azide.

2.5 Immunohistochemistry (IHC) and immunofluorescence (IF)

Free-floating brain sections at 480 µm intervals were used for IHC and IF. Human APP transgene expression was detected by immunostaining for Anti-APP, clone 1D1 (Millipore Cat# MABN2287, RRID:AB_3665093). For 1D1 IF, sections were washed in Tris Buffered Saline (1xTBS, 100mM Tris. pH 7.4 and 150 mM NaCl) 2 times for 5-10 minutes each time. The sections were then incubated in methanol with 3% Hydrogen peroxide for 15 minutes and washed in 1xTBS 3 times for 5-10 minutes each. After washing, sections were incubated for 1-2 hours at room temperature in a 1xTBS, 5% Normal Donkey Serum (NDS), 0.3% Triton X-100 blocking solution. Sections were then incubated in a 1:250 dilution of Rat Anti-1D1 primary antibody (Millipore Cat# MABN2287, RRID:AB_3665093) with 1xTBS, 5% NDS and 0.3% Triton X-100 overnight at room temperature. The following day, sections were washed in 1xTBS 3 times for 5-10 minutes each and then incubated in a 1:250 dilution of Biotin-SP (long spacer) AffiniPure™ Donkey Anti-Rat IgG (H+L) (Cat# 712-065-153, RRID: AB_2315779, Jackson ImmunoResearch) for 2 hours at room temperature. Sections were then washed in 1xTBS 3 times for 5-10 minutes each and then incubated in a 1:100 dilution of VECTASTAIN® Elite® ABC (Avidin/Biotin) - Horseradish peroxidase (HRP) (Standard) (PK-6100, RRID: AB_2336819) with 1xTBS for 1-2 hours. After incubation, sections were washed in 1xTBS 3 times for 5-10 minutes each and then incubated in a 1:250 dilution of Fluorescein-conjugated tyramide (FITC-tyramide) with 0.1M borate buffer (pH 9) for 25 minutes. Sections were washed twice in 1xTBS

and mounted on 0.5% gelatin subbed, double frosted, VWR® microscope slides. For NeuN IF, sections were washed in 1xTBS 2 times for 5-10 minutes each time. The sections were then incubated in 1xPBS with 3% hydrogen peroxide for 15 minutes and washed in 1xTBS 3 times for 5-10 minutes each time. After washing, sections were incubated for 1-2 hours at room temperature in a 1xTBS, 5% NDS, 0.3% Triton X-100 blocking solution. Sections were then incubated in a 1:250 dilution of Mouse anti-NeuN Antibody, clone A60 (Millipore Cat# MAB377, RRID:AB_2298772) in 1xTBS, 5% NDS, 0.3% Triton X-100 solution overnight at room temperature. The following day, sections were washed in 1xTBS 3 times for 5-10 minutes each and then incubated in a 1:250 dilution of Donkey anti-Mouse 488 secondary antibody with 1xTBS, 5% NDS, 0.3% Triton X-100 for 2 hours at room temperature. Sections were washed twice in 1xTBS and mounted on 0.5% gelatin subbed, double frosted, VWR® microscope slides.

To detect tdTomato by IF, sections were immunostained for Red Fluorescent Protein (RFP). Steps prior to incubation in primary antibody were as for 1D1 (*above*). Sections were then incubated in a 1:1000 dilution of Rabbit anti-RFP primary antibody (Rockland Cat# 600-401-379, RRID:AB_2209751) with 1xTBS, 5% NDS and 0.3% Triton X-100 overnight at room temperature. The next day, sections were washed in 1xTBS 3 times for 5-10 minutes each and then incubated in a 1:500 dilution of Donkey anti-Rabbit 555 with 5% NDS and 0.3% Triton X-100 for 2 hours at room temperature, washed twice in 1xTBS and mounted on 0.5% gelatin subbed, double frosted, VWR® microscope slides.

For the RFP and 1D1 co-IF, the steps and reagents remained the same for each, but the steps were combined. The Aβ IF was done by first washing sections in 1xTBS 2 times for 5-10

minutes each, then sections were incubated in 1.75 mL clear microtubes filled with citrate buffer (10mM, pH 6) and tubes were placed in a 100º C water bath for 5 minutes for antigen retrieval and then in a water bath at room temperature for 10 minutes. Sections were washed in 1xTBS 3 times for 5-10 minutes each, incubated in 88% formic acid (Cat# A119P-500, Fisher Scientific) for 7 minutes, then washed again in 1xTBS 3 times for 5-10 minutes each. Sections were then incubated for 1-2 hours at room temperature in a 1xTBS, 5% NDS, 0.3% Triton X-100 solution followed by incubation in a 1:1000 dilution of Mouse anti-Amyloid-ß (N) (82E1) Aβ Anti-Human Mouse IgG MoAb (Tecan (IBL) Cat# 10323, RRID:AB_10707424) with 1xTBS, 5% NDS, 0.3% Triton X-100 overnight at room temperature. The following day, sections were washed in 1xTBS 3 times for 5-10 minutes each and then incubated in a 1:250 dilution of Donkey anti-Mouse 488 with 1xTBS, 5% NDS, 0.3% Triton X-100 for 2 hours at room temperature. Lastly, sections were washed twice in 1xTBS and mounted on 0.5% gelatin subbed, double frosted, VWR® microscope slides. Some sections were stained with Hoechst 33258, pentahydrate (bis-benzimide) in 1xPBS (1µg/ml, ThermoFisher Scientific®, Cat# H3569) to label cell nuclei.

The co-IF for 1D1 and 6E10 was done by first washing sections in 1xTBS 2 times for 5-10 minutes each, then sections were incubated in 1.75 mL clear microtubes filled with citrate buffer (10mM, pH 6) and tubes were placed in a 60º C water bath for 15 minutes for antigen retrieval and then in a water bath at room temperature for 10 minutes. Sections were washed in 1xTBS 3 times for 5-10 minutes each and incubated in a 1:1000 dilution of Mouse anti-β-Amyloid, clone 6E10 (BioLegend Cat# 803001, RRID AB_2564653; gift from the Green Lab, University of California, Irvine) and 1:250 dilution of Rat Anti-1D1 primary antibody with 1xTBS, 5% NDS,

0.3% Triton X-100 overnight at room temperature. The following day, sections were washed in 1xTBS 3 times for 5-10 minutes each and then incubated in a 1:250 dilution of Donkey anti-Mouse 488 and a 1:250 dilution of Biotin-SP (long spacer) AffiniPure™ Donkey Anti-Rat IgG (H+L) with 1xTBS, 5% NDS, 0.3% Triton X-100 for 2 hours at room temperature. Sections were then washed in 1xTBS 3 times for 5-10 minutes each and then incubated in a 1:100 dilution of VECTASTAIN® Elite® ABC (Avidin/Biotin) - Horseradish peroxidase (HRP) (Standard) (PK-6100, RRID: AB_2336819) with 1xTBS for 1-2 hours. After incubation, sections were washed in 1xTBS 3 times for 5-10 minutes each and then incubated in a 1:250 dilution of Cy3-conjugated tyramide (Cy3-tyramide) with 0.1M borate buffer (pH 9) for 25 minutes. Sections were washed twice in 1xTBS and mounted on 0.5% gelatin subbed, double frosted, VWR® microscope slides. Slides were then incubated in a Hoechst 33258, pentahydrate (bis-benzimide) 1xPBS solution (1µg/ml, ThermoFisher Scientific®, Cat# H3569) for 10 minutes, to label cell nuclei.

IF for LAMP-1 was done by incubating sections in a 1xTBS, 5% NDS, 0.3% Triton X-100 solution for 1-2 hours at room temperature, followed by an overnight incubation in a 1:300 dilution of Rat anti-LAMP-1 (Abcam Cat# ab25245, RRID:AB_449893, gift from the Blurton-Jones Lab and the Green Lab, University of California, Irvine) in 1xTBS, 5% NDS, 0.3% Triton X-100. The following day, sections were washed in 1xTBS 3 times for 5-10 minutes each and then incubated in a 1:250 dilution of Biotin-SP (long spacer) AffiniPure™ Donkey Anti-Rat IgG (H+L) (Cat# 712-065-153, RRID: AB_2315779, Jackson ImmunoResearch) for 2 hours at room temperature. Sections were then washed in 1xTBS 3 times for 5-10 minutes each and then incubated in a 1:100 dilution of VECTASTAIN® Elite® ABC (Avidin/Biotin) - Horseradish peroxidase (HRP) (Standard) (PK-6100, RRID: AB_2336819) with 1xTBS for 1-2 hours. After

incubation, sections were washed in 1xTBS 3 times for 5-10 minutes each and then incubated in a 1:250 dilution of Fluorescein isothiocyanate (FITC) with 0.1M borate buffer (pH 9) for 25 minutes. Sections were washed twice in 1xTBS and mounted on 0.5% gelatin subbed, double frosted, VWR® microscope slides.

Thioflavin S staining was done by mounting sections onto 0.5% gelatin subbed, double frosted, VWR® microscope slides and allowing them to air dry overnight. The following day the slides were incubated in three different 100% xylene solutions for 3 minutes each. Then, they were then rehydrated through an ordered sequence of 100%, 95%, 80%, 70% ethanol solutions for 2 minutes each, followed by a 2-minute incubation in nanopure water. The slides were then placed into a 1% thioflavin S solution for 10 minutes followed by incubations in an ordered sequence of 70%, 80%, 95%, 100% ethanol solutions.

Table 2. Primary Antibody list

Antibody	Host	Vendor	Catalog #	RRID	Dilution
Human APP, clone 1D1	Rat	Millipore Sigma	MABN22 87	RRID:AB_3665093	1:250
RFP	Rabbit	Rockland	600-401-379	RRID:AB_2209751	1:1000
LAMP-1	Rat	Abcam	ab25245	RRID:AB_449893	1:300
NeuN, clone A60	Mouse	Millipore Sigma	MAB377	RRID:AB_2298772	1:250
Human Aβ	Mouse	Tecan (IBL)	10323	RRID:AB_10707424	1:1000

6E10	Mouse	BioLegend	803001	RRID AB_2564653	1:1000

Exclusions:

Our paradigm for injections of AAV-rg/Cre at C5 leads to retrograde transduction of most neurons that give rise to the corticospinal tract (almost 10,000 CSNs throughout the sensorimotor cortex per hemisphere (Steward et al., 2021). However, there can be technical issues (mis-targeted injections, broken syringe tips, aliquots of AAV-rg/Cre that have deteriorated) leading to minimal or occasionally even no retrograde transduction. For quantitative studies, several criteria were used to exclude animals with flawed or failed AAV-rg/Cre injections including: 1) assessing tdT fluorescence at the spinal cord injection site by epi-illumination of intact brains and spinal cords prior to sectioning (as in Fig. 2.6A); and 2) total number of retrogradely transduced neurons in the cortex. $Rosa^{tdT}$ mice and young $5xFAD^{+/-}/Rosa^{tdT}$ mice with low numbers of transduced neurons (fewer than 500 tdT labeled neurons across the sensorimotor cortex in sections 240µm apart) were excluded. Excluded mice are detailed in Table 2.1. The criterion relating to the number of transduced cortical neurons cannot be used for older $5xFAD^{+/-}/Rosa^{tdT}$ mice because the expected phenotype is neuron loss.

2.6 Microscopy

Images were acquired using a fluorescent Olympus BX53 widefield microscope with a 10x objective (Fig. 2.1, Fig. 2.2 A–C, Fig. 2.3 – A, C and E, Fig. 2.4, all images except B and D, Fig. 2.5 – A-F, Fig. 2.6, Fig. 2.7, all images except E and F, Fig. 2.8 and Fig. 2.9 – A-O), an Olympus

FV3000 Scanning Confocal Microscope with a 60x objective (Fig. 2.2 – B1 and C1, Fig. 2.4 – C and D), and a Zeiss LSM 900 Airyscan 2 Confocal Microscope (Fig. 2.3 – B & D with a 40x objective, Fig. 2.5 – G, H with a 40x objective and I with a 10x objective, Fig. 2.9 – P and Q with a 20x objective). For widefield imaging, the exposure was set to the brightest sample to avoid oversaturation and kept constant for all sections within that experiment. Similarly, for confocal imaging, laser power, pinhole size and gain were set to the brightest sample and kept constant for all sections within that experiment.

2.7 Quantification of corticospinal neurons (CSNs)

For quantification of tdT-labeled neurons, coronal sections at 240 µm intervals were mounted without immunostaining onto 0.1% gelatin subbed slides. Transduced neurons were identified by native tdT fluorescence rather than by immunostaining because with IHC, robust labeling of dendrites can obscure tdT-labeled CSN cell bodies. Sections were imaged at 20X using a fluorescent Olympus BX53 microscope and tdT-positive CSN cell bodies in layer V of the cortex were manually counted in each section from the medial border of M1 to the lateral border of S1. The population of tdT-labeled CSNs in the S1 cortex posterior to bregma that are separated from the main sensorimotor cortex were not counted. Counts were taken in all sections in the series that contained tdT-labeled CSNs, which was typically from 3 mm anterior to bregma to approximately 2.5 mm posterior to bregma.

We chose to count all tdT-labeled neurons in layer V in each section rather than using single-section stereological counting techniques (the optical dissector) because cell boundaries of

fluorescently labeled neurons are indistinct, and the optical dissector depends on being able to identify cell edges (caps) when focusing up and down. Another potential caveat is that there can be photobleaching with the longer periods of time required for use of the optical dissector.

2.8 Quantification of accumulations of tdT (debris)

Our results revealed the unexpected appearance of clusters of tdT-positive granules in areas containing tdT-positive neurons and their processes. To quantify these granules, we selected sections at approximately 0.74mm–0.62mm anterior to bregma (midway along the rostro-caudal axis of the sensorimotor cortex). Native tdT fluorescence in the right cortex was imaged at 20x magnification with a fluorescent Olympus BX53 microscope. The quantifications were on the right cortex because the unilateral AAV-rg/Cre injection was on the left side of the spinal cord. Multiple images were taken at 10x magnification to capture the full medio-lateral expanse of layer V containing labeled CSNs, images were tiled into a montage and imported to Fiji ImageJ. The scale was set to pixels and images were converted to 8-bit format. Then, the threshold was set to 0.36–0.38% with a dark background. After thresholding, the watershed separation command was used to accurately track the clusters of granules. If any neuronal cell bodies were selected throughout the process (identified by their morphology and location in layer V), they were removed. Lastly, the particle analysis plug-in was used with the following settings: Size ($pixel^2$) = 100–1000, circularity = 0.30–1.00.

2.9 Assessing co-localization of tdT granules with amyloid plaques, hAPP and LAMP-1

To assess co-localization of tdT granules with other markers of AD pathophysiology, sections were stained for β-amyloid, hAPP and LAMP-1 as described above with FITC. As above, we selected sections at approximately 0.74mm–0.62mm anterior to bregma and collected paired images from the right cortex of tdT granules (native tdT fluorescence) and FITC IF for the different antibodies using a 10x objective. Using the "Cell Counter" plugin on ImageJ, tdT particles were quantified from medial to lateral across layers V and VI until 100 individual granules were sampled. If the tdT-positive granule was fully within the bounds of the FITC IF for Aβ, LAMP-1 or 1D1, then tdT was identified as colocalized.

Thioflavin-S only stains the β-sheet rich core of amyloid-β plaques, so that in sections, Thioflavin-S particles are surrounded by a donut-shaped amyloid-stained plaque. TdT-positive granules were observed in the plaques surrounding the thioflavin-S core (see Results). To quantify this, we determined the proportion of tdT granules within 6 micrometers away from the thioflavin-S particle. The 6 μm parameter was chosen to account for the radius of the amyloid plaque, which has been reported to be up to 16μm diameter in an amyloidosis mouse model (Hefendehl et al., 2011). Of note, however, some amyloid plaques in the older 5xFAD mice in the present study were much larger in diameter (see Fig. 2.5G and Fig. 2.9P & Q).

Results

3.1 Pattern of expression of hAPP in brain and spinal cord of young 5xFAD$^{+/-}$/Rosa^{tdT} mice

For this study, we created a new transgenic strain by crossing 5xFAD mice (34840-JAX) with $Rosa^{tdT}$ reporter mice. These mice allow for selective and permanent retrograde labeling of corticospinal neurons (CSNs) which are amongst the neurons in cortical layer V that are thought to degenerate in 5xFAD mice. Since these mice have a different genetic background than the commercially available Jackson Laboratory 5xFAD mice (MMRRC Strain #034840-JAX), it was important to determine the overall pattern of expression of the 5xFAD transgenes. Also, to our knowledge, there have been no comprehensive studies of the overall pattern of expression of hAPP in different neuronal cell types in the parental 5xFAD transgenic strain. The mutant hAPP and hPS1 genes in 5xFAD mice are driven by a modified mouse Thy-1 promoter, but the exact pattern of Thy-1 driven expression can vary (Feng et al., 2000). A previous study described patterns of labeling in cortex, hippocampus and spinal cord using an unpurified polyclonal antiserum against human APP, but specificity for hAPP was not documented (Jawhar et al., 2012).

To determine the pattern of expression in our $5xFAD^{+/-}/Rosa^{tdT}$ transgenic strain, we immunostained coronal brain sections from young (2-month-old) mice using an antibody for hAPP (Clone 1D1, Millipore Cat# MABN2287, RRID:AB_3665093), with FITC as the reporter. To test selectivity of this antibody for hAPP, we also immunostained sections from $Rosa^{tdT}$ mice lacking the 5xFAD transgene. Immunofluorescence for hAPP was completely absent in control $Rosa^{tdT}$ mice (**Fig. 2.1A**) whereas there was robust labeling of multiple populations of neurons in $5xFAD^{+/-}/Rosa^{tdT}$ mice (**Fig. 2.1B**). This documents that with our methods of immunostaining, the 1D1 antibody specifically recognizes hAPP and not mouse APP. To our knowledge, the monoclonal 1D1 antibody has not previously been used to document expression of hAPP in

5xFAD mice, so the following describes the overall pattern of expression in some detail. For this, we first describe the pattern of labeling in young (2–3-month-old) mice and the change in the pattern of labeling as the mice age.

Previous studies have shown that neurons in layer V of the primary (M1) and secondary (M2) motor area and primary somatosensory (S1) area express the hAPP transgene at high levels (Oakley et al., 2006), and this was confirmed here by 1D1 immunofluorescence (**Fig. 2.1B-C**). Importantly, these are the neurons that have been reported to degenerate in 5xFAD mice (Oakley et al., 2006). Neurons in layers IV and VI were also labeled although fluorescence was less pronounced than in layer V.

In sections near the caudal boundary of the sensorimotor cortex (approximately 1.7 mm posterior to bregma), there were fewer 1D1-positive neurons in layer V (**Fig. 2.1D**) than in the more rostral M1 region (**Fig. 2.1C**). Labeling was more prominent in layer V and VI of the S1 area and auditory (A1) region in the lateral cortex (**Fig. 2.1D**). In more caudal sections (approximately 3.5mm posterior to bregma) where the visual cortex was prominent, labeling was also present in layers V and VI (**Fig. 2.1E).**

Robust immunofluorescence for hAPP was also observed in the pyramidal layer of the CA1 region of the hippocampus (**Fig. 2.1D**) and in more caudal sections, in the subiculum (**Fig. 2.1E, F, and G**). Levels of labeling in CA2-3 were lower than CA1 but still detectable (**Fig. 2.1D, E**). Of note, in addition to labeled neuronal cell bodies in the subiculum, there were clusters of 1D1-positive granules (**Fig. 2.1F**). These clusters were primarily in the dendritic lamina (stratum

oriens) and had a distinctly different appearance than the 1D1-positive neuronal cell bodies in the cell layer of the subiculum (more on clusters of 1D1-positive granules below). Of note, subicular neurons have been reported to degenerate in 5xFAD mice (Oakley et al., 2006) whereas minimal, if any, neurodegeneration has been reported in CA1 and CA3.

In the brains of patients with AD, the entorhinal cortex (EC) is one of the first regions to show signs of neurofibrillary tangles and neurodegeneration (Braak and Braak, 1991, Gomez-Isla et al., 1996). To our knowledge, the pattern of expression of 5xFAD transgenes has not been characterized in the EC or posterior cortical regions with antibodies specific to human APP. Accordingly, we sectioned brains in the horizontal plane from 3-month-old 5xFAD$^{+/-}$/Rosa^{tdT} mice to better visualize the EC and other posterior cortical areas and immunostained these for hAPP with the 1D1 antibody. Figure 2.1G illustrates the pattern of labeling in sections through the dorsal EC and in a more ventral section where the lateral EC is present. 1D1-positive neurons were present in layers V and VI of the EC. Notably, there is minimal hAPP fluorescence in stellate neurons in layer II of the EC, which are the cells of origin of perforant path projections to the dentate gyrus and distal dendrites of CA3 (Steward and Scoville, 1976). The lack of labeling for hAPP in stellate neurons in layer II is noteworthy because in AD patients, neurons in layer II of the EC are the most susceptible to early neurodegeneration (Gomez-Isla et al., 1996). In addition, there was little labeling of the pyramidal neurons in layer III, which project to the most distal dendrites of neurons in CA1-subiculum (Steward and Scoville, 1976). Similarly, there was essentially no 1D1 labeling in the parasubiculum and presubiculum in 3-month-old mice. In contrast, there was a high level of labeling for 1D1 in neurons in the subiculum and

accumulations of 1D1-positive clusters of 1D1 granules in the *stratum oriens* were even more apparent than in the dorsal subiculum visible in coronal sections (**Fig. 2.1G**).

As expected, based on previously reported patterns of Thy1-driven expression (Gordon et al., 1987), there were only scattered populations of 1D1-labeled neurons in most subcortical regions including thalamus, hypothalamus and brainstem of 2–3-month-old mice (**Fig. 2.2A)**. One exception was moderate levels of labeling of neuronal cell bodies in the basolateral amygdala (BLA) and posterior amygdala (PA), **Fig. 2.2B & B1).** There were also scattered 1D1-positive granules in the lateral septum (**Fig. 2.1B & C, LS** and **Fig. 2.2C & C1**); these did not appear to be inside of neuronal cell bodies (**Fig. 2.2 C1**) and instead appeared similar to 1D1-positive granules in the dendritic layer of the subiculum (**Fig. 2.1F**). The lateral septum receives glutamatergic input from 1D1-expressing neurons the hippocampus (Khakpai et al., 2013). There was also light 1D1-labeling of the descending column of the fornix (fx) (**Fig. 2.2A**), which contains axons from the hippocampus. No other structures in the thalamus and hypothalamus were 1D1-positive.

In the midbrain, scattered neurons in the deep layers of the superior colliculus and red nucleus exhibited strong immunofluorescence for hAPP along with other scattered populations of neurons in the brainstem and spinal cord. **Fig. 2.3A** illustrates a section through the midbrain at the level of the superior colliculus and red nucleus. **Fig. 2.3B** illustrates 1D1-positive neurons in the red nucleus at high magnification, confirming intra-neuronal labeling.

In the brainstem, the most noteworthy feature was the presence of large numbers of clusters of 1D1-positive granules in the pons (**Fig. 2.3C&D).** Neurons in the pontine nuclei project to the cerebellum via the middle cerebellar peduncle where they terminate as mossy fibers on cerebellar granule neurons. The middle cerebellar peduncle is one of the many white matter tracts affected in humans with AD (Toniolo et al., 2020). Although there are many neuronal cell bodies within the pons (pontine nuclei), 1D1 fluorescence did not appear to be within cell bodies. Instead, the 1D1-positive granules had the appearance of the clusters of granules in the lateral septum and dendritic lamina of the subiculum. In considering the source of these 1D1-positive granules, it should be noted that CST axons from 1D1-positive neurons in layer V of the cortex pass through the pons en route to the spinal cord and some synapse on neurons in the pons to form the cortico-pontine tract. Thus, the likely explanation of the clusters of 1D1-positive granules is that these originate from axons and/or synaptic terminals from hAPP-expressing CSNs in the cortex.

Of note, some of the clusters of 1D1-positive granules were in a petal-like cluster. Such petal-like structures have previously been associated with degenerating neuronal cell bodies in murine models of AD. Because of the absence of 1D1-expressing neurons in the pons, the likely interpretation is that petal-like clusters of 1D1-positive granules also originate from axons or synapses from hAPP-expressing CSNs in the cortex.

In the cervical spinal cord, sparsely distributed 1D1-positive neuronal cell bodies were seen in the gray matter, including a few large motoneurons (MNs) in the ventral horn (**Fig. 2.3E**). 1D1-positive axons were evident in the ventral part of the dorsal column in the position of the

descending dorsal corticospinal tract (dCST), consistent with their origin from 1D1-positive CSNs in cortical layer V **(Fig. 2.3E)**.

3.2 Pattern of transgene expression in older 5xFAD$^{+/-}$/Rosa^{tdT} mice

It was of interest to determine how 1D1 labeling patterns would change as neurons begin to degenerate in older 5xFAD mice. For this, we immunostained brain sections from 7–14-month-old 5xFAD$^{+/-}$/Rosa^{tdT} mice (see Table 2.1). In what follows, we first consider the areas in which neurodegeneration has been previously reported in 5xFAD mice, layer V of the cortex and subiculum, and then other regions.

Notably, the labeling in older 5xFAD$^{+/-}$/Rosa^{tdT} had a different appearance from that observed at 2-3 months of age. In the primary motor cortex (M1) and primary somatosensory area (S1), some 1D1-positive neurons were still evident in layer V in older mice. Figure 4A-D illustrates examples from the motor cortex of a 7-month-old 5xFAD$^{+/-}$/Rosa^{tdT} mouse. In addition to 1D1 fluorescence that appeared to be within neuronal cell bodies (**Fig. 2.4A**), there was a dramatic increase in 1D1-labeled granules that did not appear to be in neuronal cell bodies (**Fig. 2.4B, see inset**). **Figure 2.4C&D** illustrate confocal images of labeling in neuronal cell bodies in cortical layer V (arrowheads, **Fig. 2.4C&D**), in single granules (arrow in **Fig. 2.4B)**, and in clusters of granules just below layer V (traced, **Fig. 2.4D**). The clusters of granules range up to nearly 100µm in diameter, which is larger than the size of even a large pyramidal cell body in layer V.

In coronal sections, large 1D1-positive clusters were particularly prominent in stratum oriens of the hippocampus and hilus of the dentate gyrus (**Fig. 2.4E,** arrowhead). These clusters are much larger than the size of the resident neurons in either area and in the case of CA1, are in the neuropil layer rather than the cell body layer. These findings are consistent with a recent study involving immunostaining using a different antibody against human and mouse APP (Anti-APP A4 Antibody, a.a. 66-81 of APP (NT), clone 22C11) reporting no intracellular APP in dentate granule cells at 12 weeks of age in 5xFAD, although extracellular plaques were present at that age (Mabrouk et al., 2023).

A key difference between 7-month-old vs. young mice were the evident clusters of 1D1-positive granules in several white matter tracts including the ventral hippocampal commissure (VHC) and fornix (**Fig. 2.4F, G, &H)**. The VHC and fornix contain axons from 1D1-expressing hippocampal and subicular neurons.

Examples of 1D1 IF in horizontal sections through the entorhinal cortex and hippocampus at 10 months of age revealed a similar set of age-related changes (**Fig 2.4I**). In the CA1 region of the hippocampus, 1D1-positive neuronal cell bodies were still evident but there were also 1D1-positive granules. Although, there was little to no hAPP fluorescence in the granule cell layer of the dentate gyrus of 2-3-month-old mice (**Fig. 2.1D and G),** there was moderate hAPP IF in the granule cell layer in 7-month-old mice (**Fig. 2.4I**). This may coincide with the reported increase in mouse and human RNA transcripts of APP as 5xFAD mice age (Forner et al., 2021).

In subcortical areas of older mice, 1D1-positive granules were present in the red nucleus, midbrain reticular nucleus and superior colliculus, often in rosette-shaped clusters (**Fig. 2.4J&K).** As above, these granules did not appear to be within neuronal bodies as was the case at the 2–3-month time point. Of note, in the 7-month-old mice, there appeared to be few 1D1-positive neuronal cell bodies in the red nucleus (more on this below).

In considering the nature of the 1D1-positive granules, several facts are relevant. 1) hAPP expression is driven by the neuron-specific elements of the Thy-1 promoter and is thus exclusively expressed by neurons. However, the granules are not within neuronal cell bodies that express hAPP. 2) Some clusters are larger than even the very large neurons in layer V (**Fig. 2.4D**). 3) In the older mice, there are few 1D1-positive cell bodies in layer V consistent with neuronal death whereas there are large numbers of clusters of 1D1-positive granules. Together, these facts suggest 2 possibilities: 1) 1D1-positive granules contain fragments of axons and/or dendrites from 1D1-expressing neurons that have died; or, 2) the granules contain hAPP or at least fragments thereof that were released by hAPP expressing neurons.

The pattern of 1D1 IF in the entorhinal cortex of older mice was also distinctly different than in young mice. Although there were still almost no 1D1-positive neuronal cell bodies in superficial layers (I-IV), there was a dramatic increase in 1D1-positive granules in deep layers adjacent to the white matter, especially in the lateral entorhinal cortex (**Fig. 2.4I**). As above, these granules did not appear to be within neuronal cell bodies (arrowhead in layers V/VI, **Fig. 2.2C**); 2) The deeper layers are the site of termination of axons from the hippocampus and subiculum. The superficial layers also had a few scattered 1D1-positive clumps (arrowhead in layers III/IV, **Fig.**

2.4I). These results again imply accumulation of hAPP-positive granules in areas containing axons and synapses from hAPP-expressing neurons.

Immunostaining of a mouse sacrificed at 12 months of age revealed that there were few 1D1-positive neuronal cell bodies in layer V of the sensorimotor cortex (**Fig. 2.5A-C**). IF was done by using a biotinylated secondary antibody that was visualized by using the VECTASTAIN® ABC kit followed by tyramide signal amplification with Cy3 (see Methods) in contrast to the previous IF stains that were done by tyramide signal amplification with FITC. This change was in order to allow co-imaging (below). The main change in comparison to earlier ages was that there were very few 1D1-positive neurons in layer V, and instead, there were large numbers of clusters of 1D1-positive granules (**Fig. 2.5C**). At this age, the clusters had the physical appearance of Aß plaques and were confirmed to be such by co-staining with other markers. In a more caudal section containing the rostral hippocampus (**Fig. 2.5B**) the pattern of 1D1 staining in the hippocampus was similar to that at 7-10 months. However, a noteworthy change was the appearance of 1D1-positive granules in the thalamus where there are no hAPP-expressing neurons at any age. Of note, thalamo-cortical projections arise from cortical pyramidal neurons; thus, 1D1-positive clusters in the thalamus may reflect hAPP deposition by these thalamocortical axons.

1D1-positive granules presumably contain at least the N-terminus of hAPP which contains the epitope recognized by 1D1. To assess whether particles contained sequences from other parts of the total hAPP protein, we co-stained sections for 1D1 and the 6E10 antibody, the epitope for which maps to amino acids 3-8 of Aβ. **Figure 2.5D-E** illustrates immunostaining for 6E10 in the

same sections shown in A-C. **Fig. 2.5F** illustrates a merged 10X image of 1D1 and 6E10 (from the area of the section illustrated in **Fig. 2.5C**). As is evident, there is extensive co-labeling although some particles do stain for only one or the other antibody. To better define the actual association between 1D1 and 6E10 IF, one large cluster in the cortex was imaged using confocal microscopy (**Fig. 2.5G** and in rotation, **Fig. 2.5H**). IF for 1D1 (shown in red) was present in small, discrete granules that were scattered throughout the large 6E10 positive structure. These results indicate that both N and C-terminal portions of hAPP are present in plaques. Of note, although Aβ plaque density also increases with age in the cortex of 5xFAD mice (Oblak et al., 2021), it is important to emphasize that the 1D1 antibody does not recognize human Aß. The epitope for 1D1 is in the N-terminus of APP (Hofling et al., 2016), and 1D1 does not recognize human Aß expressed in transgenic mice (Hofling et al., 2016). Thus, at least an N-terminal fragment of hAPP is present in granules and co-immunofluorescence for 1D1 and the 6E10 antibody indicates that the 1D1 epitope is present in some of the same granules as the epitope for 6E10. It remains to be established whether co-labeling reflects the presence of C and N-terminal peptide fragments or whether the entire intact hAPP protein is present.

A final point is that 1D1-and 6E10-positive clusters continue to be very prominent in the pons even in the oldest mice. **Fig. 2.5I** illustrates a section through the pons in a 14-month-old $5xFAD^{+/-}/Rosa^{tdT}$ mouse co-stained for 1D1 (red) and 6E10 (green). At the time of euthanasia, this mouse was exhibiting significant deficits and appeared to be near end-of-life. These results continue to imply that either the entire hAPP protein or peptide fragments containing C and N-terminal portions of hAPP are deposited extra-cellularly in regions containing axons and synapses from hAPP expressing cortico-spinal neurons.

Taken together, our results indicate that IF for 1D1 is mostly within neuronal cell bodies in young mice although clusters of 1D1-positive granules are present in a few areas. 1D1-positive clusters of granules then increase in abundance in three general sites as mice age: 1) neuropil regions in areas that contain neurons that express hAPP at high levels; 2) white matter tracts that contain axons from neurons that express hAPP at relatively high levels; 3) areas that receive synaptic connections from neurons that express hAPP at high levels – the pons, septum, deep layer of the entorhinal cortex, and eventually in the thalamus. Given the fact that neurons in these areas, especially the pons, do not appear to express hAPP, the most plausible explanation is that hAPP in the pons arises from axons and/or synapses of the CST. Although the granules in the pons could be fragments of CST axons that have degenerated, this seems less likely in the young mice in which axon degeneration has presumably not begun. Instead, at least some of the 1D1-positive granules may be extra-neuronal aggregates of hAPP protein or fragments thereof that were deposited by hAPP expressing axons.

3.3 Tracking neurodegeneration of layer V neurons labeled via retrograde transduction with AAV-rg/Cre.

We created the new 5xFAD$^{+/-}$/Rosa^{tdT} transgenic line to track age-dependent loss of large pyramidal neurons in cortical layer V previously reported in 5xFAD mice (Oakley et al., 2006). These previous reports of neurodegeneration were based on routine neurohistological stains (Nissl stains) that are not specific to neuron type. To accurately track degeneration of a particular neuronal type over time requires that the neurons be selectively labeled, ideally with a reporter that is permanent. For this, we used a paradigm that we previously deployed to transduce

neurons in layer V that give rise to the corticospinal tract (corticospinal neurons or CSNs) (Metcalfe et al., 2022).

The paradigm takes advantage of a variant of AAV that is retrogradely transported from axons to cell bodies, (AAV-retrograde, or AAV-rg). Injections of AAV-rg expressing Cre (AAV-rg/Cre) into cervical spinal cord of $Rosa^{tdT}$ reporter mice result in robust retrograde transduction and permanent labeling of CSNs in the primary motor cortex (M1), secondary motor cortex (M2) and in a region of the secondary somatosensory cortex (S2) (Steward et al., 2021). Other neuron types that project to the spinal cord are also retrogradely transduced including neurons in the red nucleus and brainstem. The injection site in the spinal cord and distribution of labeled neurons in the cortex can be conveniently visualized in intact brains and spinal cords when viewed via epi-fluorescence imaging with excitation light of approximately 550 nm (**Fig. 2.6A**). In this mouse, epi-fluorescence imaging revealed oval areas of tdT fluorescence in both hemispheres of the brain with higher levels of fluorescence on the right because the unilateral spinal cord injection was on the left side (arrows). These oval areas reflect tdT expression by hundreds-thousands of CSNs. Labeling in the cortex ipsilateral to the injection is likely due to spread of AAV-rg/Cre across the midline at the spinal cord injection site. In most other mice, labeling was mostly contralateral to the injection. **Fig. 2.6B&C** illustrate coronal sections from a different mouse immunostained for RFP in which there were large numbers of labeled CSNs on the right (contralateral to injection site), and fewer on the left. Most mice exhibited this largely contralateral pattern of labeling. TdT labeling extends throughout the cell bodies, dendritic arbors and axons of the CSNs, which can be visualized with native tdT fluorescence without immunostaining or can be amplified by immunostaining using antibodies for Red Fluorescent

Protein (RFP, see **Fig. 2.6C**). The graph in **Fig. 2.6D** illustrates counts of tdT-labeled CSNs across a set of coronal sections taken at intervals of 240µm in one 5xFAD$^{+/-}$/Rosa^{tdT} mouse and one Rosa^{tdT} control. CSNs are labeled throughout the rostro-caudal axis of the sensorimotor cortex, with peak numbers of labeled neurons in the main sensorimotor cortex rostral to bregma.

TdT labeling is specific to neurons and is permanent: It is important to note that although injections of AAV2-rg/Cre lead to non-selective transduction of both neurons and glia, this would only occur at the injection site in the spinal cord. Neurons in the brain are transduced exclusively as a result of retrograde transport of AAV-rg along axons that project to the spinal cord, so the only cells in the brain that are transduced are neurons that project to the spinal cord. In both the current study and our previous studies, we have not observed tdT-expressing cells with glial morphology in the brains of control Rosa^{tdT} mice despite transduction of tens of thousands of neurons. This is true regardless of how long the mice survive after receiving AAV-rg/Cre.

To track neurodegeneration across age, it is important that neurons are permanently labeled with tdT. In both control Rosa^{tdT} and 5xFAD$^{+/-}$/Rosa^{tdT} mice, expression of Cre recombinase removes the stop cassette resulting in robust tdT expression. In previous studies, we have observed robust tdT labeling in CSNs up to 1 year after intra-spinal cord injections of AAV-rg/Cre in Rosa^{tdT} mice. For the present study, 5xFAD$^{+/-}$/Rosa^{tdT} and control Rosa^{tdT} mice were injected with AAV-rg/Cre between 2-3 months of age and brains were collected 2-3 weeks post-injection, allowing time for tdT to be expressed in transduced neurons. **Fig. 2.7A** shows a coronal section of a 5xFAD$^{+/-}$/Rosa^{tdT} mouse injected at 2 months of age; qualitatively, CSNs appeared

morphologically normal at 2-3 months (**Fig. 2.7A**). The 2–3-month timepoint was chosen to quantify the baseline number of CSNs in young 5xFAD$^{+/-}$/Rosa^{tdT} mice prior to the onset of age-related neurodegeneration. Figure 7B illustrates a Rosa^{tdT} injected at 2 months of age and perfused at 15 months of age, demonstrating that tdT labeling persists for at least 10 months post-injection and is likely permanent.

3.4 Characteristics of age dependent degeneration of layer V CSNs in 5xFAD$^{+/-}$/Rosa^{tdT} mice.

Complete and permanent tdT labeling of cell bodies, axons and dendrites following AAV-rg/Cre injections in 2-month-old 5xFAD$^{+/-}$/Rosa^{tdT} mice allowed us to track signs of degeneration that became apparent as the mice aged. We leveraged this innovative AAV-mediated delivery tool to further define characteristics of neurodegeneration of layer V neurons and identify degenerative changes in other neuron types. **Fig. 2.7C & D** illustrate examples of patterns of tdT labeling at 8 months and 12 months. In 8-month-old 5xFAD$^{+/-}$/Rosa^{tdT} mice, tdT labeled CSNs exhibited clear dendritic and axonal dystrophy (**Fig. 2.7C**). In layers III and above, tdT-positive dendrites from layer V neurons appeared irregular in form. Malformations of neuronal processes due to degeneration are termed neuritic dystrophies and are accompanied, or followed by, a loss of dendritic spines. In layers VI and below, which contains basal dendrites and descending axons from layer V neurons, large bulbous tdT-positive varicosities were evident along tdT-positive axons in the sub-cortical white matter (**Fig. 2.7C & D, F**). All these signs of neurodegeneration were more prominent at 12 months of age, including increases in axonal varicosities along CSN axons in layer VI (**Fig. 2.7D,** arrowhead) and large varicosities of similar appearance that were not directly along a labeled axon in layer VI (**Fig. 2.7F**, circled). These manifestations of

neurodegeneration were accompanied by decreases in the number of tdT-positive neuronal cell bodies in layer V (see below for quantitative analyses).

A conspicuous feature of labeling in older 5xFAD$^{+/-}$/Rosa^{tdT} mice was the presence of rosette-shaped clusters of tdT-positive granules; these resembled the clusters of 1D1-positive granules described above (**Fig. 2.7C, D, E**). In the motor cortex, the tdT granules were primarily in cortical layer VI below the tdT-positive CSNs with minimal presence in layer V. Notably, the tdT-labeled granules were found only in areas of the cortex where tdT labeled CSNs were present. The primary location of the granules, along with their increase in quantity coinciding with a loss of tdT-labeled neurons, suggest that the granules derive from axonal and/or dendritic fragments of tdT labeled neurons that are degenerating. Hence, we term the tdT-positive granules "degeneration debris" from degenerating CSNs.

Extracellular accumulations of tdT-positive granules were especially prominent in the pons where axons from tdT labeled CSNs traverse (**Fig. 2.7G**). The tdT-positive particles were similar in appearance to the 1D1-positive granules in the pons illustrated in Figure 5 and included rosette-shaped clusters (**Fig. 2.7G&I**). We also observed large tdT-positive axonal varicosities in the tegmentum dorsal to the pons where tdT-labeled descending CST axons were present (**Fig. 2.7G&H**).

It is important to emphasize that tdT IF did not appear to be within neuronal bodies in the pons at any age. To confirm this conclusion, sections through the pons were co-stained for RFP to reveal tdT and NeuN to reveal neuronal cell bodies. TdT-labeled axons were evident in the pons of a

12-month-old 5xFAD$^{+/-}$/Rosa^{tdT} mouse (**Fig. 2.7J**), which were presumably CST axons from layer V neurons, along with tdT-positive granules. However, no tdT-labeled elements were co-localized with NeuN-positive neuronal cell bodies (**Fig. 2.7J-L**). The presence of both dT-positive and 1D1-positive granules in the pons further supports the interpretation that these originate from axons from 1D1-expressing layer V CSNs.

We were curious whether a different fluorescent protein expressed by CSNs would also accumulate in extra-neuronal granules as the neurons degenerate. For this, CSNs were labeled by injecting AAV-rg/GFP into the cervical spinal cord of 5-month-old 5xFAD$^{+/-}$/Rosa^{tdT} and Rosa^{tdT} mice and mice were allowed to survive until 8 months of age. Immunostaining for GFP revealed GFP-positive layer V pyramidal neurons along with spherical particles that appeared to be dendritic varicosities in layer IV and above and axonal varicosities below layer V and in the subcortical white matter (**Fig. 2.7M**). However, there were no clusters of GFP granules resembling the rosette-like accumulations of tdT-positive granules below layer V (**Fig. 2.7B, C, E**).

Quantification of neurodegeneration: Having established that labeling of CSNs is permanent and selective, and signs of neurodegeneration were present, we quantified these features of neurodegeneration as mice age. Using sections from young 5xFAD$^{+/-}$/Rosa^{tdT} and Rosa^{tdT} mice (2-4 months of age), middle-aged (6-10 months of age) and older mice (12-14 months of age), tdT-labeled CSNs were quantified in a 1-in-8 series of sections spaced 240µm apart encompassing the rostro-caudal axis of the sensorimotor cortex. For this, we excluded cases in which injections were suboptimal (for exclusion criteria, see Methods and Table 2.1). Counts of

the total number of tdT-labeled neurons in the young 5xFAD$^{+/-}$/Rosa^{tdT} mice **(Fig. 2.8A)** and control Rosa^{tdT} mice reached up to 1500 (**Fig. 2.8B**). This information provides the baseline for age-dependent CSN degeneration.

Counts of tdT-positive CSNs revealed a dramatic decrease in 5xFAD$^{+/-}$/Rosa^{tdT} mice beginning at 6-10 months and progressing at 11+ months compared to 2-4 months. (**Fig. 2.8B**). In contrast, in control Rosa^{tdT} mice, there was no decrease in the number of tdT-labeled layer V CSNs (**Fig. 2.8B**). It should be noted that if cases in which injections were suboptimal were included, this would shift average values down because some 5xFAD$^{+/-}$/Rosa^{tdT} mice had no labeled neurons at all. These data confirm and extend previous reports of age-dependent degeneration of layer V neurons in 5xFAD$^{+/-}$/Rosa^{tdT} mice, document that at least some of them are CSNs, and reveal that degeneration can be tracked by tdT labeling.

In parallel with the decline in tdT-labeled layer V CSNs, tdT labeled granules in the sensorimotor cortex became more numerous as the mice aged **(Fig. 2.8C)**. We quantified the granules in cortical layer V and VI of 5xFAD$^{+/-}$/Rosa^{tdT} and Rosa^{tdT} mice at 2-4, 6-10 and 12-14 months of age using the analyze particles plug-in on ImageJ. The inclusion criteria accounted for the various sizes and shapes ranging from large clumps to smaller granules. Numbers of tdT granules were low at 2-4 months of age and increased dramatically with age in 5xFAD$^{+/-}$/Rosa^{tdT} mice as CSN counts decreased **(Fig. 2.8D)**. There were no tdT-labeled granules in Rosa^{tdT} mice at any age **(Fig. 2.8D)**.

Age-related degeneration of neurons in the red nucleus: We were also curious to assess whether neurons in the red nucleus, some of which express hAPP (see **Fig. 2.3A&B; Fig. 2.4J&K** above) would show signs of degeneration. Large numbers of tdT labeled neurons were seen in the red nucleus in young mice **(Fig. 2.8E)** but far fewer were seen in 12–14-month-old 5xFAD$^{+/-}$/Rosa^{tdT} mice (**Fig. 2.8F** illustrates a 12-month-old mouse). Quantification of tdT-positive neurons in the red nucleus of 2-month-old and 12-month-old 5xFAD$^{+/-}$/Rosa^{tdT} mice confirmed a loss of tdT-positive neurons (**Fig. 2.8G**) accompanied by the appearance of tdT-positive debris (circled, **Fig. 2.8F**). To assess whether neuron loss in the red nucleus was evident in routine histological stains, we stained sections through the red nucleus from the above cases with Cresyl violet (**Fig. 2.8H**). In young mice, the red nucleus was easily distinguishable as a collection of large, darkly stained neurons (magnocellular division) and a collection of somewhat smaller neurons in the ventro-medial region of the nucleus (parvocellular division, see **Fig. 2.8H**). In old 5xFAD mice, there were very few large, healthy-appearing neurons making it difficult to distinguish the actual boundaries of the nucleus (**Fig. 2.8I**). Instead of the large neurons characteristic of young mice, the area of the nucleus contained large numbers of small cells (possibly glia). Counts of the number of large cells with neuronal morphology in the nucleus in young vs. old mice confirmed extensive loss of large neurons (**Fig. 2.8J**). It should be emphasized that these counts should be considered provisional; validation with a neuron-specific marker is needed to confirm these results. Nevertheless, these results, taken together with the loss of tdT in 5xFAD mice, strongly suggest degeneration of red nucleus neurons, which to our knowledge, has not previously been reported.

Co-localization of tdT and hAPP in granules: The overall distribution of tdT-labeled debris resembled the distribution of extracellular accumulations of 1D1-positive granules suggesting possible co-localization. To investigate whether the tdT co-labeled with hAPP positive granules, we performed Co-IF for hAPP, using the FluoReporter™ FITC, and Red Fluorescent Protein to label tdT. The IHC was done on tissue from young 5xFAD$^{+/-}$/Rosa^{tdT} and Rosa^{tdT} mice and *older* (12 months of age) when both tdT- and 1D1-stained clusters of granules were prominent. Co-IF revealed that many tdT-positive granules were co-labeled with hAPP tdT (**Fig. 2.9A-C**). Quantifications of three 5xFAD$^{+/-}$/Rosa^{tdT} mice revealed that, on average, 85% (SD = 0.095) of the tdT granules were co-localized with hAPP. This co-localization supports the conclusion that both the hAPP and tdT-positive granules originate from tdT-labeled layer V CSNs expressing hAPP.

Co-localization of tdT granules with Aß and other markers of neurodegeneration: Due to the co-localization of hAPP and tdT in granules, we explored whether tdT granules were also associated with β-amyloid (Aβ) plaques. For this, sections from a 12-month-old 5xFAD mouse were co-immunostained for RFP to identify tdT and an antibody that reacts to the N-terminal of Aβ (Amyloid Beta (N3pE) (8E1) Aβ Anti-Human Mouse IgG MoAb) (**Fig. 2.9D-F**). As illustrated in **Fig. 2.9D-F**, many tdT-positive granules were co-localized with accumulations of Aβ. Quantification of three 5xFAD$^{+/-}$/Rosa^{tdT} mice revealed an average of 88.33% (SD = 0.083) of tdT granules were co-localized with Aβ. Other sections were immunostained with thioflavin-S which marks the core of many Aβ aggregates. TdT was visualized by native fluorescence (no IF) (**Fig. 2.9G-I**). An average of 79% (SD = 0.065) of the tdT-positive granules were within 6 micrometers away from the thioflavin-S particles, often within the Aß-stained area surrounding

the thioflavin-S particle. Taken together, the co-localization studies indicate that at least some of the granules contain hAPP, tdT and Aß, suggesting that all three originate from degenerating CSNs. These results also suggest that there must be some unique property of tdT protein that leads to its persistence after neurons degenerate and association with hAPP and Aß.

In dendritic or axonal swellings, lysosomes have been reported to form clusters (Sharoar et al., 2021). To investigate whether the tdT accumulations are within axonal swellings and associating with lysosomal clusters, we immunostained for LAMP-1 and Hoechst (**Fig. 2.9J-O**). Some of the smaller tdT-positive granules appeared to be associated with Hoechst and LAMP-1 (**Fig. 2.9M, N**), whereas the larger tdT clusters did not appear to be associated with either (**Fig. 2.9M, O**). The minimal colocalization of tdT labeled granules with LAMP-1 can also be seen in a higher magnification confocal image (**Fig. 2.9Q**). Quantifications of three 5xFAD$^{+/-}$/Rosa^{tdT} mice revealed an average of 78% (SD = 0.157) of the tdT granules were co-localized with LAMP-1-stained areas. These data suggest that some of the accumulations are associated with the hAPP transgene outside of cells and are not within the large axonal varicosities.

As with 1D1-positive clusters, the large size of the tdT-positive clusters of granules (nearly 100 µm in diameter) suggests that they are not inside a cell body. To assess this directly, we immunostained sections with Hoechst to label nuclei. As illustrated in **Figure 2.9L-O**, the tdT accumulations did not appear to surround a Hoechst-positive nucleus, suggesting that most of the clusters are not inside a cell body. A high magnification confocal image, in a 5xFAD$^{+/-}$/Rosa^{tdT} mouse at 7 months old, shows the 1D1-positive clusters surrounded by tdT positive granules and, separately (Arrowheads, **Fig. 2.9P**), shows 1D1 and RFP co-labeled neurons (**Fig. 2.9P**).

It is not surprising that the mutant hAPP (at least a fragment containing the N-terminus with the 1D1 epitope) is found in the same granules as Aß because both are likely to derive in part from CSNs that express hAPP. However, tdT is an exogenous cytoplasmic protein, and thus how it gets from the CSNs that express the protein into the Aß/hAPP granules is not apparent. There is no compelling reason to predict that tdT, a soluble cytoplasmic protein, would bind to either Aß or hAPP, although it could be assembled into aggregates inside CSNs prior to being deposited extracellularly. Further studies will be required to explore these possibilities directly.

Discussion

This study provides several novel insights about the cell biology of age-related neurodegeneration in 5xFAD mice. To emphasize at the outset, our findings and interpretations apply to 5xFAD mice and may not reflect degenerative processes in humans or even other murine AD models. With this caveat, key findings are: 1) Location and expression of hAPP transgenes differ between young and old 5xFAD$^{+/-}$/Rosa^{tdT} mice; 2) As 5xFAD$^{+/-}$/Rosa^{tdT} mice age, there is a dramatic increase in hAPP-positive granules that are not within neuronal cell bodies; 3) hAPP-positive granules are especially prominent in areas containing dendrites, axons and synapses from neurons expressing the hAPP transgenes; 4) Selective retrograde labeling of CSNs reveals extensive degeneration with age in 5xFAD$^{+/-}$/Rosa^{tdT} mice; 5) As tdT-positive CSNs degenerate, tdT-labeled debris appears, providing another quantitative measure to track neurodegeneration of tdT-positive CSNs; 6) There is extensive age-related degeneration of neurons in the red nucleus of 5xFAD$^{+/-}$/Rosa^{tdT} mice, which has not been previously reported to

our knowledge; 7) As mice age, tdT-positive degeneration debris accumulates in the same areas with extracellular granules containing hAPP; 8) Co-immunostaining reveals substantial co-localization of hAPP and tdT in granules that co-localize with Aß-containing plaques. Taken together, our findings establish that some proteins derived from hAPP-expressing neurons accumulate in extracellular granules in areas containing axons and synaptic terminals from hAPP-expressing neurons. The clusters of particles often have a rosette-like or petal shaped structure even in areas that do not contain neuronal cell bodies that express hAPP. In what follows, we discuss implications and caveats of our findings.

IHC for hAPP reveals previously un-described selectivity in transgene expression.

The Thy1-promoter drives transgene expression in 5xFAD mice, and its pattern of expression was largely consistent with previously described patterns of Thy1-YFP expression. However, some aspects of selectivity of expression should be noted: 1) Transgene expression was selective to particular neuronal types in the cortex, but varied across cortical areas; 2) Some of the neuronal types that express the transgene at high levels have been reported to exhibit age-related neurodegeneration (neurons in cortical layer V and subiculum) but we did not observe evidence of degeneration of other neurons that express the transgene at moderately high levels (neurons in the BLA); 3) There was a notable absence of transgene expression in neurons in the entorhinal cortex that project to the dentate gyrus and hippocampus; 4) 1D1-positive particles that did not appear to be within neuronal cell bodies or cell bodies of any cell were present in some brain regions (more below).

IHC for hAPP reveals previously un-described features of neurodegeneration in 5xFAD mice.

The spatial and age-dependent differences in hAPP transgene expression observed in 5xFAD$^{+/-}$/Rosa^{tdT} mice suggests previously un-described, or at least under-described, aspects of neurodegeneration. In young 5xFAD$^{+/-}$/Rosa^{tdT} mice, hAPP labeling was largely within neuronal cell bodies except in the lateral septum and pons. As mice aged, hAPP labeling was increasingly in granules that were not apparently within neuronal cell bodies. These granules were especially prominent in the cortex and subiculum where neurons degenerate. Notably, the clusters of 1D1 granules in the motor cortex were most prominent in cortical layer VI, below the neurons in layer V that express the transgene at high levels. The 1D1-positive granules also became more abundant in fornix and lateral septum as the 5xFAD$^{+/-}$/Rosa^{tdT} mice aged. The fornix contains axons from the subiculum, where hAPP is expressed at high levels. The lateral septum receives projections from the hippocampus and the basolateral amygdala, where there is a high level of 1D1 expression in neuronal cell bodies. It is possible that as 1D1 positive neurons are degenerating, they release hAPP. The presence of APP was previously reported in swollen degenerating axons that were surrounding amyloid plaques and neuritic plaques (Dickson, 1997; DeTure and Dickson, 2019; Mabrouk et al., 2023).

Especially dramatic accumulations of hAPP granules were observed in the pons. Of note, CST axons from cortical layer V neurons pass through the pons *en route* to the spinal cord and terminate on neurons in the pontine nuclei. However, we did not observe hAPP-labeled neuronal cell bodies in the pons. These findings strongly support the conclusion that extracellular particles

of hAPP are deposited by axons and/or synaptic terminals from hAPP-expressing neurons located in the cortex, not by degenerating hAPP-expressing neuronal cell bodies in the pons.

Some extracellular clusters of hAPP resemble what have previously been termed “PANTHOS”, which were interpreted as the remains of degenerated neuronal cell bodies. The proposed process is that autophagic vacuoles within the neuronal cell body generate a ß-amyloid ‘core’ (Lee et al., 2022). If this is the case, then PANTHOS structures should appear only where neuronal cell bodies have degenerated. However, our results reveal rosette-like clusters of 1D1-positive particles (PANTHOS-like) in axon tracts and areas of termination of axons from 1D1-positive neurons in structures that do not contain 1D1-expressing neuronal cell bodies. These results suggest that PANTHOS structures can originate from degenerating axons and/or synaptic terminals. Our results are consistent with another recent study showing that extracellular Aß develops in the dendritic lamina of the dentate gyrus even though the granule cells express the 5xFAD transgene at low levels. These results were interpreted as indicating that extracellular Aß in the dendritic zone of the dentate gyrus originates from axons and terminals that innervate granule cells (Mabrouk et al., 2023). As discussed further below, some clusters of tdT granules from CSNs also had a PANTHOS-like appearance.

The change in hAPP localization (from within neuronal cell bodies to clusters of granules that are not within cell bodies) coincides with degeneration of certain neuron types in cortical layer V and the subiculum. Our results characterizing age-related appearance of clusters of hAPP granules may be useful for identifying unreported areas of neurodegeneration in 5xFAD mice.

Permanent labeling of corticospinal, and other neurons that project to the spinal cord, enabled quantification of neurodegeneration of defined neuron types in 5xFAD mice.

We developed the 5xFAD$^{+/-}$/Rosa^{tdT} line to quantify age-dependent neurodegeneration of CSNs and the approach achieved that goal. Counts of tdT-expressing CSNs after retrograde transduction with AAV-rg/Cre revealed loss of 80.92% of CSNs. Our results also revealed previously undescribed neurodegeneration in the red nucleus, which gives rise to the rubrospinal tract, involved in motor control (Vadhan et al., 2024). The neurons in the red nucleus also receive inputs from the motor cortex and cerebellum. Thus, age-related degeneration of these neurons could contribute to the motor symptoms that develop in 5xFAD mice. Neurodegeneration may be occurring in other areas of the brain where clusters of hAPP granules were observed, but our model was created to track neurodegeneration in neurons with projections to the spinal cord. Of note, Cre-dependent induction of tdT provided by 5xFAD$^{+/-}$/Rosa^{tdT} mice could be used for selective labeling of other neuron types in these mice to track neurodegeneration.

Permanent labeling of corticospinal and other neurons that project to the spinal cord reveals other aspects of neurodegeneration.

The 5xFAD$^{+/-}$/Rosa^{tdT} model also revealed previously undescribed aggregation of proteins expressed by neurons undergoing degeneration in 5xFAD mice. It is well-established that Aß accumulates in extracellular Aß plaques in 5xFAD mice, as well as in human AD. However, we were surprised that tdTomato, expressed by degenerating neurons, also accumulates in

extracellular granules and co-localized with hAPP. It is exceedingly unlikely that the tdT granules could have come from any source other than the tdT-expressing neurons. We were further surprised that tdT in granules continued to generate native fluorescence weeks, and perhaps months, after the neurons that produced it had degenerated. It remains unclear how tdT survives as a functional fluorescent protein for this duration of time. Additionally, the presence of petal-like accumulations of extracellular tdT in white matter tracts containing tdT labeled CST axons supports the speculation that petal-like structures are the remains of degenerated axonal swellings. This appearance of axonal varicosities in tdT labeled layer V CSNs, in conjunction with high 1D1 labeling in layer V, provides compelling evidence that axonal varicosities are on axons from 1D1-expressing CSNs.

Because tdT is a soluble protein, it is also unclear how it remains in the same location as hAPP granules. This suggests there must be a strong interaction between the tdT protein and hAPP. This could be part of the intracellular pathophysiology due to expression of the 5xFAD transgenes. For example, the soluble protein encoded by the transgene may cross-link with other proteins. It may be possible to use the association between extracellular tdT and hAPP as a biochemical tool to further characterize the components of the aggregates.

In contrast to tdT, we did not observe granules outside of neuronal cell bodies when a different fluorescent protein (GFP) was expressed by CSNs in the $5xFAD^{+/-}/Rosa^{tdT}$ mice that were injected with AAV-rg/GFP. Instead, GFP appeared to be within cell bodies, dendrites and axons of GFP labeled neurons. Of note, in our model, tdT is expressed as a transgene whereas GFP is expressed via a viral vector which could result in differences in levels of expression.

Limitations of 5xFAD as a model of human AD

A limitation of the 5xFAD mouse model is that it is not representative of how AD manifests in humans. First, the transgenes are driven by the Thy-1 promoter, so expression is limited to certain neuron types. In contrast, in humans carrying FAD mutant alleles, most or all neurons express the gene although levels of expression probably vary by neuron type. Second, 5xFAD mice carry a total of 5 different FAD mutant alleles in two different genes, which is certainly not the case in any human. FAD makes up a small amount of the cases of AD, so the 5xFAD mouse is not representative of most human cases. Third, human AD is characterized by a slow progression of pathology that includes extracellular amyloid-β plaques and intracellular neurofibrillary tau tangles (Knopman et al., 2021). The 5xFAD model, an amyloidosis model, exhibits a rapid and abundant amyloid-β burden. Phosphorylated tau aggregates have been reported in 5xFAD mice (Shin et al., 2021), but this is somewhat surprising because the 5xFAD mutations don't involve tau. Finally, 5xFAD mice display prominent age-dependent motor deficits, perhaps because the transgene is expressed in CSNs and neurons in the red nucleus. Motor symptoms are not a prominent feature of AD in humans (Masse et al., 2021).

Finally, it is important to note that our transgenic line of $5xFAD^{+/-}/Rosa^{tdT}$ was generated by crossing different strains and thus has a different genetic background than the commercially available 5xFAD-B6SJL background mice. The $5xFAD^{+/-}/Rosa^{tdT}$ mice and $Rosa^{tdT}$ mice have been propagated in our facility over multiple generations, which results in genetic background drift that may introduce variability in disease pathology and behavior. For all these reasons, our

findings described herein define aspects of neurodegeneration that may be unique to 5xFAD mice and perhaps even specifically 5xFAD$^{+/-}$/Rosa^{tdT} mice. Nevertheless, our results reveal the existence of fundamental cell biological aspects of neurodegeneration that operate when different neuronal populations express these hAPP mutant proteins.

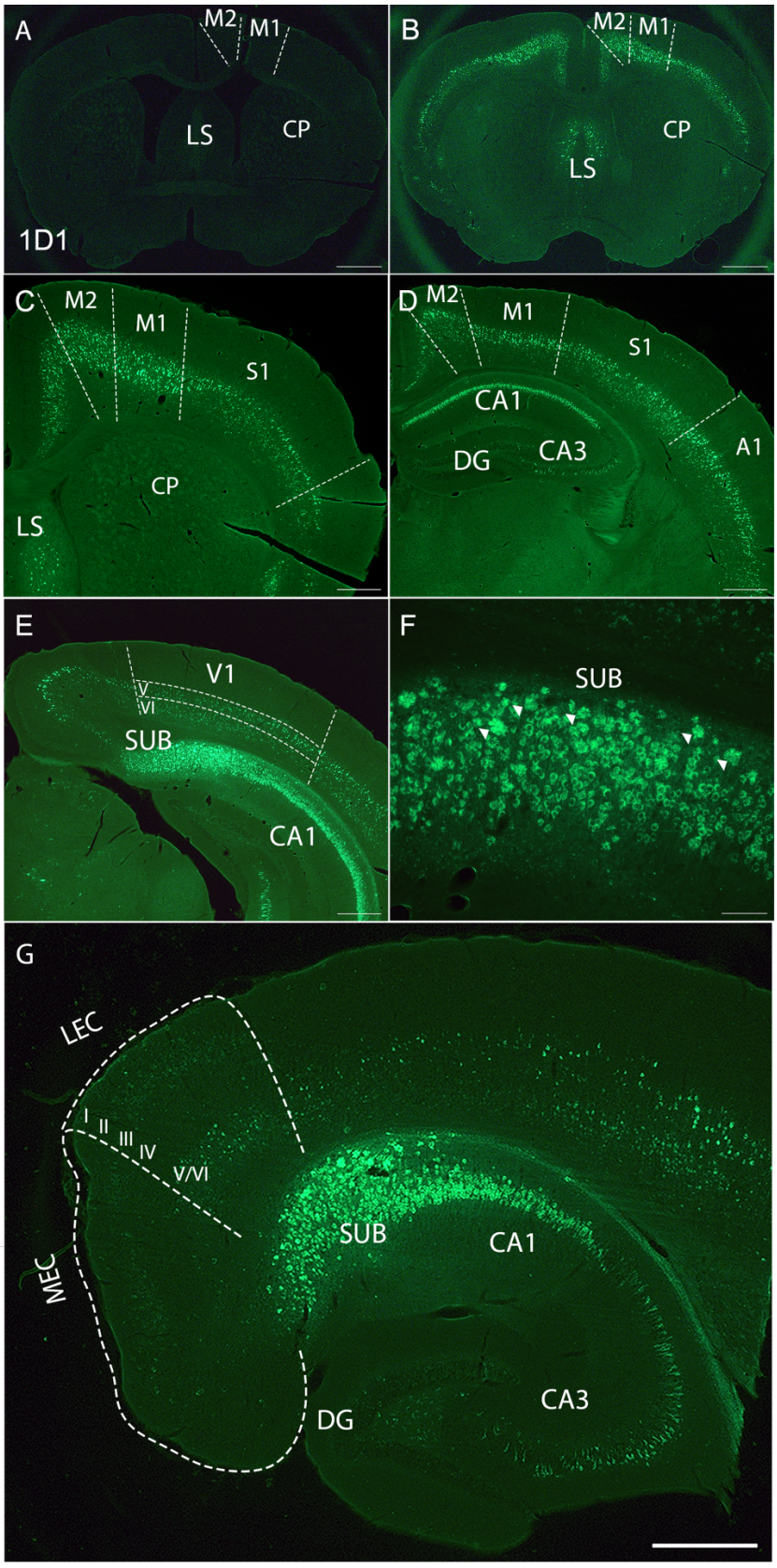

A
M2
M1
LS
CP
1D1
B
M2
M1
CP
LS
C
M2
M1
S1
CP
LS
D
M2
M1
S1
CA1
DG
CA3
A1
E
V1
V
VI
SUB
CA1
F
SUB
G
LEC
I
II
III
IV
V/VI
MEC
SUB
CA1
DG
CA3

Figure 2.1 Immunofluorescence (IF) for hAPP in the cortex, hippocampus and entorhinal cortex of young 5xFAD$^{+/-}$/Rosa^{tdT} and Rosa^{tdT} mice.

(A) 2-month-old female Rosa^{tdT} mouse stained with 1D1 antibody against hAPP. Absence of labeling indicates specificity for hAPP, indicating no cross-reactivity with mouse APP. M1 and M2 indicate primary and secondary motor cortex; LS = lateral septum; CP = caudate putamen. **(B-F)** Examples of immunofluorescence for hAPP in a 2-month-old male 5xFAD$^{+/-}$/Rosa^{tdT} mouse. **(B&C)** Sections at the level of the primary motor cortex approximately 1mm anterior to bregma. S1 = primary sensory cortex. **(D)** Pattern of immunofluorescence in cortex and hippocampus approximately 2mm caudal to bregma. Note lower levels of labeling in the CA3 vs. CA1 region of the hippocampus and absence of labeling in the dentate gyrus (DG). A1 = primary auditory cortex. **(E)** Pattern of immunofluorescence in caudal neocortex, V/VI = layers V/VI of the visual cortex (V1), CA1 and subiculum (SUB), approximately 3.5 mm caudal to bregma. **(F)** Higher magnification view of subiculum; arrowheads indicate clusters of 1D1-positive granules. **(G)** Pattern of labeling in a male 3-month-old 5xFAD$^{+/-}$/Rosa^{tdT}. Note high levels of neuronal labeling in the subiculum (SUB) and CA1 region of the hippocampus and low levels of labeling in CA2, CA3 and dentate gyrus (DG) and lateral and medial entorhinal cortex (LEC and MEC respectively); Roman numerals indicate layers. Scale bar: 1mm in **A & B**, 500 μm in **C, E, G,** 200μm in **D, F & H**.

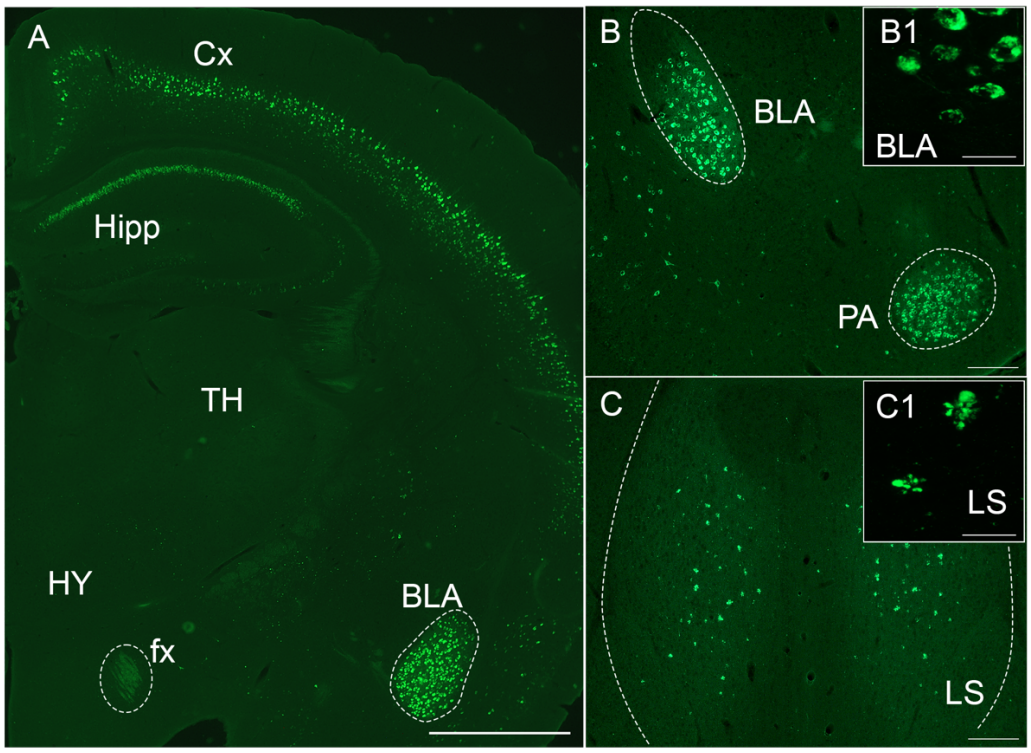


Figure 2.2 Expression of hAPP in subcortical regions in young 5xFAD$^{+/-}$/Rosa^{tdT} mice.

(A-C) Representative images from a 2-month-old female 5xFAD$^{+/-}$/Rosa^{tdT} mouse. **(A)** Immunofluorescence of hAPP in the cortex (Cx), hippocampus (Hipp), BLA and in columns of the fornix. No apparent hAPP immunofluorescence in the thalamus (TH) and hypothalamus (HY). Fx indicates light 1D1-labeling of axons in the descending fornix. **(B)** hAPP positive neurons in the basolateral amygdala (BLA) and posterior amygdala (PA) **(B1)** Higher magnification view of hAPP positive neurons in the BLA. **(C)** hAPP-positive granules in the lateral septum. **(C1)** Higher magnification image of rosette shaped cluster of 1D1 granules. Scale bar: 1mm in **A,** 200µm in **B&C**; 30µm in **B1 & C1**.

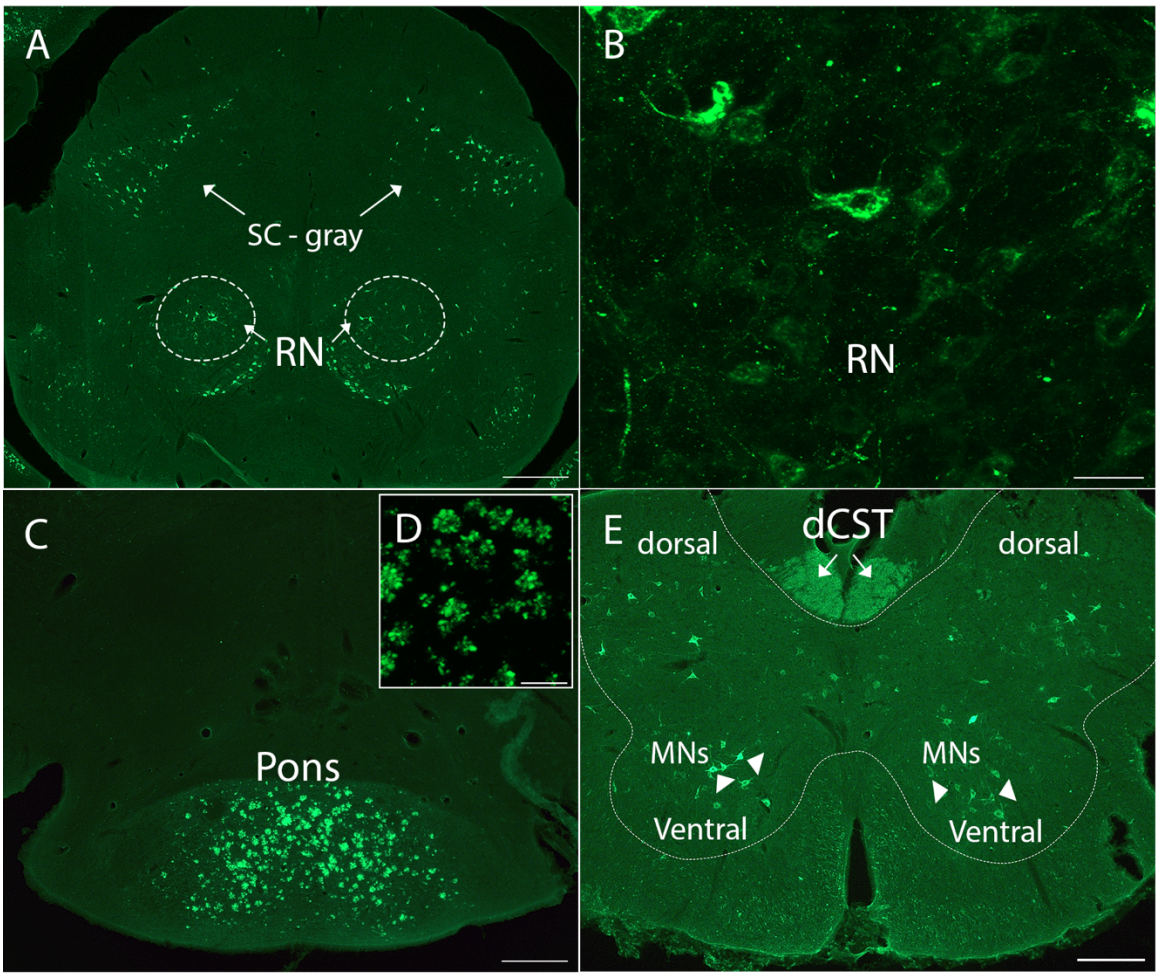


Figure 2.3 Expression of hAPP in the brainstem and spinal cord of young 5xFAD$^{+/-}$/Rosa^{tdT} mice

(A-E) Representative images from a 2-month-old female 5xFAD$^{+/-}$/Rosa^{tdT} mouse. **(A)** hAPP positive neurons in the red nucleus (RN) and gray matter of the superior colliculus (SC – gray). **(B)** Higher magnification of the RN. **(C & D)** 1D1 positive granules in the pons. **(E)** hAPP positive axons in the dorsal corticospinal tract in the dorsal column of the spinal cord (dCST, arrows). Sparse labeling of presumed motor neurons (MNs) in the ventral horn of the spinal cord (arrowheads). Scale bar: 200µm in **A, C & E**; 30µm in **B & D.**

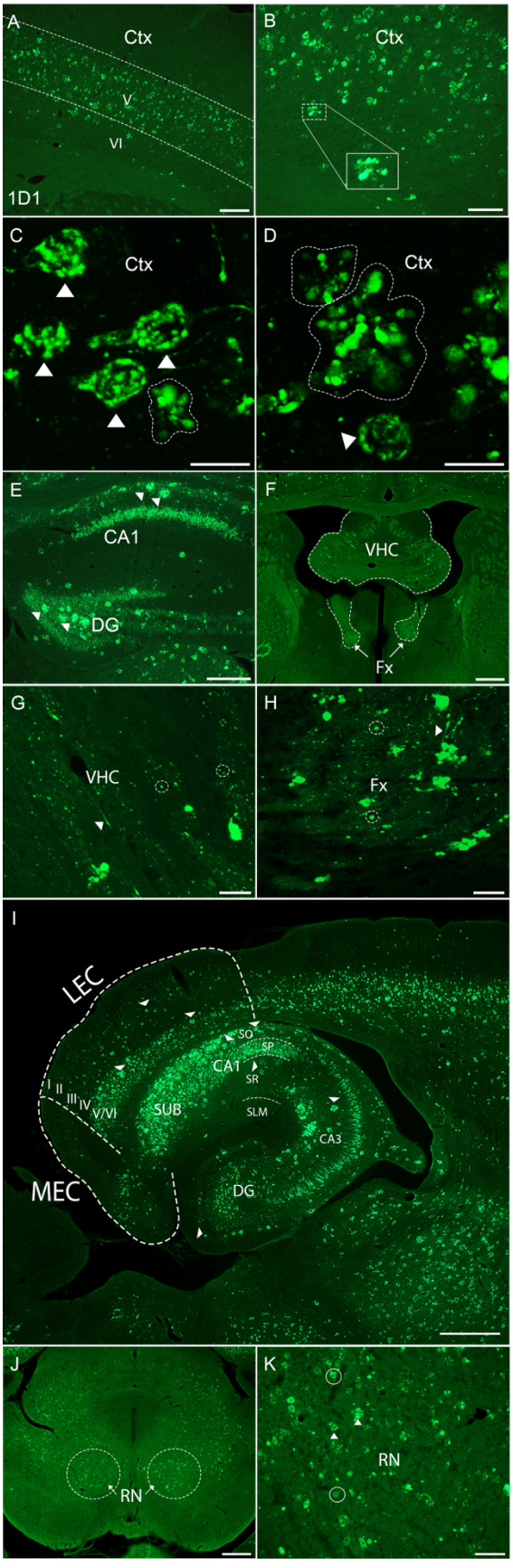

A
Ctx
V
VI
1D1
B
Ctx
C
Ctx
D
Ctx
E
CA1
DG
F
VHC
Fx
G
VHC
H
Fx
I
LEC
MEC
SO
SP
SR
CA1
I II III IV V/VI
SUB
SLM
CA3
DG
J
RN
K
RN

Figure 2.4 1D1-positive granules in older 5xFAD$^{+/-}$/Rosa^{tdT} mouse.

(A-H and J-K) Representative images from 7-month-old male 5xFAD$^{+/-}$/Rosa^{tdT} mice. **(A)** 1D1-positive granules are primarily in cortical layer VI. **(B)** Higher magnification image of 1D1-positive neurons and rosette-shaped clusters of granules within the primary motor cortex. **(C & D)** 1D1 positive rosette-shaped clusters in the motor cortex (outline traced). **(E)** 1D1-positive rosette shaped clusters in CA1 and dentate gyrus (arrowheads). **(F)** 1D1-positive fibrils in the ventral hippocampal commissure (VHC) and the descending column of the fornix (Fx) (arrowheads, **F & G**) along with 1D1-positive granules (circled, **I & J**). **(K & L)** 1D1-positive neuronal cell bodies in the red nucleus (RN) (**L**, circles) and 1D1-positive granules **(L,** arrowheads). **(I)** Pattern of labeling in 10-month-old male 5xFAD$^{+/-}$/Rosa^{tdT} mouse. Note appearance of labeling in deep layers of the LEC, increased labeling in SUB and CA1 and appearance of labeling in CA3 and the hilus of the DG. Arrowheads indicate 1D1 positive clusters of granules scattered throughout the SUB, MEC, LEC, DG, *stratum oriens* (SO) and *stratum radiatum* (SR) of CA1 and in CA3 (arrowheads, **D**). Scale bar: 200µm in **A**; 100µm in **B**; 20µm in **C & D**, 300µm in **E**; 500 µm in **F**; 30 µm in **G & H**; 200µm in **I**; 500µm in **J**; and 100µm **K**.

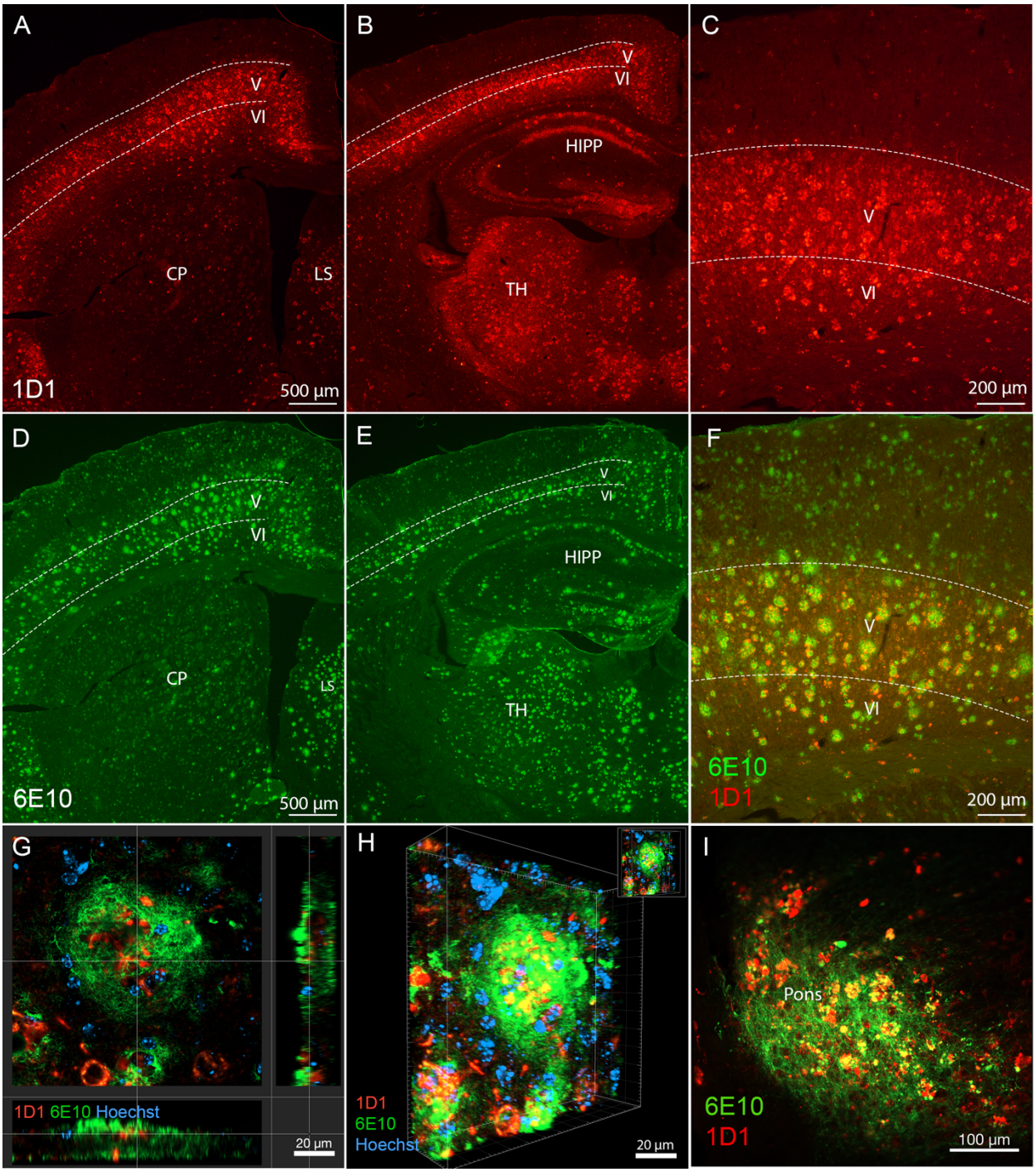


Figure 2.5 Staining pattern of 1D1 and 6E10 in a 12-month-old male 5xFAD$^{+/-}$/Rosa^{tdT} mouse.

(A&B) IF for 1D1 coronal sections. Note labeling in layer V/VI of the cortex, throughout caudate putamen (CP), lateral septum (LS), hippocampus (HIPP), and thalamus (TH). **(C)** 10X

image of IF for 1D1 across layer V/VI of the portion of the sensorimotor cortex illustrated in A. **(D)** IF for 6E10 in the same sections shown in **A-C**. **(G)** Confocal image of 1D1 and 6E10 in a plaque in layer V/VI of the cortex. Note small 1D1-positive granules embedded in the larger 6E10-positive plaque. **(H)** Rotated view of image shown in **G**. **(I)** Confocal image of 1D1 and 6E10 labeling in the pons of a 14-month-old 5xFAD$^{+/-}$/Rosa^{tdT} mouse**. Scale bar:** 500µm in **A, B, D & E;** 200µm in **C & F;** 20µm in **G & H** and 100µm in **I**.

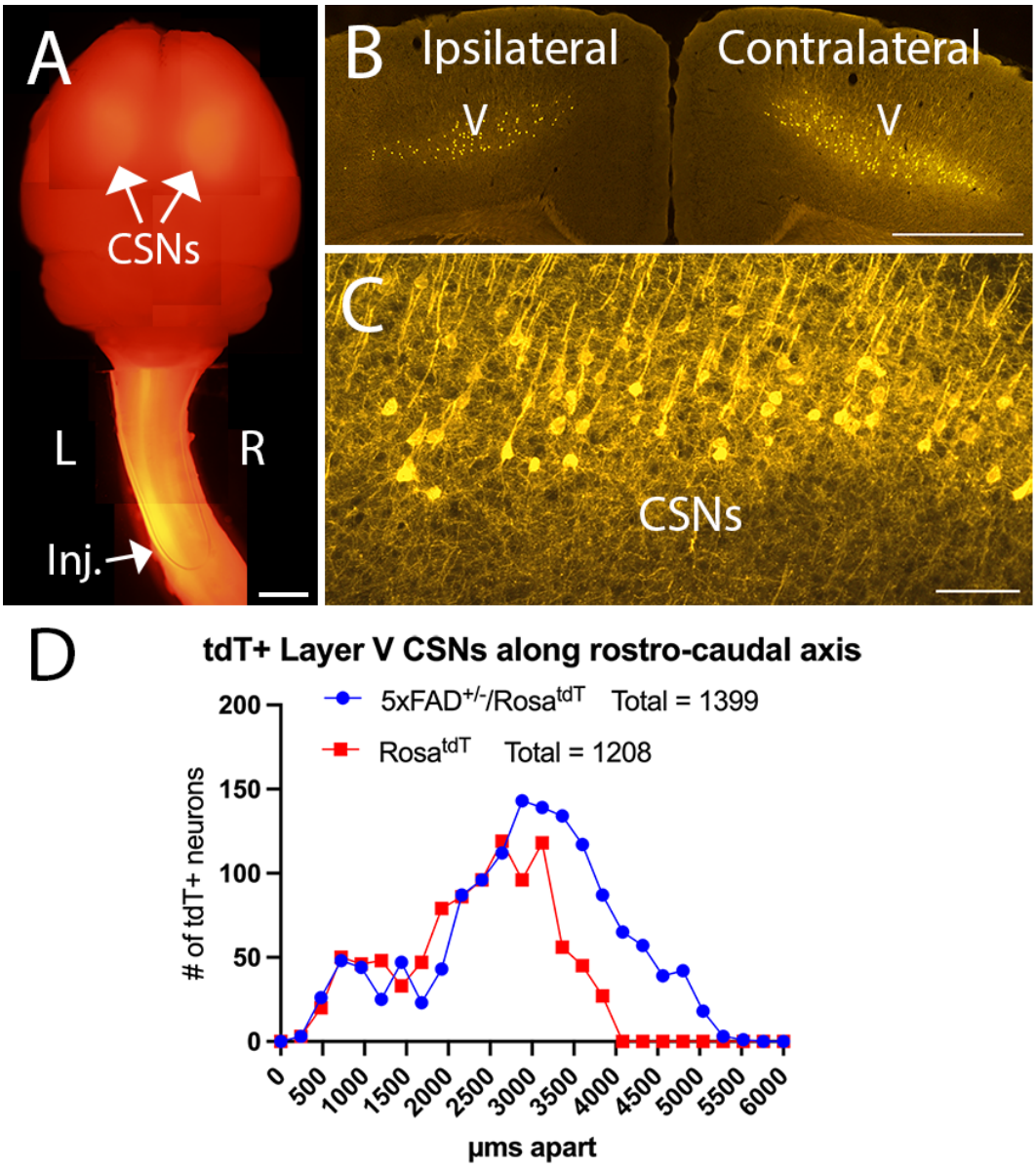


Figure 2.6 Retrograde transduction and induction of tdT expression in CSNs via AAV-rg/Cre injections at C5.

(A) Intact Rosa^{tdT} brain and spinal cord imaged for tdT with epifluorescence illumination. The unilateral injection site is visible on the left (L) side of the spinal cord. Oval shaped areas of red fluorescence reveal areas containing tdT expressing CSNs. **(B)** IF for Red Fluorescent Protein

(RFP) reveals robust labeling of CSNs in the cortex contralateral to the injection with some labeling on the ipsilateral side. **(C)** High magnification views illustrating tdT labeled CSN cell bodies and dendritic arbors. **(D)** Examples of counts of retrogradely labeled CSNs along the rostro-caudal axis in 2-month-old 5xFAD$^{+/-}$/Rosa^{tdT} and Rosa^{tdT} mice tdT. (See Fig. 8 for full quantification). Scale bar: 2mm in **A**; 1mm in **B;** 100µm in **C.**

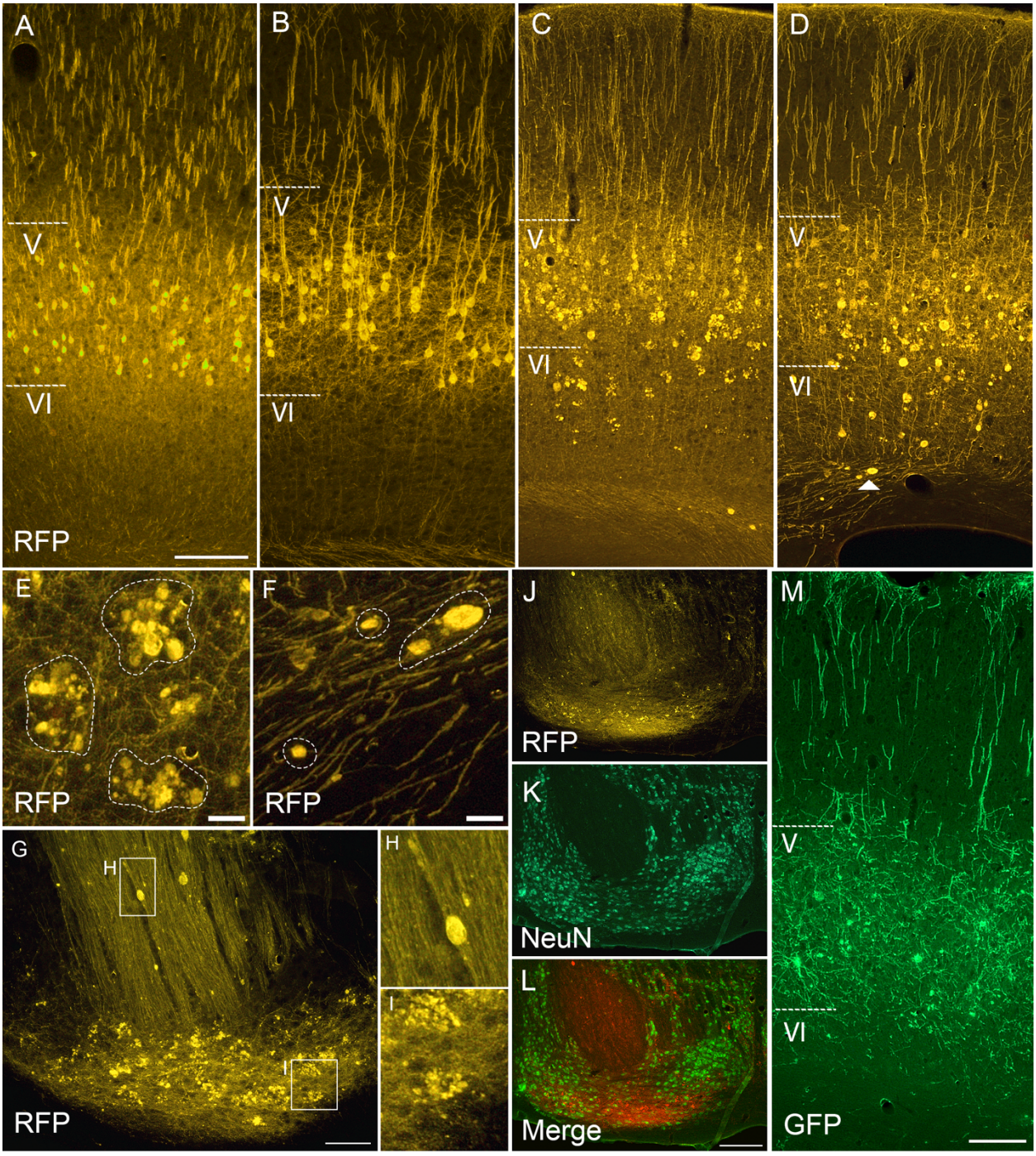


Figure 2.7 Neurodegenerative changes can be tracked by tdT fluorescence.

(A) TdT-labeled CSNs (IF for RFP) in a 2-month-old female 5xFAD$^{+/-}$/Rosa^{tdT} mouse. **(B)** No signs of neurodegeneration in female Rosa^{tdT} mouse injected at 2 months and perfused at 15

months of age. **(C)** TdT-labeled CSNs in male 5xFAD$^{+/-}$/Rosa^{tdT} mouse at 12 months of age. **(D)** Example of tdTomato-labeled CSNs in male 5xFAD$^{+/-}$/Rosa^{tdT} mouse at 8 months of age; **(E)** High magnification view of the tdT accumulations in the cortex; **(F)** dystrophic axons of the tdT positive CSNs in a male 5xFAD$^{+/-}$/Rosa^{tdT} mouse at 12 months of age. **(G)** TdT-labeled particles in the pons of a male 14-month-old 5xFAD$^{+/-}$/Rosa^{tdT}; **(H)** high magnification of axonal varicosities; **(I)** rosette shaped tdT-positive clusters. **(J)** TdT labeled granules in the pons of a male 12-month-old 5xFAD$^{+/-}$/Rosa^{tdT} mouse; **(K)** same section stained for NeuN; **(L)** Merge of J and K reveals little to no overlap. **(M)** GFP IF in the cortex of female 5xFAD$^{+/-}$/Rosa^{tdT} mice injected with AAV-rg/GFP at 5-months that survived until 8 months of age. Scale bar: 200µm in **A-D**; 50µm in **E & F**; 100µm in **G** (same scale bar for **H & I**); 200µm in **J-L;** 200µm in **M.**

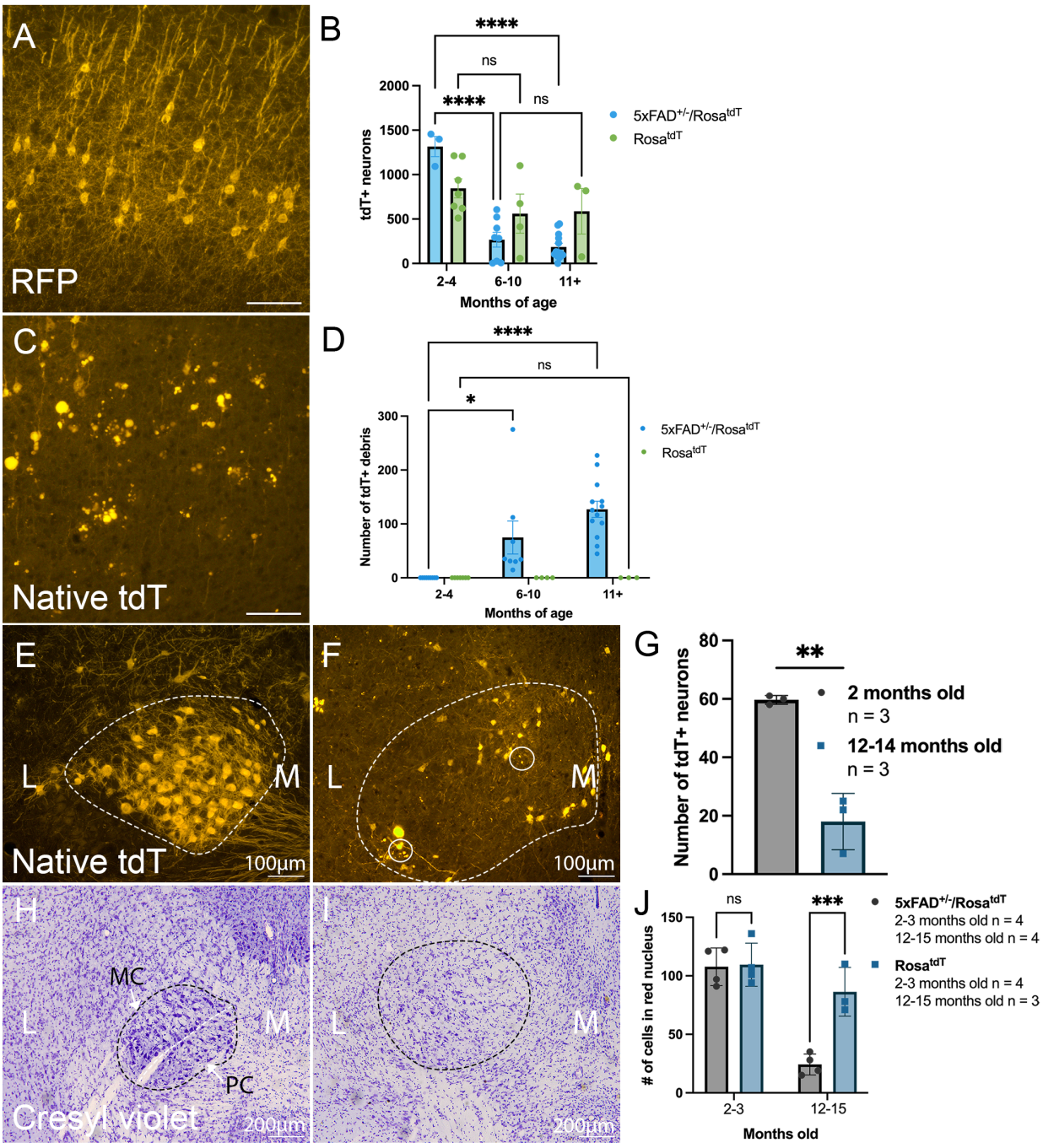


Figure 2.8 Neurodegenerative changes tracked by tdT fluorescence.

(A) tdTomato-labeled CSNs (IF for RFP) in 2-month-old 5xFAD$^{+/-}$/Rosa^{tdT} mouse. **(B)** CSNs decline with age in 5xFAD$^{+/-}$/Rosa^{tdT} but not in Rosa^{tdT}. Mean CSN counts in 5xFAD$^{+/-}$/Rosa^{tdT} and Rosa^{tdT}mice across age groups (2-4, 6-10, and 11+ months). Two-way ANOVA revealed a

significant main effect of age ($F(2,32) = 20.26$, $p < 0.0001$), but no significant main effect of genotype ($F(1,32) = 0.587$, $p = 0.4492$). Sidak's multiple comparisons test revealed that CSN count was significantly lower in 5xFAD$^{+/-}$/Rosa^{tdT} mice at 6-10 months ($p < 0.0001$) and 11+ months ($p < 0.0001$) compared to 2-4 months. In contrast, CSN count in Rosa^{tdT} mice did not significantly change across age groups ($p > 0.72$, for all comparisons). Bars represent mean ± SEM. **(C)** tdTomato-labeled granules in 5xFAD$^{+/-}$/Rosa^{tdT} mouse at 12 months of age. **(D)** Quantification of tdT-positive debris reveals progressive accumulation with age in 5xFAD$^{+/-}$/Rosa^{tdT} mice but absence in Rosa^{tdT} mice. Two-way ANOVA revealed significant effects of genotype ($F(1,38) = 17.08$, $p = 0.0002$) and age ($F(2,38) = 5.574$, $p = 0.0075$). Rosa^{tdT} mice did not have debris at any age. In 5xFAD$^{+/-}$/Rosa^{tdT} mice, tdT+ debris counts increased significantly with age. Debris was significantly different in the 6–10-month group ($p = 0.0297$) and 11+ month group ($p < 0.0001$) compared to the 2–4-month group. Bars represent mean ± SEM. **(E)** tdT-labeled neurons in the red nucleus at 2 months of age vs; **(F)** tdT-labeled red nucleus neurons at 12-14 months of age. **(G)** Counts of tdT labeled neurons in 2-month-old vs. 12–14-month-old 5xFAD$^{+/-}$/Rosa^{tdT} mice. Bars represent mean ± SD. Unpaired t-test: $t = 7.391$, $DF = 4$, $p = 0.0018$. **(H)** Cresyl violet stain reveals large darkly-stained cells (presumed neurons) in the red nucleus of a 2-month-old 5xFAD$^{+/-}$/Rosa^{tdT} **(I)** Cresyl violet stain of 14-month-old 5xFAD$^{+/-}$/Rosa^{tdT} reveals very few large neurons **(J)** Quantification of cresyl violet stained cells in 5xFAD$^{+/-}$/Rosa^{tdT} vs. Rosa^{tdT} at 12–15-months of age. Two-way ANOVA showed significant main effects of genotype ($F = 14.25$, $DF = 1$, $p = .0031$), age ($F = 39.79$, $DF = 1$, $p < 0.0001$), along with a significant interaction ($F = 12.73$, $DF = 1$, $p = 0.0044$). Post-hoc analysis by Sidak's multiple comparison test revealed no difference between genotypes at 2 months of age ($t = 0.1523$, $DF = 11$, $p = 0.9860$) but significant differences at 12-15 months of age ($t = 5.004$, $DF =$

11, p = 0.0008). Bars represent mean ± SD. Medial (M) and lateral (L). Scale bar: 100μm in **A, C, E & F,** 200μm in **H & I**.

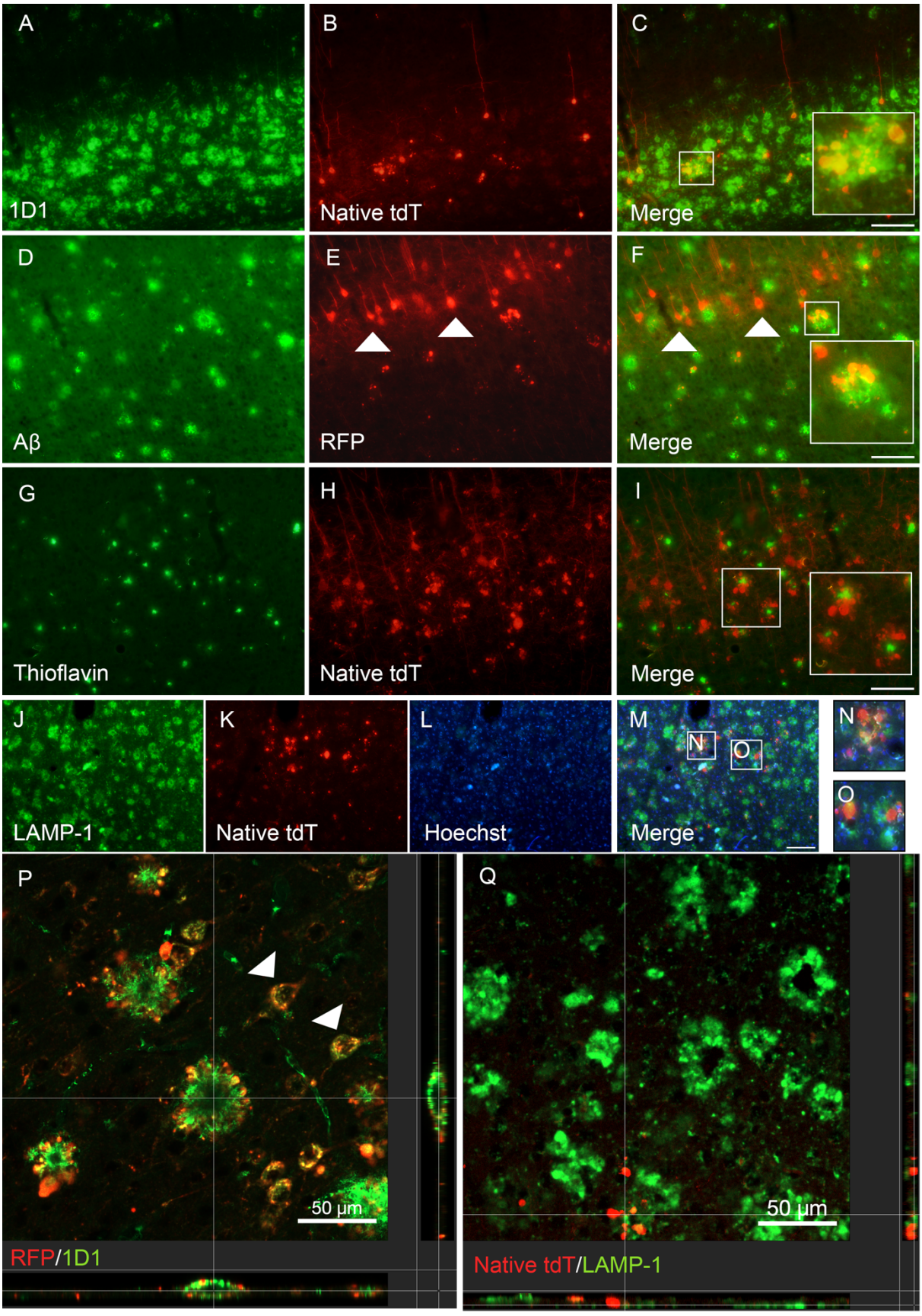

A
1D1
B
Native tdT
C
Merge
D
Aβ
E
RFP
F
Merge
G
Thioflavin
H
Native tdT
I
Merge
J
LAMP-1
K
Native tdT
L
Hoechst
M
N
O
Merge
N
O
P
50 μm
RFP/1D1
Q
50 μm
Native tdT/LAMP-1

Figure 2.9 Characterization of tdT-positive granules in older 5xFAD$^{+/-}$/Rosa^{tdT} mice.

(A-C) hAPP transgene colocalizes with tdT labeled accumulations in cortical layer V/VI, shown in a 12-month-old female 5xFAD$^{+/-}$/Rosa^{tdT}. **(D-F)** In a representative image from a 12-month-old female 5xFAD$^{+/-}$/Rosa^{tdT}. Aβ appears to colocalize with tdT accumulations in the cortex. Note that larger tdT-positive profiles are neuronal cell bodies (white arrows). **(G-I)** Thioflavin S stain shows the amyloid-β core surrounded by tdT positive accumulations in a 12-month-old female 5xFAD$^{+/-}$/Rosa^{tdT}. **(J-O)** LAMP-1, Hoechst and native tdT expression in the cortex. Some tdT granules colocalize with LAMP-1 and Hoechst **(N)** and others appear isolated, **(O),** in a 12-month-old female 5xFAD$^{+/-}$/Rosa^{tdT}. **(P)** High magnification view of RFP labeled neurons and granules colocalized with hAPP transgene in cortical layer V/VI in 8-month-old 5xFAD$^{+/-}$/Rosa^{tdT} female mouse. **(Q)** Occasional colocalization of LAMP-1 and tdT-positive accumulations shown in a higher magnification image, in a 12-month-old female 5xFAD$^{+/-}$/Rosa^{tdT}. Scale bar: 100μm in **A-O**; 50μm in **P** and **Q**.

References

1. Braak, H. & Braak, E. Neuropathological stageing of Alzheimer-related changes. *Acta Neuropathol* 82, 239–259 (1991).
2. DeTure, M. A. & Dickson, D. W. The neuropathological diagnosis of Alzheimer's disease. Molecular Neurodegeneration 14, 32 (2019).
2. Dickson, D. W. The pathogenesis of senile plaques. J Neuropathol Exp Neurol 56, 321–339 (1997).
3. Drummond, E. & Wisniewski, T. Alzheimer's Disease: Experimental Models and Reality. Acta neuropathologica 133, 155 (2016).
4. Eimer, W. A. & Vassar, R. Neuron loss in the 5XFAD mouse model of Alzheimer's disease correlates with intraneuronal Aβ42 accumulation and Caspase-3 activation. Molecular Neurodegeneration 8, 2 (2013).
5. Feng, G. et al. Imaging Neuronal Subsets in Transgenic Mice Expressing Multiple Spectral Variants of GFP. Neuron 28, 41–51 (2000).
6. Forner, S. et al. Systematic phenotyping and characterization of the 5xFAD mouse model of Alzheimer's disease. Sci Data 8, 270 (2021).
7. Gallardo, D. & Steward, O. Development and characterization of a novel transgenic strain to selectively label neurons that degenerate in 5xFAD mice. *Experimental Neurology* 405, 115914 (2026).
8. Gómez-Isla, T. et al. Profound Loss of Layer II Entorhinal Cortex Neurons Occurs in Very Mild Alzheimer's Disease. J. Neurosci. 16, 4491–4500 (1996).
9. Gordon, J. W. et al. Regulation of Thy-1 gene expression in transgenic mice. Cell 50, 445–452 (1987).

10. Haass, C., Kaether, C., Thinakaran, G. & Sisodia, S. Trafficking and proteolytic processing of APP. Cold Spring Harb Perspect Med 2, a006270 (2012).

11. Hefendehl, J. K. et al. Long-Term In Vivo Imaging of β-Amyloid Plaque Appearance and Growth in a Mouse Model of Cerebral β-Amyloidosis. J Neurosci 31, 624–629 (2011).

12. Herzig, M. C. et al. Abeta is targeted to the vasculature in a mouse model of hereditary cerebral hemorrhage with amyloidosis. Nat Neurosci 7, 954–960 (2004).

13. Hofling, C. *et al.* Differential transgene expression patterns in Alzheimer mouse models revealed by novel human amyloid precursor protein-specific antibodies. Aging Cell 15, 953–963 (2016).

14. Jawhar, S., Trawicka, A., Jenneckens, C., Bayer, T. A. & Wirths, O. Motor deficits, neuron loss, and reduced anxiety coinciding with axonal degeneration and intraneuronal Aβ aggregation in the 5XFAD mouse model of Alzheimer's disease. Neurobiology of Aging 33, 196.e29-196.e40 (2012).

15. Johns, P. Chapter 12 - Dementia. in Clinical Neuroscience (ed. Johns, P.) 145–162 (Churchill Livingstone, 2014). doi:10.1016/B978-0-443-10321-6.00012-6.

16. Khakpai, F., Zarrindast, M. R., Nasehi, M., Haeri-Rohani, A. & Eidi, A. The role of glutamatergic pathway between septum and hippocampus in the memory formation. EXCLI J 12, 41–51 (2013).

17. Knopman, D. S. et al. Alzheimer disease. Nat Rev Dis Primers 7, 33 (2021).

18. Lee, J.-H. et al. Faulty autolysosome acidification in Alzheimer's disease mouse models induces autophagic build-up of Aβ in neurons, yielding senile plaques. Nat Neurosci 25, 688–701 (2022).

19. Mabrouk, R., Miettinen, P. O. & Tanila, H. Most dystrophic neurites in the common 5xFAD Alzheimer mouse model originate from axon terminals. Neurobiology of Disease 182, 106150 (2023).

20. Masse, F. A. A. et al. Progression of Gait Changes in Older Adults With Mild Cognitive Impairment: A Systematic Review. Journal of Geriatric Physical Therapy 44, 119 (2021).

21. Metcalfe, M. et al. Harnessing rAAV-retro for gene manipulations in multiple pathways that are interrupted after spinal cord injury. (2022) doi:10.1016/j.expneurol.2021.113965.

22. Moechars, D., Lorent, K., De Strooper, B., Dewachter, I. & Van Leuven, F. Expression in brain of amyloid precursor protein mutated in the alpha-secretase site causes disturbed behavior, neuronal degeneration and premature death in transgenic mice. The EMBO Journal 15, 1265–1274 (1996).

23. Oakley, H. et al. Intraneuronal β-Amyloid Aggregates, Neurodegeneration, and Neuron Loss in Transgenic Mice with Five Familial Alzheimer's Disease Mutations: Potential Factors in Amyloid Plaque Formation. J. Neurosci. 26, 10129–10140 (2006).

24. Oblak, A. L. et al. Comprehensive Evaluation of the 5XFAD Mouse Model for Preclinical Testing Applications: A MODEL-AD Study. Front Aging Neurosci 13, 713726 (2021).

25. Sadleir, K. R., Popovic, J. & Vassar, R. ER stress is not elevated in the 5XFAD mouse model of Alzheimer's disease. Journal of Biological Chemistry 293, 18434–18443 (2018).

26. Schindelin, J. et al. Fiji: an open-source platform for biological-image analysis. Nat Methods 9, 676–682 (2012).

27. Sharoar, M. G., Palko, S., Ge, Y., Saido, T. C. & Yan, R. Accumulation of saposin in dystrophic neurites is linked to impaired lysosomal functions in Alzheimer's disease brains. Mol Neurodegener 16, 45 (2021).

28. Shin, J., Park, S., Lee, H. & Kim, Y. Thioflavin-positive tau aggregates complicating quantification of amyloid plaques in the brain of 5XFAD transgenic mouse model. Sci Rep 11, 1617 (2021).

29. Steward, O. et al. Rostro-Caudal Specificity of Corticospinal Tract Projections in Mice. Cereb Cortex 31, 2322–2344 (2021).

30. Steward, O. & Scoville, S. A. Cells of origin of entorhinal cortical afferents to the hippocampus and fascia dentata of the rat. Journal of Comparative Neurology 169, 347–370 (1976).

31. Terry, R. D. The Fine Structure of Neurofibrillary Tangles in Alzheimer's Disease. Journal of Neuropathology & Experimental Neurology 22, 629–642 (1963).

32. Terry, R. D. et al. Physical basis of cognitive alterations in alzheimer's disease: Synapse loss is the major correlate of cognitive impairment. Annals of Neurology 30, 572–580 (1991).

33. Thal, D. R., Rüb, U., Orantes, M. & Braak, H. Phases of A beta-deposition in the human brain and its relevance for the development of AD. Neurology 58, 1791–1800 (2002).

34. Toniolo, S. et al. Cerebellar White Matter Disruption in Alzheimer's Disease Patients: A Diffusion Tensor Imaging Study. J Alzheimers Dis 74, 615–624 (2020).

35. Vadhan, J. & Das, J. M. Neuroanatomy, Red Nucleus. in StatPearls (StatPearls Publishing, Treasure Island (FL), 2024).

36. Zheng, Y. et al. Involvement of Receptor Tyrosine Kinase Tyro3 in Amyloidogenic APP Processing and β-Amyloid Deposition in Alzheimer's Disease Models. PLOS ONE 7, e39035 (2012).

37. 2024 Alzheimer's disease facts and figures. Alzheimer's Dement., 20: 3708-3821 (2024).

Chapter 3 - Progression of neurodegeneration in 5xFAD Alzheimer's disease mouse model following mTOR activation

Abstract

Alzheimer's disease (AD) pathology is characterized by progressive neurodegeneration, accumulation of amyloid-β (Aβ) plaques and neurofibrillary tangles. To investigate whether mTOR activation could prevent or delay neuronal death, we created a triple transgenic model by crossing 5xFAD, $Rosa^{tdT}$ and $PTEN^{flox/flox}$ mice. The $5xFAD^{+/-}/PTEN^{f/f}/Rosa^{tdT}$ mouse model allows for permanent cre-dependent expression of tdT in the cell bodies, dendrites and axons of the neurons that have PTEN deleted. Here, we assessed whether deletion of PTEN, which leads to activation of mTOR, delays or reduces age-dependent neurodegeneration or progression of functional deficits in 5xFAD mice. At 2-4 months of age, $5xFAD^{+/-}/PTEN^{f/f}/Rosa^{tdT}$ mice received intra-spinal cord injections of AAV-retrograde (rg)/Cre. The AAV-rg/Cre transduced neurons retrogradely and resulted in permanent labeling of corticospinal neurons (CSNs) in layer V of the sensorimotor cortex. The brains and spinal cords were collected at 2-4 months, 6-10 and 11-17 months of age. Quantifications of tdT labeled neurons and accumulations revealed no differences between 5xFAD mice with PTEN deleted and 5xFAD controls.

Introduction

Alzheimer's disease (AD) is defined primarily by cognitive decline, but motor deficits have also been recognized as a pathological feature (Albers et al., 2015). Motor decline is even thought to precede cognitive decline in AD (Verghese et al., 2007; Buchman et al., 2007; Boyle et al., 2009;

Albers et al., 2015). The rest of the characteristic neuropathological markers of AD also begin decades before cognitive changes are clinically detectable. Early in disease onset, AD is characterized by the accumulation of extracellular amyloid beta (Aβ) plaques and intraneuronal neurofibrillary tangles (Terry, 1963). As the disease advances, neurodegeneration becomes a primary pathological feature, encompassing synapse loss, dendritic atrophy, axonal destabilization, and ultimately neuron death (Terry et al., 1991; Thal et al., 2002). Extracellular aggregated Aβ deposits are commonly surrounded by degenerating neuronal processes, and together these are termed neuritic plaques. Some of these pathological features are recapitulated in animal models of AD (Drummond and Wisniewski, 2016), and characterizing the progression of pathology in these models is crucial for understanding disease mechanisms and developing effective treatments. Particularly, there is a need for studies on neurodegeneration of motor pathway neurons as it is fundamental to the progression of AD pathology.

Mouse models are widely used to study AD and neurodegeneration, due in part to their comparatively short lifespan. However, very few well-characterized murine models of AD exhibit age-related neurodegeneration within the lifetime of a mouse. One model that does exhibit extensive neurodegeneration is the 5xFAD transgenic strain. 5xFAD mice express two mutant human genes, amyloid precursor protein (APP) and presenilin 1 (PSEN1), carrying five familial AD mutations (three in APP, two in PSEN1). The two transgenes are inserted into a single locus and driven by the neuron-specific elements of the mouse Thy-1 promoter, which restricts expression to select forebrain neuron populations (Oakley et al., 2006). Using an antibody recognizing both mouse and human protein, total APP expression in the 5xFAD brain has been found to be approximately 1.8 times that of non-transgenic controls (Sadleir et al.,

2018). These mice display robust amyloid plaque accumulation and neurodegeneration in layer V of the cerebral cortex (Oakley et al., 2006; Eimer and Vassar, 2013; Bhatt et al., 2014).

The extensive neurodegeneration of cortical layer V in 5xFAD mice is of particular interest, as this layer contains corticospinal neurons (CSNs), which form the corticospinal tract. Having a defined population of neurons that degenerate in the 5xFAD model, CSNs (Gallardo and Steward 2026), provides a functionally defined and anatomically traceable neuronal population in which to study the progression of neurodegeneration. To target CSNs, they can be selectively and reliably identified through retrograde labeling from their spinal axon terminals (Ozdinler et al., 2014). Retrograde adeno-associated virus delivery carrying Cre (AAV-rg/Cre), combined with a Cre-dependent tdTomato (tdT) reporter (Madisen et al., 2010; Tervo et al., 2016), enables specific labeling of CSNs when injected into the spinal cord (Steward et al., 2021; Gallardo and Steward 2026).

Our CSN targeting and tracking platform (Gallardo and Steward, 2026) allows us to test whether activating an intrinsic growth signaling pathway can protect CSNs from degeneration. Deletion of phosphatase and tensin homolog (PTEN), a negative regulator of the mammalian target of rapamycin (mTOR) pathway, has been shown to promote growth across multiple mouse models (Park et al., 2008; Liu et al., 2010; Gallent and Steward, 2018; Yonan and Steward, 2023). In the visual system, PTEN-deletion-mediated activation of mTOR signaling in injured retinal ganglion cells was reported to not only promote axon regeneration but also cell survival (Park et al., 2008). The pro-survival effects may extend to CSNs. Notably, our lab has shown that PTEN deletion and Cre-dependent tdT labeling can be driven within the same CSNs (Metcalfe and Steward, 2023), and cervical level 5 (C5) retrograde injections reliably label CSNs originating in

the sensorimotor cortex (Steward et al., 2021). Thus, we have established a platform in which mTOR can be activated in permanently labeled CSNs.

In AD, mTOR signaling is well documented to be dysregulated (Li et al., 2005; Tramutola et al., 2015), and the field has largely framed the dysregulation (overactivation) as a contributing factor to neurodegeneration. The inhibition of mTOR has been proposed as a therapeutic strategy to enhance autophagic clearance of Aβ. However, as a lab focused on spinal cord injury, the pro-survival and pro-growth effects of mTOR activation observed in CNS injury models raise the possibility that mTOR activation may be neuroprotective.

In this study, we characterized the progression of CSN degeneration in 5xFAD mice across age and tested whether constitutive activation of the mTOR pathway, achieved through conditional deletion of PTEN, could prevent or delay this degeneration. Using retrograde-AAV delivery of Cre into the cervical spinal cord together with a Cre-dependent tdT reporter, we selectively labeled and manipulated CSNs, enabling tracking of age-dependent neurodegeneration in neurons with PTEN deletion. We hypothesized that PTEN deletion, and the resulting activation of mTOR signaling, would protect CSNs from age-related neurodegeneration in 5xFAD mice.

Methods

2.1 Experimental Animals

All procedures involving animals were approved by the Institutional Animal Care and use Committee (IACUC) at the University of California, Irvine (UCI) in accordance with the National Institute of Health (NIH) guidelines. Mice had *ad lib* access to food and water and were housed at 25°C with a 12h light/dark cycle.

Breeding strategy: To produce the transgenic mice for these studies, hemizygous 5xFAD (B6SJL-Tg (APPSwFlLon, PSEN1*M146L*L286V) 6799Vas/Mmjax; Strain #: 34840-JAXRRID:MMRRC_034840-JAX) mice were crossed with PTEN$^{flox/flox\ (f/f)/}$Rosa^{tdT} mice developed in our lab (reported in Gallent and Steward, 2018). Homozygous PTEN$^{f/f}$/Rosa^{tdT} had been maintained in our breeding colony over multiple generations before being crossed with 5xFAD mice. The PTEN$^{f/f}$/Rosa^{tdT} were developed by crossing Rosa^{tdT} (B6;129S6-Gt(ROSA)26Sortm9(CAG-tdTomato)Hze/J, Strain #:007905, RRID:IMSR_JAX:007905) mice and PTEN$^{f/f}$ (B6.129S4-Ptentm1Hwu/J, Strain #:006440, RRID:IMSR_JAX:006440) mice. All mice of the F1 generation from the 5xFAD$^{+/-}$ x PTEN$^{f/f}$/Rosa$^{tdT\ +/+}$ cross were hemizygous at both PTEN$^{f/f}$/Rosa^{tdT} loci and approximately 50% of the mice were hemizygous for 5xFAD. Genotypes were determined by real time PCR with probes designed for hAPP and hPSEN1 (Transnetyx, Cordova, TN). When sufficient numbers of 5xFAD $^{+/-}$/PTEN$^{f/f}$/Rosa$^{tdT\ +/+}$ were obtained, breeding pairs were created with 5xFAD $^{+/-}$/PTEN$^{f/f}$/Rosa$^{tdT\ +/+}$ crossed with PTEN$^{f/f}$/Rosa$^{tdT\ +/+}$ to generate 5xFAD$^{+/-}$/PTEN$^{f/f}$/Rosa$^{tdT\ +/+}$ and 5xFAD $^{-/-}$/PTEN$^{f/f}$/Rosa$^{tdT\ +/+}$ controls. Another colony of 5xFAD$^{+/-}$/Rosa$^{tdT\ +/+}$ and Rosa$^{tdT\ +/+}$ controls. Similarly, all mice of the F1 generation from the 5xFAD$^{+/-}$ x Rosa$^{tdT\ +/+}$ cross were hemizygous at the Rosa^{tdT} locus and approximately 50% of the mice were hemizygous for 5xFAD. When enough 5xFAD $^{+/-}$/Rosa$^{tdT\ +/+}$ were obtained, breeding pairs were created with Rosa$^{tdT\ +/+}$/5xFAD $^{+/-}$ crossed with Rosa$^{tdT\ +/+}$ to generate Rosa$^{tdT\ +/+}$/ 5xFAD$^{+/-}$ and Rosa$^{tdT\ +/+}$/5xFAD $^{-/-}$ controls. Genotyping of progeny of these breeders was done with PCR probes designed according to the protocol provided by Jackson lab (protocol ID = 22421) with confirmation of presence, or absence of hAPP by IF against hAPP protein using the clone 1D1 primary antibody (RRID:AB_3665093). Details on the age of mice when injected with AAV-rg/Cre and age at tissue collection are in

Table 3.1. In initial studies, mice received AAV-rg/Cre injections at 5 months of age. However, we discovered early signs of neurodegeneration at this age by presence of tdT-labeled accumulations (as in Results below, tdT accumulations appear as the number of neurons decreases) and so transitioned to injecting mice with AAV-rg/Cre between 2-4 months of age to label neurons with tdT and delete PTEN before neurodegeneration began.

Table 3.1 Mice used for immunohistology

2-4 Months of age

Months of age	Months of age at injection	5xFAD$^{+/-}$ /PTEN$^{f/f}$/Rosa^{tdT}	5xFAD$^{+/-}$ /Rosa^{tdT}	PTEN$^{f/f}$/Rosa^{tdT}	Rosa^{tdT}
2	2	6 (3 F, 3 M)	6 (4 M, 2 F)	5 (4 M, 1 F)	-
3	2	-	-	4 (3 F, 1 M)	5 (5 F)
4	2	-	-	-	1 (1 M)
3	3	-	3 (1 M, 2 F)	-	1 (1 F)
4	3	4 (3 M, 1 F)	-	1 (1 F)	-

6-10 Months of age

Months of age	Months of age at injection	5xFAD$^{+/-}$ /PTEN$^{f/f}$/Rosa^{tdT}	5xFAD$^{+/-}$ /Rosa^{tdT}	PTEN$^{f/f}$/Rosa^{tdT}	Rosa^{tdT}
6	2	1 (1 M)	-	1 (1 M)	-
8	2	1 (1 F)	-	4 (2 F, 2 M)	-
10	2	2 (2 M)	-	4 (4 M)	-
5	4	-	3 (1 F, 2 M)	-	-
6	4	-	-	-	-
8	4	-	5 (1 F, 4 M)	3 (2 M, 1 F)	4 (2 F, 2 M)

11+ Months of age

Months of age	Months of age at injection	5xFAD$^{+/-}$/PTEN$^{f/f}$/Rosa^{tdT}	5xFAD$^{+/-}$/Rosa^{tdT}	PTEN$^{f/f}$/Rosa^{tdT}	Rosa^{tdT}
11	2	2 (1 F, 1 M)	-	-	-
12	2	1 (1 M)	2 (2 M)	1 (1 M)	-
14	2	-	2 (1 F, 1 M)	1 (1 F)	1 (1 F)
15	2	3 (2 F, 1 M)	-	2 (1 F, 1 M)	2 (2 F)
17	2	1 (1 F)	-	-	-
12	3	1 (1 F)	2 (2 F)	-	-
14	3	-	-	-	-
15	3	-	2 (2 F)	2 (2F)	-
12	4	-	4 (3 F, 1 M)	-	-
16	4	1 (1 M)	-	-	-

Mice used for bioluminescence imaging: As a pilot study, Camk2a-cre mice (B6.Cg-Tg (Camk2a-cre) T29-1Stl/J; MGI:2177650 JAX: 005359) were used (n = 13). The mice were chosen for the study due to the large availability in our breeding colony.

2.2 Surgical procedures

For 5xFAD$^{+/-}$/PTEN$^{f/f}$/Rosa^{tdT}, 5xFAD$^{+/-}$/Rosa^{tdT}, PTEN$^{f/f}$/Rosa^{tdT} and Rosa^{tdT} studies, surgical methods are as reported in Gallardo and Steward 2026 and are described in detail below. Mice received unilateral intra-spinal cord injections of AAV-retrograde(rg)/Cre (Addgene viral prep #24593-AAVrg) at cervical level 5 (C5). Injections were unilateral in order to transduce neurons on the contralateral side of the brain leaving most neurons on the ipsilateral side as non-transduced control. For surgery, mice were anesthetized with continuous isoflurane (2-2.5%)

administration, their eyes were swabbed with Vaseline to prevent drying, and the scalp was shaved and cleaned with Betadine®. A laminectomy was performed at C5 to expose the spinal cord and AAV-rg/Cre was injected 0.5 mm left of the midline and 0.5 mm deep (3E9 viral genome copies (GC) per mouse) using a Hamilton microsyringe fitted with a pulled glass micropipette. The needle was kept in place for 1 minute after completing the injection. Following injection, the muscle layers were sutured, and the skin was closed by wound clips.

For bioluminescence imaging, Camk2a-cre mice received unilateral intra-spinal cord injections of AVV-rg-Firefly Luciferase (fLuc) (addgene??) at thoracic level 9 (T9). Injections were unilateral, into the left side of the spinal cord. During surgery, mice were anesthetized with continuous isoflurane (2-2.5%) administration, their eyes were swabbed with Vaseline to prevent drying, and the scalp was shaved and cleaned with Betadine®. A laminectomy was performed at T9 to expose the spinal cord and AAV-rg-fLUC was injected 0.5 mm left of the midline and 0.5 mm deep (3E9 viral genome copies (GC) per mouse) using a Hamilton microsyringe fitted with a pulled glass micropipette. As above, the needle was kept in place for 1 minute after completing the injection. Following injection, the muscle layers were sutured, and the skin was closed by wound clips.

2.3 Post-operative care

After surgery, mice were immediately placed in cages with Alpha-Dri bedding with half of the cage placed on a circulating water warming pad set to 37^{o}C. Placing the cage partially on top of warming pads allows mice to remove themselves from the heat source, if desired. Mice were kept on the warming pad for 3 days post-surgery and received lactated Ringer's solution once a day (1ml/20g, subcutaneously), enrofloxacin once a day (Baytril® 2.5mg/kg, subcutaneously)

and buprenorphine twice a day (0.01mg/kg, subcutaneously). Mice were monitored twice daily for 3 days post-surgery for general health and signs of distress. If bladders of mice were full, indicating difficulty to urinate due to surgery, the bladders were manually expressed twice daily. Bladder expression was required for a small number of animals and for a maximum of 3 days post-surgery. After 3 days, the cages were removed from the warming pads and were transferred back to the mouse housing room set at 25°C. Once in the housing room, mice were routinely monitored by vivarium staff and research staff.

2.5 Bioluminescence imaging

Images of *in vivo* bioluminescence were taken on an In Vivo Imaging System (IVIS) platform. Mice were administered 6 mg of potassium D-luciferin salt substrate D-Luciferin (Goldbio, Cat. #: LUCNA-100) via intraperitoneal injection (IP) 20 minutes prior to imaging, along with shaving the head and back to reduce interference of fur with bioluminescence imaging. Images were taken with a 10-minute exposure. The Living Image software was used for image analysis and quantifications per manufacturer recommendations. Bioluminescence data are reported in all cases as photon radiance, measured in photons per second per square centimeter per steradian ($P/S/cm^2/Sr$). Equal size Region of Interest (ROI) areas were drawn (1.25 cm diameter circle on the head and an oval 1.76 cm wide/2.78 cm high on the back) and used for quantification analysis.

For bioluminescent imaging of brain slices, mice were sacrificed with 195 mg/kg Fatal-Plus (Pentobarbital) and brains were collected immediately. Brains were sectioned coronally on a vibratome at 400µm, while submerged in cold aCSF (125 mM NaCl, 3 mM KCl, 1.2 mM NaH_2PO_4, 7.7 mM MgSO4, 26 mM $NaHCO_3$, 10 mM D-glucose) infused with a 95% O_2/5%

CO_2 gas mixture. Slices were kept on a slice incubation chamber and allowed to equilibrate in >1 mL/min flow aCSF maintained with a 95% O_2/5% CO_2 gas mixture combined with 0.16 mg/mL D-luciferin substrate for 30 minutes. Prior to imaging, 0.16 mg/mL D-luciferin was added to the aCSF.

2.6 Tissue collection

Tissue collection, histology, and IHC were as reported previously in Gallardo and Steward 2026 and are described in detail below. Mice were euthanized using Fatal Plus®, followed by transcardiac perfusion with 4% paraformaldehyde (PFA). Brains and spinal cords were removed intact and imaged under a fluorescent microscope to visualize tdT fluorescence from the site of injection to the cortex. Brains and spinal cords were kept in 4% PFA for at least 24 hours. The tissue was then submerged in 27% sucrose for 24 hours for cryoprotection and frozen in Tissue-Tek O.C.T. embedding medium. Brains were then sectioned at 30µm coronally using a cryostat. Sections were stored free-floating in phosphate-buffered saline (1xPBS, 20mM, pH7.4) with 0.1% sodium azide.

2.7 Immunohistochemistry (IHC) and immunofluorescence (IF)

Free-floating brain sections at 480 µm intervals were used for all histology, including IHC and IF. Quantifications of tdT labeled neurons and debris were done by visualizing native tdT fluorescence, without antibody staining. In some cases, to amplify signal from tdT by IF, sections were immunostained for Red Fluorescent Protein (RFP). Sections were washed in Tris Buffered Saline (1xTBS, 100mM Tris. pH 7.4 and 150 mM NaCl) 2 times for 5-10 minutes each time. The sections were then incubated in methanol with 3% Hydrogen peroxide for 15 minutes and washed in 1xTBS 3 times for 5-10 minutes each. After washing, sections were incubated for

1-2 hours at room temperature in a 1xTBS, 5% Normal Donkey Serum (NDS), 0.3% Triton X-100 blocking solution. Sections were then incubated in a 1:1000 dilution of Rabbit anti-RFP primary antibody (Rockland Cat# 600-401-379, RRID:AB_2209751) with 1xTBS, 5% NDS and 0.3% Triton X-100 overnight at room temperature. The next day, sections were washed in 1xTBS 3 times for 5-10 minutes each and then incubated in a 1:500 dilution of Donkey anti-Rabbit 555 with 5% NDS and 0.3% Triton X-100 for 2 hours at room temperature, washed twice in 1xTBS and mounted on 0.5% gelatin subbed, double frosted, VWR® microscope slides.

For PTEN detection, sections were washed in 1xTBS 2 times for 5-10 minutes each time. The sections were then incubated in 1xTBS with 3% Hydrogen peroxide for 15 minutes and washed in 1xTBS 3 times for 5-10 minutes each. After washing, sections were incubated for 1-2 hours at room temperature in a 1xTBS, 5% NDS, 0.3% Triton X-100 blocking solution. Sections were then incubated in a 1:250 dilution of Rabbit anti-PTEN primary antibody (Cell Signaling Technology #9188 L, RRID:AB_2253290) with 1xTBS, 5% NDS and 0.3% Triton X-100 overnight at room temperature. The next day, sections were washed in 1xTBS 3 times for 5-10 minutes each and then incubated in a 1:250 dilution of Biotin-SP (long spacer) AffiniPure F(ab')$_2$ Fragment Donkey Anti-Rabbit IgG (H+L) (Jackson Immuno Research Labs, Cat. No. 711-066-152, RRID:AB_2340594) with 1xTBS, 5% NDS, 0.3% Triton X-100 for 2 hours at room temperature. Sections were then washed in 1xTBS 3 times for 5-10 minutes each and then incubated in a 1:100 dilution of VECTASTAIN® Elite® ABC (Avidin/Biotin) - Horseradish peroxidase (HRP) (Standard) (PK-6100, RRID: AB_2336819) with 1xTBS for 1-2 hours. After incubation, sections were washed in 1xTBS 3 times for 5-10 minutes each and then incubated in a 1:250 dilution of FITC-conjugated tyramide (FITC-tyramide) with 0.1M borate buffer (pH 9)

for 25 minutes. Sections were washed twice in 1xTBS and mounted on 0.5% gelatin subbed, double frosted, VWR® microscope slides.

For detection of pS6, sections were washed in 1xTBS 2 times for 5-10 minutes each time. The sections were then incubated in 1xTBS with 3% Hydrogen peroxide for 15 minutes and washed in 1xTBS 3 times for 5-10 minutes each. After washing, sections were incubated for 1-2 hours at room temperature in a 1xTBS, 5% NDS, 0.3% Triton X-100 blocking solution. Sections were then incubated in a 1:500 dilution of Rabbit anti-pS6 primary antibody (Cell Signaling Technology Cat# 2211, RRID:AB_331679, Phospho-S6 Ribosomal Protein (Ser235/236)) with 1xTBS, 5% NDS and 0.3% Triton X-100 overnight at room temperature. The next day, sections were washed in 1xTBS 3 times for 5-10 minutes each and then incubated in a 1:250 dilution of Biotin-SP (long spacer) AffiniPure F(ab') $_2$ Fragment Donkey Anti-Rabbit IgG (H+L) (Jackson Immuno Research Labs, Cat. No. 711-066-152, RRID:AB_2340594) with 1xTBS, 5% NDS, 0.3% Triton X-100 for 2 hours at room temperature. Sections were then washed in 1xTBS 3 times for 5-10 minutes each and then incubated in a 1:100 dilution of VECTASTAIN® Elite® ABC (Avidin/Biotin) - Horseradish peroxidase (HRP) (Standard) (PK-6100, RRID: AB_2336819) with 1xTBS for 1-2 hours. After incubation, sections were washed in 1xTBS 3 times for 5-10 minutes each and then incubated in a 1:250 dilution of FITC-conjugated tyramide (FITC-tyramide) with 0.1M borate buffer (pH 9) for 25 minutes. Sections were washed twice in 1xTBS and mounted on 0.5% gelatin subbed, double frosted, VWR® microscope slides.

Table 3.2. Primary antibody list

Antibody	Host	Vendor	Catalog #	RRID	Dilution
RFP	Rabbit	Rockland	600-401-379	RRID: AB_2209751	1:1000
PTEN	Rabbit	Cell signaling	9188L	RRID: AB_2253290	1:250
pS6 (Ser235/236)	Rabbit	Cell signaling	2211	RRID: AB_331679	1:250

Exclusions:

Our paradigm for injections of AAV-rg/Cre at C5 leads to retrograde transduction of most neurons that give rise to the corticospinal tract (almost 10,000 CSNs throughout the sensorimotor cortex per hemisphere (Steward et al., 2021). However, there can be technical issues (mis-targeted injections, broken syringe tips, aliquots of AAV-rg/Cre that have deteriorated) leading to minimal or occasionally even no retrograde transduction. Several criteria were used to exclude animals with flawed or failed AAV-rg/Cre injections including: 1) assessing tdT fluorescence at the spinal cord injection site by epi-illumination of intact brains and spinal cords prior to sectioning; and 2) total number of retrogradely transduced neurons in the cortex. Young (2–4-month-old) $Rosa^{tdT}$, $5xFAD^{+/-}/Rosa^{tdT}$, $5xFAD^{+/-}/PTEN^{f/f}/Rosa^{tdT}$mice with low numbers of transduced neurons (fewer than 500 tdT labeled neurons across the sensorimotor cortex in sections 240µm apart) were excluded. There were no young (2-4 month old) $PTEN^{f/f}/Rosa^{tdT}$ mice that needed to be excluded. The criterion relating to the number of transduced cortical neurons cannot be used for older $5xFAD^{+/-}/Rosa^{tdT}$ and $5xFAD^{+/-}/PTEN^{f/f}/Rosa^{tdT}$ mice because the expected phenotype is neuron loss. We did not exclude any mice of any genotype from older groups (6-10 and 11-17 months of age). Quantifications of tdT-positive neurons in $5xFAD^{+/-}$

/Rosa^{tdT} and 5xFAD$^{+/-}$/PTEN$^{f/f}$/Rosa^{tdT}, without exclusions are shown in **Figure. 3.4D** for reference, but the data was not used to interpret the results.

2.8 Quantification of corticospinal neurons (CSNs)

For quantification of tdT-labeled neurons, coronal sections at 240 µm intervals were mounted without immunostaining onto 0.1% gelatin subbed slides. Transduced neurons were identified by native tdT fluorescence rather than by immunostaining because with IHC, robust labeling of dendrites can obscure tdT-labeled CSN cell bodies. TdT-positive CSN cell bodies in layer V of the cortex were manually counted in each section from the medial border of M1 to the lateral border of S1 using a fluorescent Olympus BX53 microscope at 20x magnification. The population of tdT-labeled CSNs in the S1 cortex posterior to bregma that are separated from the main sensorimotor cortex were not counted. Counts were taken in all sections in the series that contained tdT-labeled CSNs, which was typically from 3 mm anterior to bregma to approximately 2.5 mm posterior to bregma.

We chose to count all tdT-labeled neurons in layer V in each section rather than using single-section stereological counting techniques (the optical dissector) because cell boundaries of fluorescently labeled neurons are indistinct, and the optical dissector depends on being able to identify cell edges (caps) when focusing up and down. Another potential caveat is that there can be photobleaching with the longer periods of time required for use of the optical dissector.

2.9 Quantification of extracellular accumulations of tdT

Our results revealed the unexpected appearance of extracellular tdT-positive aggregates in areas containing tdT-positive neurons and their processes. To quantify these aggregates, we selected sections at approximately 0.74mm–0.62mm anterior to bregma (midway along the rostro-caudal axis of the sensorimotor cortex). Native tdT fluorescence in the right cortex was imaged at 20x magnification with a fluorescent Olympus BX53 microscope. The quantifications were on the right cortex because the unilateral AAV-rg/Cre injection was on the left side of the spinal cord. Multiple images were taken at 10x magnification to capture the full medio-lateral expanse of layer V containing labeled CSNs, images were tiled into a montage and imported to Fiji ImageJ (Schneider et al., 2012). The scale was set to pixels and images were converted to 8-bit format. Then, the threshold was set to 0.36–0.38% with a dark background. After thresholding, the watershed separation command was used to accurately track the clumps of debris. If any neuronal cell bodies were selected throughout the process (identified by their morphology and location in layer V), they were removed. Lastly, the particle analysis plug-in was used with the following settings: Size (pixel^2) = 100–1000, circularity = 0.30–1.00.

2.10 Fluorescence quantification of pS6 positive neurons in layer V

To quantify pS6 fluorescence, we selected a section at approximately 0.74mm–0.62mm anterior to bregma and imaged both right and left cortex at 20x magnification with a fluorescent Olympus BX53 microscope. Using image J software (Schneider et al., 2012), a region of interest within cortical layer V of the motor cortex was selected by drawing a square (width: 320 μm, height: 290 μm). The same ROI was selected in each channel of the multi-channel images. Then, using the freehand tool, Ps6 positive neuronal cell bodies were traced. Co-labeling of pS6 with tdT was determined by comparison with the tdT-only channel and the merged image. Fluorescence

intensity of pS6 was determined by the following formula: CTCF = Integrated Density − (Area × mean background) (Gavet and Pines, 2010).

2.11 Fluorescence quantification of 1D1 positive neurons in layer V

Similarly to quantification of pS6 fluorescence (Section 2.10), we quantified 1D1 fluorescence by selecting a section at approximately 0.74mm–0.62mm anterior to bregma and imaged both right and left cortex at 20x magnification with a fluorescent Olympus BX53 microscope. Using image J software (Schneider et al., 2012), a region of interest within cortical layer V of the motor cortex was selected by drawing a square (width: 320 μm, height: 290 μm). The same ROI was selected in each channel of the multi-channel images. Then, using the freehand tool, 1D1 positive neuronal cell bodies were traced. Co-labeling of 1D1 with tdT was determined by comparison with the tdT-only channel and the merged image. Fluorescence intensity of 1D1 was determined by the following formula: CTCF = Integrated Density − (Area × mean background) (Gavet and Pines, 2010).

Results

3.1 Simultaneous activation of tdTomato expression and deletion of PTEN in CSNs

To confirm and validate our model before assessing neuronal survival post-activation of the mTOR pathway, we developed 5xFAD$^{+/-}$/PTEN$^{f/f}$/Rosa^{tdT} mice to selectively delete PTEN and label a subset of the layer V neurons that degenerate in 5xFAD mice, CSNs. Mice were injected between 2-4 months of age with AAV-rg/Cre into cervical level 5 of the spinal cord to retrogradely transduce layer V CSNs and turn on tdTomato expression while deleting PTEN in

those same neurons. The brain tissue was collected at 2-4, 6-10, and 11-17 months of age (**Fig. 3.1A**). As expected, neurons in layer V of the motor cortex were robustly transduced and expressed tdT in both 5xFAD$^{+/-}$/PTEN$^{f/f}$/Rosa^{tdT}, 5xFAD$^{+/-}$/Rosa^{tdT}, PTEN$^{f/f}$/Rosa^{tdT} and Rosa^{tdT} (representative image of a 2-month-old 5xFAD$^{+/-}$/Rosa^{tdT} shown in **Fig. 3.1B**).

To confirm PTEN deletion in neurons labeled with tdT, sections were immunostained for PTEN (FITC) and tdT was observed without immunostaining (native tdT). Native tdT fluorescence revealed tdT-labeled layer V cell bodies in a young, 2-month-old PTEN$^{f/f}$/Rosa^{tdT} mouse, 2 weeks post-PTEN deletion (**Fig. 3.1C**); imaging the same section for PTEN (FITC) revealed PTEN was present all throughout the cortex except for layer V neurons that were completely negative for PTEN, appearing as "ghost cells" (**Fig. 3.1D**). A merged image of C and D documents that ghost cells are tdT-positive (Circled, **Fig. 3.1E**) demonstrating that transduction, deletion of PTEN and activation of tdT in CSNs was successful in our control model.

Next, as a control, we aimed to validate PTEN deletion in our 5xFAD$^{+/-}$/PTEN$^{f/f}$/Rosa^{tdT} model. In a 6-month-old 5xFAD$^{+/-}$/PTEN$^{f/f}$/Rosa^{tdT} mouse, 4 months post-PTEN deletion, we observed tdT-labeled CSNs in layer V of the motor cortex (**Fig. 3.1F**), PTEN-negative cell bodies termed "ghost cells" (**Fig. 3.1G**), and both are overlapping in the merged image (**Fig. 3.1H**). Given that PTEN negative, "ghost cells," are seen in layer V in older-aged 5xFAD$^{+/-}$/PTEN$^{f/f}$/Rosa^{tdT} and they co-label with tdT positive CSNs, these data demonstrate selective labeling of tdT and persistent deletion of PTEN in CSNs.

3.2 hAPP transgene expression is maintained after deletion of PTEN in 5xFAD$^{+/-}$ /PTEN$^{f/f}$/Rosa^{tdT} mice

Control for the possibility that PTEN deletion alters 5xFAD transgene expression: The rationale of this experiment is to delete PTEN and activate mTOR expression in CSNs in order to delay or prevent neurodegeneration driven by 5xFAD transgene expression. Thus, the logic of the experiment requires that PTEN deletion and mTOR activation does not interfere with the expression of the transgenes. To assess this, we co-immunostained brain sections from $5xFAD^{+/-}/PTEN^{f/f}/Rosa^{tdT}$ mice for RFP to identify transduced neurons expressing tdT (**Fig. 3.2A, D**) and 1D1 to label hAPP transgene expression (**Fig. 3.2B, E**). The representative images are a 6-month-old $5xFAD^{+/-}/PTEN^{f/f}/Rosa^{tdT}$ mouse, 4 months post-PTEN deletion (**Fig. 3.2A-F**). In the merged image (**Fig. 3.2C & F**), 1D1/RFP co-immunofluorescence (Co-IF) revealed that transduced tdT-positive neurons overlapped with 1D1 positive neurons (hAPP expressing), thus PTEN-deleted hAPP expressing neurons were identified. We then measured 1D1 fluorescence from co-labeled and 1D1-positive only neurons by tracing the neurons, measuring integrated density and accounting for the background using corrected total cell fluorescence (CTCF) (in Methods). There was no significant difference ($t(26) = 0.8396$, $p = 0.4088$) in the levels of 1D1 fluorescence between co-labeled and 1D1-positive only neurons at 1-month post-PTEN deletion (**Fig. 3.2G**). However, there was a significant difference ($t(24) = 5.404$, $p < 0.0001$) at 4 months post-deletion, as 1D1 fluorescence levels began to drop in 1D1-positive only neurons, but 1D1-fluorescence levels in co-labeled neurons were maintained (**Fig. 3.2H**). One interpretation of these data is that expression of the transgene decreases as mice age, perhaps as a result of age-related pathophysiology, but that deletion of PTEN maintains hAPP expression as the mice age.

3.3 mTOR activation due to PTEN deletion is maintained in $5xFAD^{+/-}/PTEN^{f/f}/Rosa^{tdT}$ mice

Control for the possibility that mTOR activation due to PTEN deletion does not persist as 5xFAD animals age. The logic of the experiment assumes that because PTEN is deleted permanently by genetic recombination, activation of mTOR will also be permanent across the mouse's lifetime. It is possible, however, that mTOR activation does not persist as animals age, either due to aging alone, or aging in the context of the 5xFAD mutations. To assess this, we used a well-documented immunohistochemical measure of mTOR activation – phosphorylation of ribosomal protein S6 (pS6). A 5xFAD$^{+/-}$/PTEN$^{f/f}$/Rosa^{tdT} mouse received an injection of AAV-rg/Cre at 2 months and was perfused at 6 months of age. Coronal sections through the sensorimotor cortex were immunostained using a pS6 antibody that identified endogenous levels of ribosomal pS6 phosphorylated at Serine 235/236 (FITC secondary). Retrogradely-transduced neurons were identified by their native tdT fluorescence. Representative images of native tdT are shown in **Fig. 3.3A** – right cortex and **Fig. 3.3D** – left cortex. Immunostaining for pS6 in the same sections revealed that pS6 was present in both hemispheres (**Fig. 3.3B** – right cortex and **Fig. 3.3E** – left cortex). In the merged image of tdT and pS6 fluorescence, tdT-positive neurons co-labeled with pS6 in layer V of the sensorimotor cortex (**Fig. 3.3C** – right cortex and **Fig. 3.3F** – left cortex). Co-labeling suggests that mTOR activation was successful and sustained in CSNs, rather than being transient.

To determine if PTEN-deletion resulted in mTOR activation higher than endogenous levels, we first had to establish a control. We took advantage of our model's paradigm – we unilaterally injected AAV-rg/Cre into the spinal cord; thus the majority of transduced CSNs, shown by tdT-labeling, were on the contralateral cortex (right cortex, **Fig. 3.3A**). As expected, we observed

fewer tdT-labeled neurons in the ipsilateral cortex (left cortex, **Fig. 3.3D**). Along with fewer tdT-positive neurons, we qualitatively observed few pS6-positive neurons in the left cortex (**Fig. 3.3E**). Due to the low quantity of tdT-positive neurons, we also observed few pS6 neurons overlapping with tdT-positive neurons (**Fig. 3.3F**). Given the difference in number of transduced neurons between the left and right cortex, we now had an internal control paradigm.

Next, we used the internal control and PTEN-deleted model to quantitatively assess whether PTEN-deletion resulted in over-activation of the mTOR pathway in $5xFAD^{+/-}/PTEN^{f/f}/Rosa^{tdT}$ mice. We assessed this by quantifying levels of pS6 fluorescence in the left and right cortex of $5xFAD^{+/-}/PTEN^{f/f}/Rosa^{tdT}$ mice by determining integrated density within each cell and accounting for the background using corrected total cell fluorescence (CTCF) (in Methods). (**Fig. 3.3G & H**). In a 3-month-old mouse, 1-month post-PTEN-deletion, we quantified pS6 fluorescence in neurons co-labeled with tdT (PTEN-deleted neurons) of the right cortex. Along with this, we quantified pS6 fluorescence in tdT- negative neurons (non-PTEN deleted neurons) of the left cortex. Shown on a log scale graph, the levels of pS6 are significantly higher in tdT-positive (PTEN-deleted neurons ($t(21) = 4.501$, $p = 0.0002$)) between the two groups of cells (**Fig. 3.3G**). These data confirm continued mTOR activation in PTEN-deleted neurons 1-month post-PTEN deletion.

To determine whether mTOR activation was sustained post-PTEN-deletion, we carried out the same assessment for a 6-month-old mouse, 4 months post-deletion. Assessment of pS6 fluorescence by determining integrated density within each cell and calculating CTCF confirmed higher levels of S6 phosphorylation in CSNs in tdT-positive neurons in the right

cortex versus tdT-negative neurons in the left cortex ($t(98) = 12.18$, $p < 0.0001$) (**Fig. 3.3H**). These results indicate that phosphorylation of ribosomal S6 persists in PTEN-deleted neurons at 4 months post-deletion is even higher than at 1 month.

3.4 PTEN deletion does not alter normal CSN counts in PTEN$^{f/f}$/Rosa^{tdT} mice

To first test whether PTEN deletion alone leads to CSN loss, as a control, we quantified tdT labeled neurons between 2-4, 6-10 and 11-17 months comparing PTEN$^{f/f}$/Rosa^{tdT} and Rosa^{tdT} mice. We quantified tdT-labeled CSNs in a 1-in-8 series of 30 μm sections spanning the rostro-caudal extent of the sensorimotor cortex of the right hemisphere (contralateral to the injection) (**Fig. 3.4A**). Numbers of tdT labeled neurons were comparable across age in PTEN$^{f/f}$/Rosa^{tdT} and Rosa^{tdT} mice. Neuron numbers were slightly lower by 6-10 months of age and 11-17 months of age in both genotypes but only by about 36% in PTEN$^{f/f}$/Rosa^{tdT} and 30% in Rosa^{tdT} mice by 11-17 months of age. A two-way ANOVA comparing genotype (PTEN$^{f/f}$/Rosa^{tdT} and Rosa^{tdT}) and age revealed a significant main effect of age ($F(2, 34) = 3.762$, $p = 0.0334$) but no significant differences between genotype ($F(1, 34) = 0.07134$, $p = 0.7910$) and no significant age x genotype interaction ($F(2, 34) = 0.09532$, $p = 0.9093$). Post-hoc analysis with Tukey's multiple comparisons correction test revealed no significant differences amongst any of the pairwise comparisons (all adjusted $p > 0.1087$) (**Fig. 3.4A**). After correction with Tukey's multiple comparisons test the significant main effect of age was not associated with a specific pairwise comparison. These results reveal that PTEN deletion does not lead to greater neuronal loss in PTEN$^{f/f}$/Rosa^{tdT} mice when compared to Rosa^{tdT} at their matched age groups, because of this we did not include them in the rest of our analyses.

3.5 CSN neuron loss and accumulation of tdT-positive debris are not altered by PTEN deletion in 5xFAD$^{+/-}$/PTEN$^{f/f}$/Rosa^{tdT} mice

To determine whether PTEN deletion reduced neurodegeneration in 5xFAD mice, we quantified tdT labeled neurons in 3 age ranges (2-4, 6-10 and 11-17 months of age) in 5xFAD$^{+/-}$/PTEN$^{f/f}$/Rosa^{tdT} and 5xFAD$^{+/-}$/Rosa^{tdT} mice. **Fig. 3.4B** shows a representative image of tdT labeled CSNs in layer V of the motor cortex of 5xFAD$^{+/-}$/Rosa^{tdT} mice. **Figure 3.4C** illustrates counts of the total number of labeled CSNs, done in the same manner as **Fig. 3.4B** – in a 1-in-8 series of 30 μm sections spanning the rostro-caudal extent of the sensorimotor cortex of the right hemisphere. In the 5xFAD$^{+/-}$/Rosa^{tdT} and 5xFAD$^{+/-}$/PTEN$^{f/f}$/Rosa^{tdT} neuronal counts decreased substantially, about 86% in 5xFAD$^{+/-}$/Rosa^{tdT} and 85% in 5xFAD$^{+/-}$/PTEN$^{f/f}$/Rosa^{tdT} to what was seen in young mice. In the 5xFAD$^{+/-}$/Rosa^{tdT} mice, the neuronal counts were approximately between 1,000-1,500 in young mice (2-4 months old) and were reduced to less than 500 past 11 months of age (**Fig. 3.4C**). In 5xFAD$^{+/-}$/PTEN$^{f/f}$/Rosa^{tdT} mice, neuronal counts ranged from approximately 500-2,500 in the young mice (2-4 months of age) to below 1,000 past 11 months of age (**Fig. 3.4C**). Analysis by two-way ANOVA revealed a significant main effect of age ($F(2, 38) = 40.37$, $p < 0.0001$), but no significant main effect of genotype ($F(1, 38) = 0.4503$, $p = 0.5062$) and no significant interaction effect of age and genotype ($F(2, 38) = 0.03547$, $p = 0.9652$). Tukey's multiple comparisons test revealed that tdT-labeled CSNs were significantly lower in 5xFAD$^{+/-}$/PTEN$^{f/f}$/Rosa^{tdT} and 5xFAD$^{+/-}$/Rosa^{tdT} mice at 6-10 months (adjusted $p < 0.0001$, for both genotypes) and 11+ months (adjusted $p < 0.0001$, for both genotypes) compared to 2-4 months. In contrast, CSN counts in 5xFAD$^{+/-}$/PTEN$^{f/f}$/Rosa^{tdT} and 5xFAD$^{+/-}$/Rosa^{tdT} mice did not significantly differ when compared to each other at 2-4, 6-10, and 11+ months of age ($p > 0.6$, for all comparisons) (**Fig. 3.4C**). These results suggest that PTEN-deletion does not

prevent or delay CSN neurodegeneration in our 5xFAD model. While we are only interpreting the quantifications of tdT-positive neurons based on our exclusion criteria, we have included the full quantification data for reference (**Fig. 3.4D**).

While testing whether activation of a growth program by deleting PTEN would result in neurons resisting neurodegeneration, it was important to address previous studies that suggest that PTEN deletion and mTOR activation might exacerbate neurodegeneration in 5xFAD mice. Specifically, the idea here is that mTOR is a negative regulator of the autophagy pathway, so activation of mTOR due to PTEN deletion would decrease clearance autophagy and clearance of cellular waste. The decrease in autophagy is thought to result in an intraneuronal accumulation of aberrant proteins and increase neurodegeneration in the context of AD. Thus, to assess whether PTEN deletion enhances age-dependent degeneration of CSNs we reviewed our previous results from tdT-labeled CSN counts in 5xFAD$^{+/-}$/PTEN$^{f/f}$/Rosa^{tdT} and 5xFAD$^{+/-}$/Rosa^{tdT} mice (**Fig. 3.4C**). Since there are no significant differences in CSN degeneration between the two genotypes at any age group, as reported above, the data suggests that PTEN deletion neither reduces nor enhances neurodegeneration.

5xFAD female mice have been reported to have a more aggressive Aβ pathology compared to male mice (Forner et al., 2021; Poon et al., 2023). Due to differences in pathology, we assessed whether female mice show greater neuron loss than males. We compared tdT-positive neuron counts in male and female 5xFAD$^{+/-}$/Rosa^{tdT} and 5xFAD$^{+/-}$/PTEN$^{f/f}$/Rosa^{tdT}. We looked at mice of 11-17 months of age since the greatest amount of neurodegeneration occurs past 9 months of age (Crowe and Ellis-Davies, 2013; Eimer and Vassar, 2013). Female mice of both genotypes had fewer tdT-positive neurons than male mice in both age groups (**Fig. 3.4E**).

The males had approximately three times as many tdT-positive neurons than as females. Analysis by two-way ANOVA revealed a significant main effect of sex ($F(1, 18) = 6.034$, $p = 0.0244$), no significant main effect of genotype ($F(1, 18) = 0.1048$, $p = 0.7499$) and no interaction ($F(1, 18) = 0.003441$, $p = 0.9539$), revealing that fewer tdT-positive CSNs survive to 11-17 months of age in female mice compared to males, regardless of PTEN deletion. However, post-hoc comparisons with Sidak's correction found no significant difference between males and females within either genotype ($5xFAD^{+/-}/PTEN^{f/f}/Rosa^{tdT}$, $p = 0.2189$; $5xFAD^{+/-}/Rosa^{tdT}$, $p = 0.1547$). These data reveal that fewer CSNs survive in females compared to males by 11-17 months of age but the sex difference doesn't depend on PTEN deletion.

As reported in Chapter 2, as the mice aged, we found that tdT remained in the cortex even when tdT labeled neurons were no longer present. The accumulations were found primarily in layers V/VI (**Fig. 3.4F**). To assess whether the tdT-positive accumulations differed across age, we quantified tdT-positive particles in sections at approximately midway along the rostro-caudal axis of the sensorimotor cortex. We term these particles "tdT-debris". For this analysis, we imaged the right cortex and used the particle analysis plug-in on FIJI (image J) (details in Methods). Assessment and quantifications of tdT-positive accumulations revealed that the average number of tdT-positive accumulations ranged from 14.5-333 across the groups of 6-10 and 11-17 months of age in 5xFAD mice (**Fig. 3.4G**). However, tdT-positive accumulations were not present in 2-4 months of age across any of the genotypes. With this data we found that tdT-positive accumulations increased as the 5xFAD groups aged (**Fig. 3.4G**), and this increase corresponded to the age ranges at which CSN count decreased **(Fig. 3.4C**). Thus, the temporal relationship between tdT+ accumulations and CSN counts, along with our previously published

findings (Gallardo and Steward, 2026), suggests that the tdT-positive accumulations could be used as a secondary measure of neurodegeneration.

Next, to assess whether PTEN-deletion delayed or prevented accumulation of tdT-positive debris in 5xFAD (5xFAD$^{+/-}$/PTEN$^{f/f}$/Rosa^{tdT}) vs. non-PTEN deleted 5xFAD mice (5xFAD$^{+/-}$/Rosa^{tdT}), we compared debris counts across age in the two genotypes. As reported in Gallardo and Steward (2026), debris counts increased with age in non-PTEN deleted 5xFAD mice. Mixed effects ANOVA revealed a significant main effect of age ($F(1.347, 31.65) = 20.20$, $p < 0.0001$) but no significant main effect of genotype ($F(1, 47) = 1.719$, $p = 0.1962$) and no significant interaction ($F(2, 47) = 2.143$, $p = 0.1286$). A post-hoc analysis with Tukey's multiple comparisons correction test revealed no significant differences between 5xFAD$^{+/-}$/PTEN$^{f/f}$/Rosa^{tdT} and 5xFAD$^{+/-}$/Rosa^{tdT} mice at 2-4, 6-10 months and 11-17 months of age (**Fig. 3.4G**). Together, our data suggest that PTEN-deletion does not prevent or delay age-related increases in tdT-positive debris.

3.6 Pilot study for in vivo tracking of CSNs across age

To assess progression and timing of neuronal degeneration *in vivo,* we tested a model that uses firefly luciferase (fLuc) to report neuronal expression of AAV cargos. Mice were injected with an AAV-retrograde (rg)-fLuc into thoracic level 9 (T9) of the spinal cord to selectively transduce neurons that have projections to that region of the spinal cord, corticospinal neurons (CSNs). Luminescence imaging provides a means to repeatedly assess signal from CSNs over time, and potentially track neurodegeneration of CSNs across age in the same cohort of animals.

We first assessed whether bioluminescent signal was selectively emitting from the motor cortex. We imaged coronal slice cultures taken from CamKIIa mice that had been previously injected with AAV-rg-fLuc and emission of luminescence in the brain had been visualized on the IVIS *in vivo* (details in Methods) prior to euthanizing the animal and collecting the brain. The slices were maintained with aCSF and D-Luciferin while imaging under the IVIS, allowing for emission of bioluminescence. Bioluminescent signal was detected on the IVIS and depicted as a heat map in the motor cortex in areas that are known to have axons of CSNs (i.e. internal capsule) (**Fig. 3.5A**). These data revealed that bioluminescent signal was in brain regions that contained CSNs.

To determine whether bioluminescent signal was specifically coming from CSNs, we imaged sections with a Princeton ProEM-HS EM-CCD camera to achieve higher spatial resolution. Luminescence appeared near the surface of the cortex, in layer V, presumably labeling the apical dendritic tufts, layer V pyramidal neurons and the axons running down to the internal capsule (**Fig. 3.5B**). Our results showed that bioluminescence signal was morphologically consistent with all structures of CSNs.

Next, we aimed to validate the model as a platform for tracking neurodegeneration. To do this, we assessed whether bioluminescent signal persisted in control mice over the course of weeks. Bioluminescent signal was tracked in the spinal cord and brain throughout age. The signal was visualized by administering D-Luciferin prior to imaging on the IVIS and was detected in both the cortex and at the injection site. We used control CamKIIa mice since we did not expect neurodegeneration to occur in this model and intended to use it to assess the stability of bioluminescence signal over time. The mice were injected at 2 months of age with AAV-rg-fLuc,

as mentioned above, and imaged over the course of one month. Standard photographs of mice were captured and overlaid with images of bioluminescence signal. Bioluminescence was shown in a heat map indicating relative photon radiance (**Fig. 3.5C**). The mice were imaged periodically, every 1-4 days, and bioluminescent signal was recorded. Our data revealed that luminescence peaked 11-12 days post-injection in the brain and 7-9 days post-injection in the spinal cord. However, luminescence rapidly decreased in both the brain and spinal cord after the peak (**Fig. 3.5D**). The decline in luminescent signal occurred in control mice where neurodegeneration was not expected, suggesting that the decrease in bioluminescent signal was not due to neuronal loss.

Together, our data revealed that while the model was successful in targeting CSNs to produce bioluminescent signal, the signal did not persist. This loss of signal over time precludes use of this approach for tracking age-related neurodegeneration *in vivo*.

Discussion

Activation of the Mammalian target of Rapamycin (mTOR) pathway, via PTEN deletion, has been widely studied in the context of neuronal regeneration in the central nervous system (Liu et al., 2010) and has been found to promote neuronal survival after spinal cord injury (Park et al., 2008). Given this, we hypothesized that constitutive activation of the AKT/mTOR pathway via PTEN deletion might preserve corticospinal neurons (CSNs) from degeneration in a neurodegenerative model, the 5xFAD mouse model. However, our results demonstrate that PTEN deletion did not delay or prevent CSN degeneration, nor did it accelerate neurodegeneration as would be predicted by other hypotheses.

Our results also validated our model demonstrating that PTEN was successfully deleted by the presence of PTEN-negative cells "ghost cells" overlapping with tdT-positive neurons. We demonstrated that mTOR was activated by confirming the phosphorylation of ribosomal S6, a downstream target of mTOR activation. PS6 was elevated at 1 month and at 4 months, demonstrating sustained mTOR activation. Lastly, we demonstrated that PTEN deletion/mTOR activation didn't alter hAPP transgene expression in 5xFAD mice by fluorescence quantification of hAPP immunofluorescence.

4.1 PTEN deletion did not delay CSN degeneration in the 5xFAD$^{+/-}$/PTEN$^{f/f}$/Rosa^{tdT} model.

The possible explanations that may account for the lack of neuroprotection following PTEN deletion are as follows: First, while PTEN deletion and downstream mTOR activation have been shown to promote neuronal survival in injury models (Park et al., 2008), the neurons were otherwise healthy. In the 5xFAD$^{+/-}$/PTEN$^{f/f}$/Rosa^{tdT} model, rapid intraneuronal amyloid accumulation is occurring simultaneously with mTOR activation. Thus, amyloid accumulation may exceed a threshold beyond which neuroprotective signaling, through mTOR pathway activation, is not sufficient to counteract neurodegeneration. In other words, PTEN deletion may be neuroprotective in models with functional neurons, but the aggressive early-onset amyloidosis pathology of 5xFAD mice may be too extensive.

Second, mTOR signaling has itself been reported to be upregulated in AD (Li et al., 2005; Tramutola et al., 2015), suggesting that there is a possibility the pathway may be hitting a limit

of activation prior to our manipulation. If so, deleting PTEN may not be doing much more to further activate mTOR signaling in a way that would allow for neuronal survival.

Third, the timing of AAV-rg/Cre injections, and thus PTEN deletion, were done prior to what appeared to be substantial neuron loss. We determined that neuronal loss occurred by a decrease in tdT-positive neurons along with an appearance of tdT-positive debris, but it's possible that neurodegeneration began before this temporal window. It's possible that we are intervening past the time that neuroprotective mechanisms can take effect.

Finally, we acknowledge that our statistical power to detect a protective effect was limited by sample size, which may have obscured a true but small effect of genotype on CSN survival. This limitation should be considered when interpreting the results for neurodegeneration quantification.

4.2 Future directions: longitudinal in vivo tracking of CSN survival

A major limitation of our current 5xFAD$^{+/-}$/PTEN$^{f/f}$/Rosa^{tdT} model is the inability to pinpoint exactly when CSN degeneration begins and how it progresses over time within the same mouse. *In vivo* bioluminescent imaging of CSNs across multiple timepoints would allow us to longitudinally track CSNs and better determine the start and rate of degeneration, rather than using multiple mice. Using the same mouse would remove a source of variation, that results from using multiple mice, that could affect the rate of neurodegeneration. However, in our bioluminescence imaging experiments, we observed a sharp reduction in bioluminescence after

12 days post-AAV-rg-fLuc injection in a non-neurodegenerative model (CamKIIa mice, controls). Since neurodegeneration was not expected in this model, it suggests that the early decline in luminescence is more likely due to loss of viral expression rather than neurodegeneration. If the bioluminescent signal had persisted for months, we would've been able to test this platform in 5xFAD$^{+/-}$/PTEN$^{f/f}$/Rosa^{tdT} mice and track their neurodegeneration. In 5xFAD mice, CSN loss or dysfunction would be expected to reduce or eliminate their ability to process D-luciferin and therefore produce bioluminescence. Thus, a decline in signal would reflect neurodegeneration and be detectable across age.

Figures

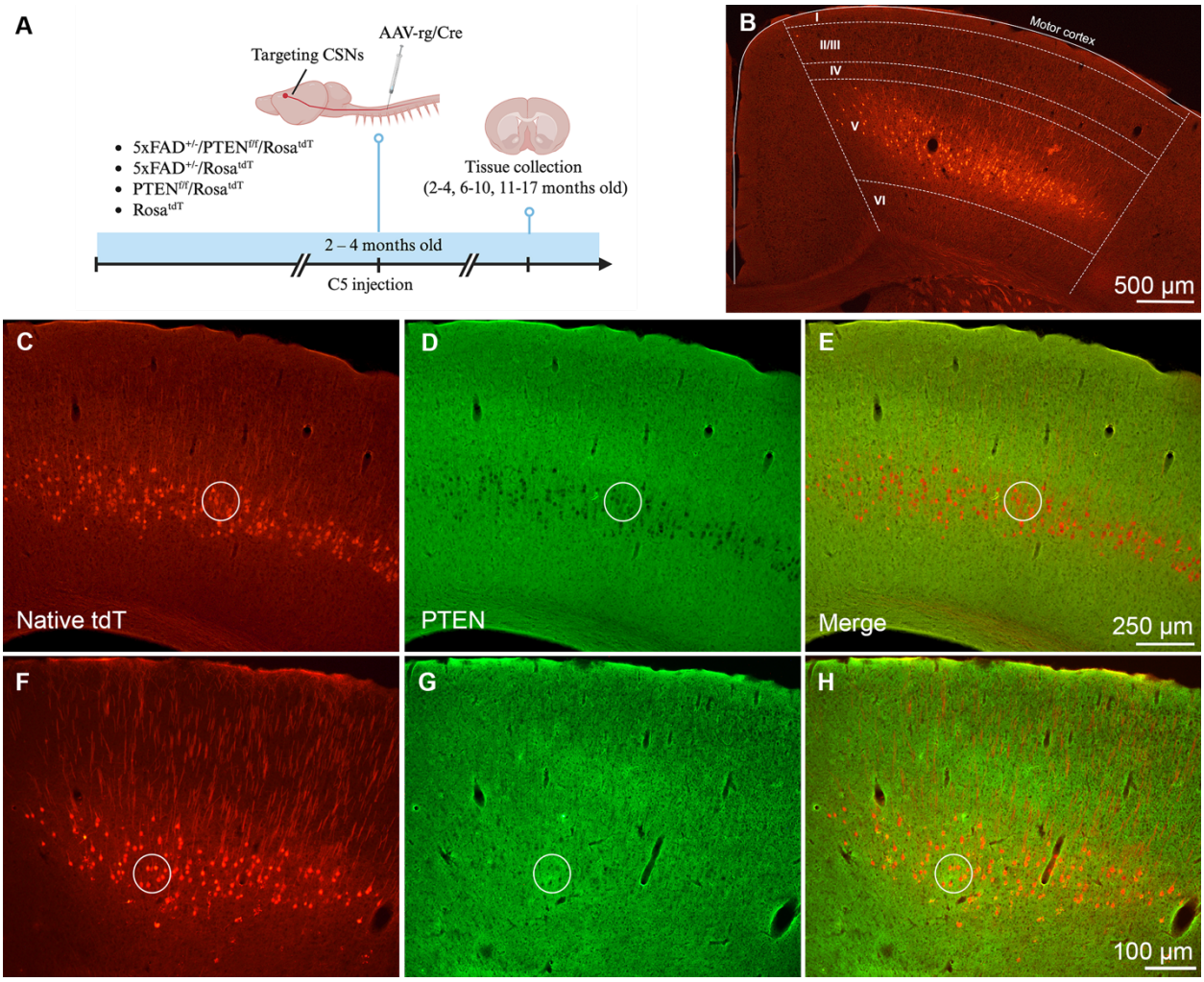


Figure 3.1. PTEN is deleted in corticospinal neurons of 5xFAD$^{+/-}$/ PTEN$^{f/f}$/Rosa^{tdT} and PTEN$^{f/f}$/Rosa^{tdT} mice.

(A) A schematic of the experimental timeline. AAV-rg/Cre was injected into vertebral level C5 of the spinal cord at 2–4 months of age to retrogradely label CSNs with tdT and simultaneous PTEN deletion. Tissue was collected at 2–4, 6–10 or 11–17 months of age across four genotypes: 5xFAD$^{+/-}$/ PTEN$^{f/f}$/Rosa^{tdT}, 5xFAD$^{+/-}$/Rosa^{tdT}, PTEN$^{f/f}$/Rosa^{tdT} and Rosa^{tdT}. **(B)** Native tdT

labeling of CSNs in layer V of the motor cortex in a 2-month-old 5xFAD$^{+/-}$/Rosa^{tdT} mouse. **(C-H)** PTEN deletion in tdT-labeled CSNs, visualized by loss of PTEN immunostaining within tdT+ neurons (circled). Native tdT (**C, F**), PTEN immunostaining (**D, G**) and merged images (**E, H**) are shown in a PTEN$^{f/f}$/Rosa^{tdT} mouse injected with AAV-rg/Cre 2 weeks prior to tissue collection at 2 months of age (**C-E**) and injected with AAV-rg/Cre at 2 months of age and collected at 12 months of age (**F-H**). Circled regions highlight tdT+ neurons with absent PTEN signal, confirming Cre-mediated recombination. Scale bars: 500µm (**B**), 250 µm (**C-E**), 100 µm (**F-H**).

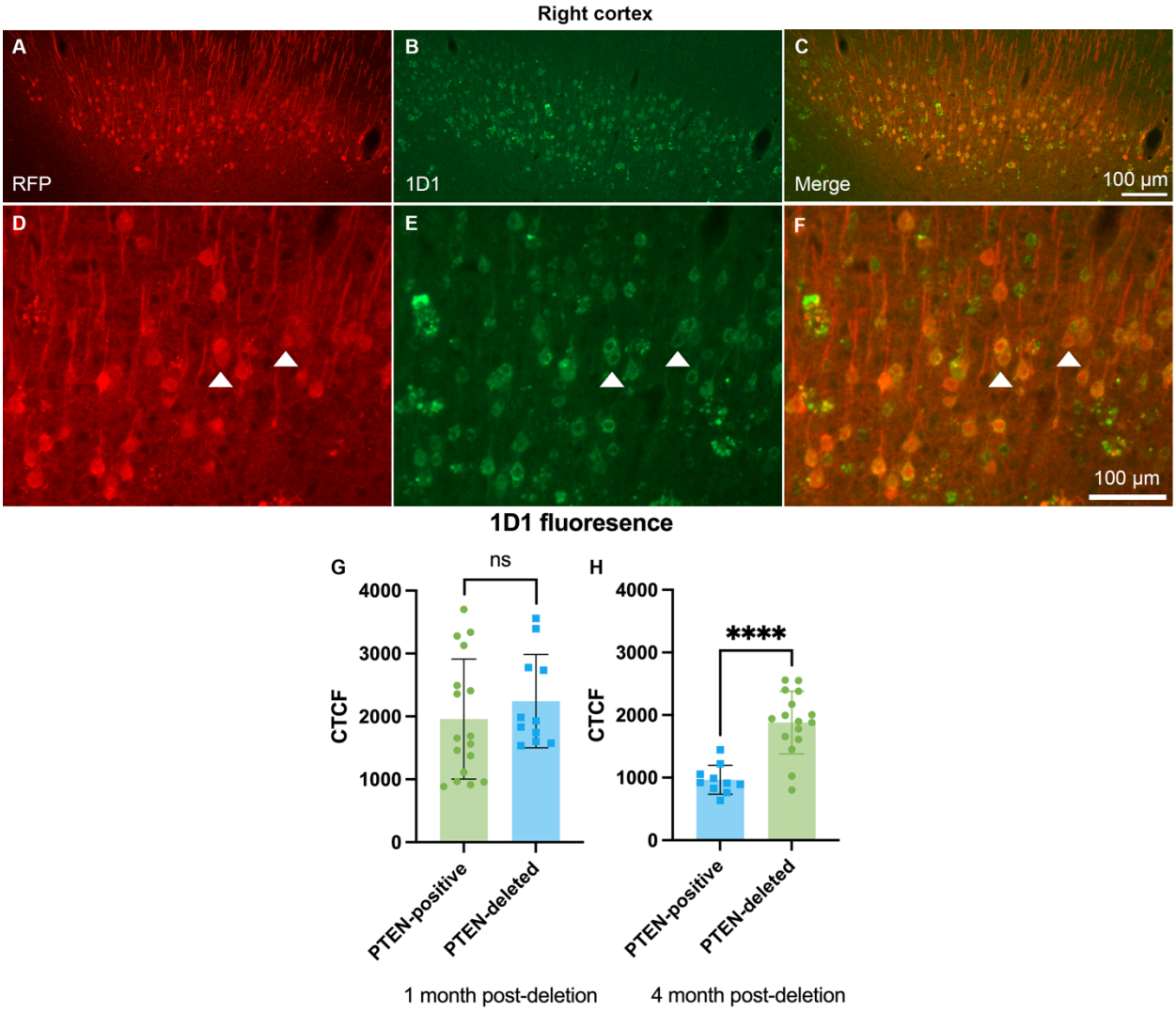


Figure 3.2. PTEN deletion maintains hAPP transgene expression as the 5xFAD$^{+/-}$/ PTEN$^{f/f}$/Rosa^{tdT} mice age.

(A-C) Representative image of the right cortex, contralateral to the AAV-rg/Cre injection into the left side of the spinal cord, containing tdT-positive PTEN-deleted CSNs in a 6-month-old 5xFAD$^{+/-}$/PTEN$^{f/f}$/Rosa^{tdT} mouse. **(A)** RFP staining, **(B)** 1D1 staining and **(C)** merged image. **(D-F)** Higher magnification image of the same coronal brain section as **(A-C)**. **(D)** RFP staining, **(E)** 1D1 staining and **(F)** merged image. 1D1 fluoroscence signal is comparable at **(G)** 1 month and

(H) 4 months post-deletion in the PTEN deleted neurons, indicating that PTEN deletion does not diminish hAPP transgene expression. Scale bar: **(A-F)** 100 μm.

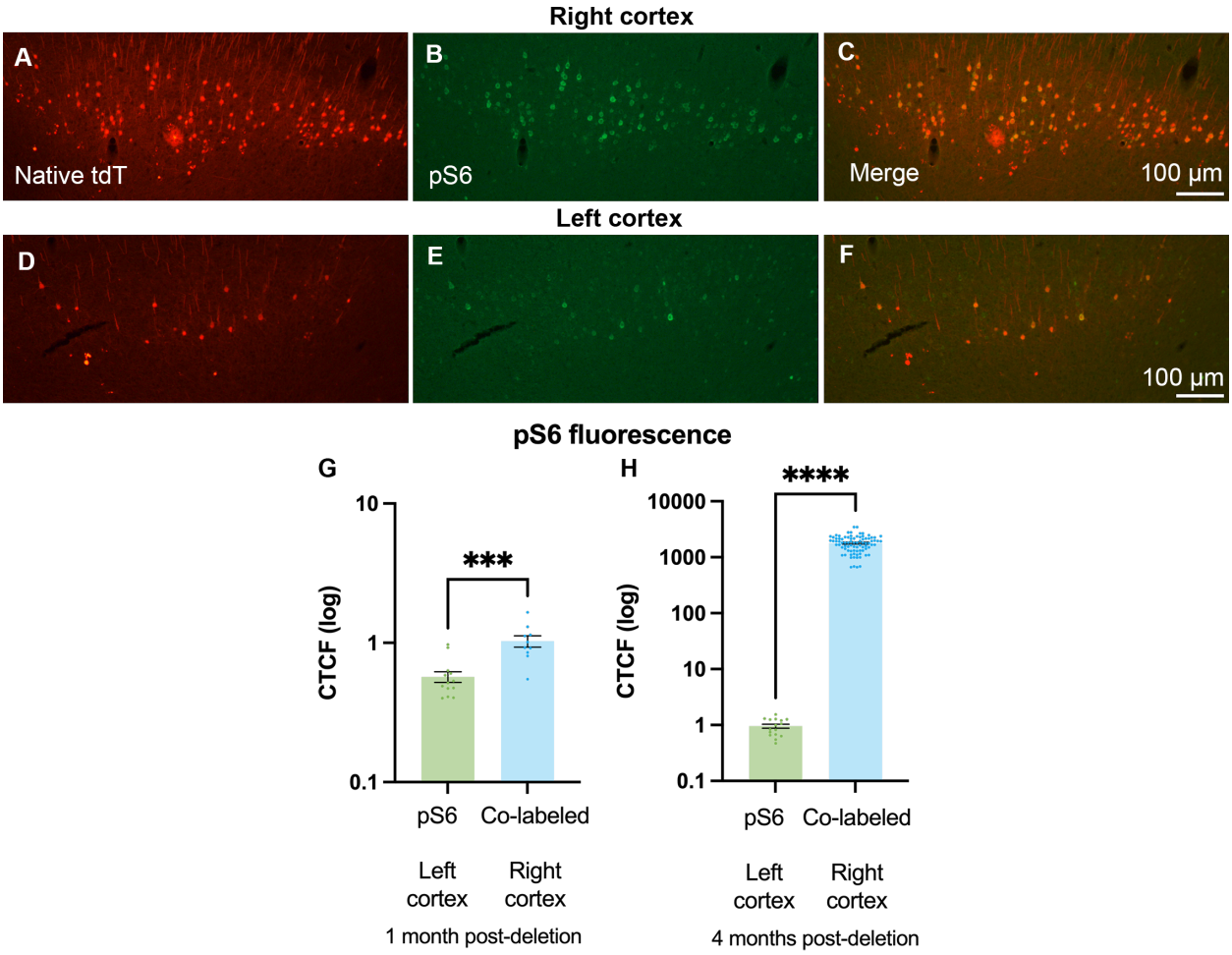


Figure 3.3. Successful activation of the mTOR pathway persists 4 months post-PTEN deletion.

(A-F) Phospho-S6 (pS6 Ser235/236) immunostaining shows activation of the mTOR pathway following PTEN deletion. Shown in the **(A-C)** right cortex and **(D-F)** left cortex of a 5xFAD$^{+/-}$/PTEN$^{f/f}$/Rosa^{tdT} mouse injected at 3 months of age with tissue collected at 4 months of age. **(G)** Quantification of pS6 fluorescence in cells co-labeling with tdT and non-co-labeled **(G)** 1-month post-PTEN deletion (injected at 3 months of age with tissue collected at 4 months of age) and

(H) 4 months post-PTEN deletion (injected at 2 months of age with tissue collected at 6 months of age).

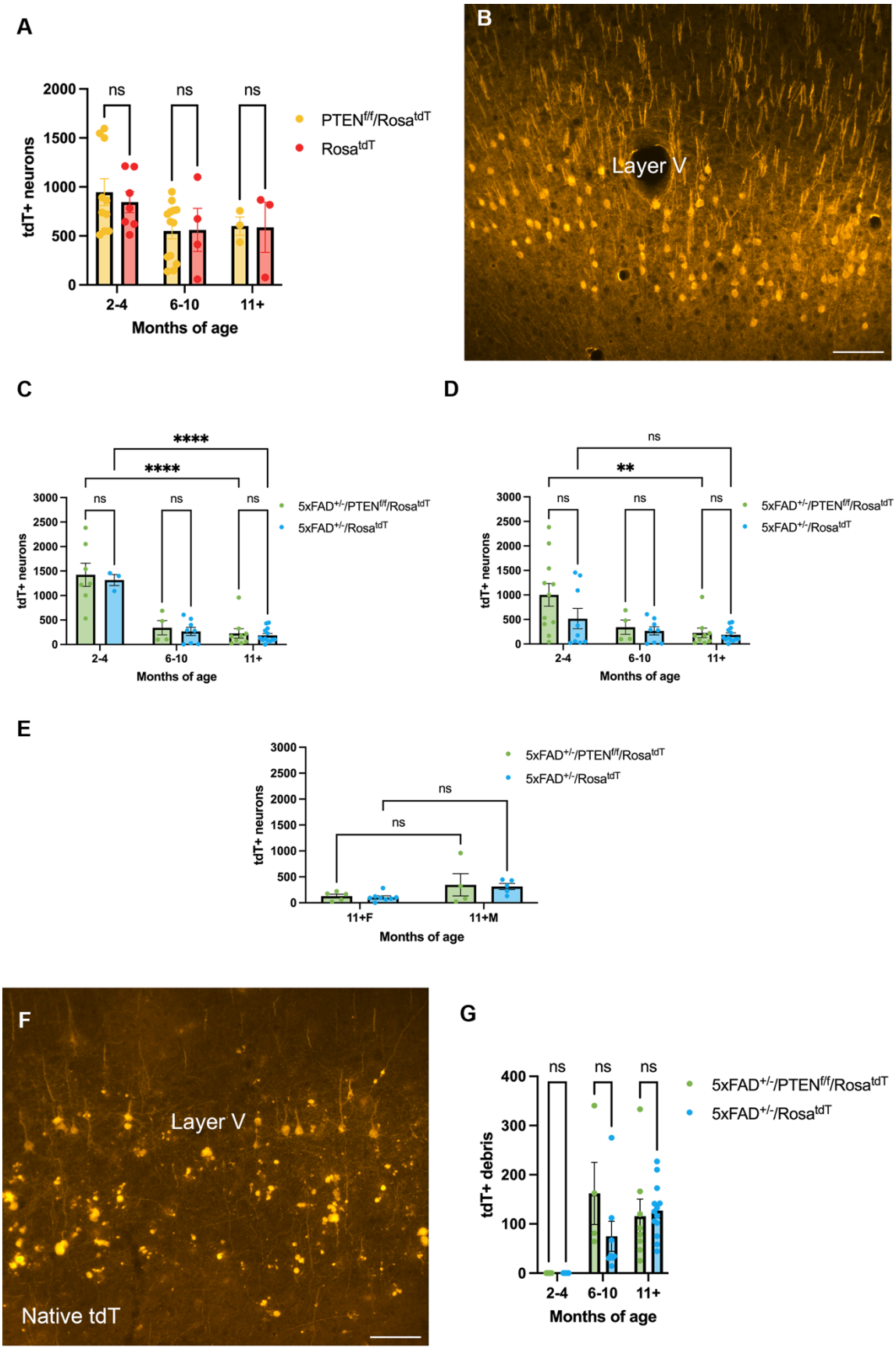

A
2000
1500
1000
500
0
tdT+ neurons
ns
ns
ns
2-4
6-10
11+
Months of age
PTEN^f/f/Rosa^tdT
Rosa^tdT
B
Layer V
C
****
****
ns
ns
ns
3000
2500
2000
1500
1000
500
0
tdT+ neurons
2-4
6-10
11+
Months of age
5xFAD^+/-/PTEN^f/f/Rosa^tdT
5xFAD^+/-/Rosa^tdT
D
ns
**
ns
ns
ns
3000
2500
2000
1500
1000
500
0
tdT+ neurons
2-4
6-10
11+
Months of age
5xFAD^+/-/PTEN^f/f/Rosa^tdT
5xFAD^+/-/Rosa^tdT
E
3000
2500
2000
1500
1000
500
0
tdT+ neurons
ns
ns
11+F
11+M
Months of age
5xFAD^+/-/PTEN^f/f/Rosa^tdT
5xFAD^+/-/Rosa^tdT
F
Layer V
Native tdT
G
400
300
200
100
0
tdT+ debris
ns
ns
ns
2-4
6-10
11+
Months of age
5xFAD^+/-/PTEN^f/f/Rosa^tdT
5xFAD^+/-/Rosa^tdT

Figure 3.4. Quantifications of tdT-labeled neurons decline as accumulations increase with age.

(A) Neuronal quantifications of tdT-positive neurons in 2-4, 6-10, and 11-17 months old $PTEN^{f/f}/Rosa^{tdT}$ and $Rosa^{tdT}$ mice show no significant differences. **(B)** Representative image of tdT-labeled neurons in layer V of a 2-month-old $5xFAD^{+/-}/Rosa^{tdT}$ mouse. **(C)** Neuronal quantifications of tdT-positive neurons in $5xFAD^{+/-}/PTEN^{f/f}/Rosa^{tdT}$, $5xFAD^{+/-}/Rosa^{tdT}$ show a decline in tdT-positive neurons. **(D)** Full neuronal quantifications of tdT-positive neurons in $5xFAD^{+/-}/PTEN^{f/f}/Rosa^{tdT}$, $5xFAD^{+/-}/Rosa^{tdT}$, without exclusions. **(E)** Neuronal quantifications of tdT-positive neurons in male and female $5xFAD^{+/-}/PTEN^{f/f}/Rosa^{tdT}$ and $5xFAD^{+/-}/Rosa^{tdT}$ 11-17 month old mice show no significant differences between sex in each genotype. **(F)** Representative image of tdT-positive accumulations found in layer V/VI of the cerebral cortex of a 12-month-old $5xFAD^{+/-}/Rosa^{tdT}$ mouse. **(G)** Quantifications of tdT-labeled accumulations in $5xFAD^{+/-}/PTEN^{f/f}/Rosa^{tdT}$ and $5xFAD^{+/-}/Rosa^{tdT}$ between 2-4, 6-10, 11-17 months of age, showing increase in accumulations with age. Scale bar: A & F 200μm.

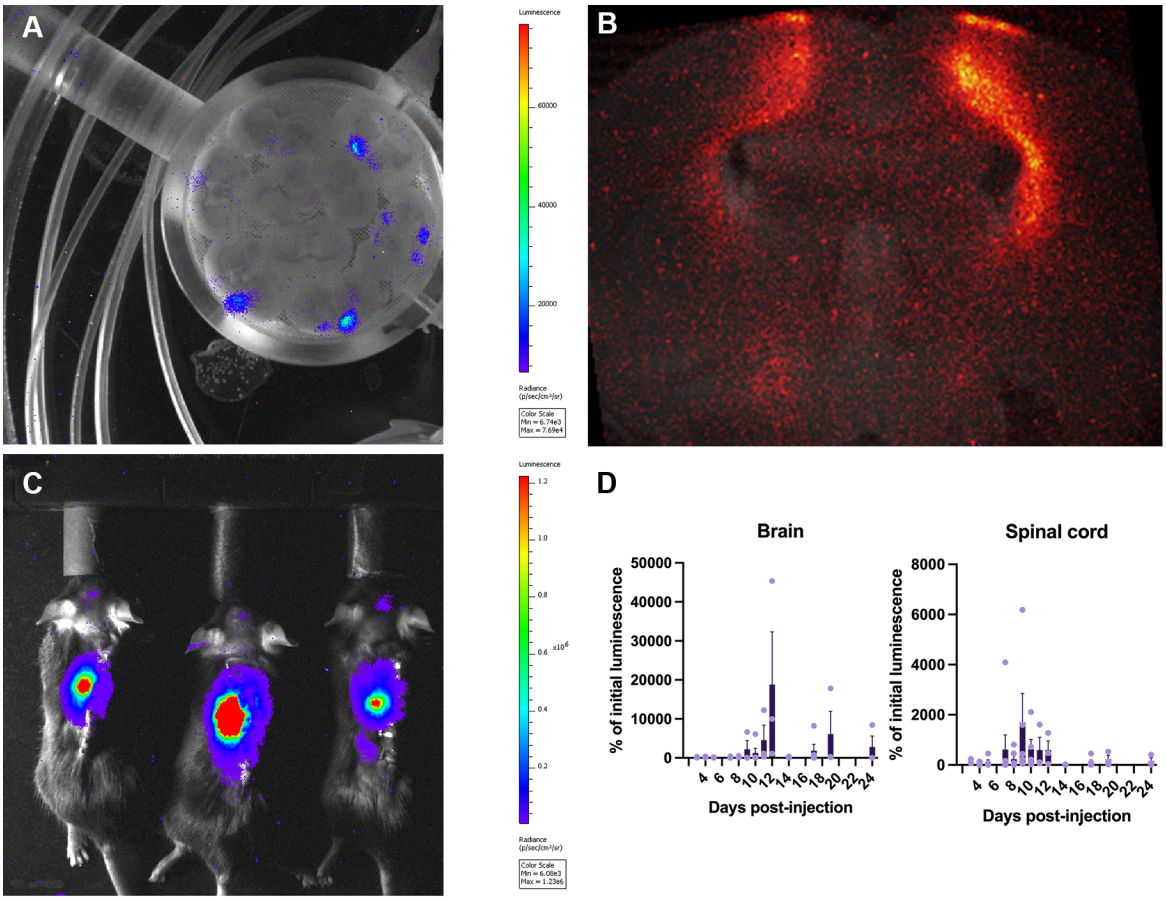


Figure 3.5. Longitudinal bioluminescent labeling of CSNs in brain and spinal cord declines.

(A) Bioluminescent imaging in coronal brain slices, with signal localized to the motor cortex and internal capsule. **(B)** Representative coronal brain section showing bilateral bioluminescent signal throughout the presumed neuronal cell bodies and dendritic tufts of CSNs in the motor cortex and their axons. **(C)** *In vivo* bioluminescent imaging showing signal in the brain and spinal cord. **(D)** Quantification of bioluminescent signal, shown as % of initial luminescence across days post-injection (PI) in the brain and spinal cord. Peak signal intensity and subsequent decline past 12 days PI are seen.

References

1. Oakley, H. et al. Intraneuronal beta-amyloid aggregates, neurodegeneration, and neuron loss in transgenic mice with five familial Alzheimer's disease mutations: potential factors in amyloid plaque formation. J Neurosci 26, 10129–10140 (2006).
2. Gallent, E. A. & Steward, O. Neuronal PTEN deletion in adult cortical neurons triggers progressive growth of cell bodies, dendrites, and axons. Exp Neurol 303, 12–28 (2018).
3. Eimer, W. A. & Vassar, R. Neuron loss in the 5XFAD mouse model of Alzheimer's disease correlates with intraneuronal Aβ42 accumulation and Caspase-3 activation. Molecular Neurodegeneration 8, 2 (2013).
4. Tervo, D. G. R. et al. A Designer AAV Variant Permits Efficient Retrograde Access to Projection Neurons. Neuron 92, 372–382 (2016).
5. Yonan, J. M. & Steward, O. Vector-mediated PTEN deletion in the adult dentate gyrus initiates new growth of granule cell bodies and dendrites and expansion of mossy fiber terminal fields that continues for months. Neurobiol Dis 184, 106190 (2023).
6. Metcalfe, C. D. et al. An introduction to the sources, fate, occurrence and effects of endocrine disrupting chemicals released into the environment. Environ Res 207, 112658 (2022).
7. Terry, R. D. et al. Physical basis of cognitive alterations in alzheimer's disease: Synapse loss is the major correlate of cognitive impairment. Annals of Neurology 30, 572–580 (1991).
8. Thal, D. R., Rüb, U., Orantes, M. & Braak, H. Phases of A beta-deposition in the human brain and its relevance for the development of AD. Neurology 58, 1791–1800 (2002).
9. Forner, S. et al. Systematic phenotyping and characterization of the 5xFAD mouse model of Alzheimer's disease. Sci Data 8, 270 (2021).

10. Drummond, E., Nayak, S., Pires, G., Ueberheide, B. & Wisniewski, T. Isolation of Amyloid Plaques and Neurofibrillary Tangles from Archived Alzheimer's Disease Tissue Using Laser-Capture Microdissection for Downstream Proteomics. Methods Mol Biol 1723, 319–334 (2018).
11. Boyle, P. A., Buchman, A. S., Wilson, R. S., Leurgans, S. E. & Bennett, D. A. Association of Muscle Strength With the Risk of Alzheimer Disease and the Rate of Cognitive Decline in Community-Dwelling Older Persons. Arch Neurol 66, (2009).
12. O'Leary, T. P., Mantolino, H. M., Stover, K. R. & Brown, R. E. Age-related deterioration of motor function in male and female 5xFAD mice from 3 to 16 months of age. Genes Brain and Behavior 19, e12538 (2020).
13. Scarmeas, N. et al. Motor signs predict poor outcomes in Alzheimer disease. Neurology 64, 1696–1703 (2005).
14. Terry, R. D. THE FINE STRUCTURE OF NEUROFIBRILLARY TANGLES IN ALZHEIMER'S DISEASE: Journal of Neuropathology and Experimental Neurology 22, 629–642 (1963).
15. Albers, M. W. et al. At the interface of sensory and motor dysfunctions and Alzheimer's disease. Alzheimers Dement 11, 70–98 (2015).
16. Madisen, L. et al. A robust and high-throughput Cre reporting and characterization system for the whole mouse brain. Nat Neurosci 13, 133–140 (2010).
17. Steward, O. et al. Rostro-Caudal Specificity of Corticospinal Tract Projections in Mice. Cereb Cortex 31, 2322–2344 (2021).
18. Park, K. K. et al. Promoting axon regeneration in the adult CNS by modulation of the PTEN/mTOR pathway. Science 322, 963–966 (2008).

19. Metcalfe, M. & Steward, O. PTEN deletion in spinal pathways via retrograde transduction with AAV-rg enhances forelimb motor recovery after cervical spinal cord injury; sex differences and late-onset pathophysiologies. Preprint at https://doi.org/10.1101/2023.03.20.533502 (2023).
20. Bhattacharya, S., Haertel, C., Maelicke, A. & Montag, D. Galantamine Slows Down Plaque Formation and Behavioral Decline in the 5XFAD Mouse Model of Alzheimer's Disease. PLoS ONE 9, e89454 (2014).
21. Crowe, S. E. & Ellis-Davies, G. C. R. Spine pruning in 5xFAD mice starts on basal dendrites of layer 5 pyramidal neurons. Brain Struct Funct 219, 571–580 (2014).
22. Poon, C. H. et al. Sex Differences between Neuronal Loss and the Early Onset of Amyloid Deposits and Behavioral Consequences in 5xFAD Transgenic Mouse as a Model for Alzheimer's Disease. Cells 12, 780 (2023).
23. Schneider, C. A., Rasband, W. S. & Eliceiri, K. W. NIH Image to ImageJ: 25 years of image analysis. Nat Methods 9, 671–675 (2012).

Chapter 4 - Motor behavior in 5xFAD Alzheimer's disease mouse model following mTOR activation

Abstract

Alzheimer's disease (AD) is clinically defined by progressive cognitive decline, accumulation of amyloid-β (Aβ) plaques and neurofibrillary tangles, but late-stage AD also involves significant neurodegeneration and motor deficits. Some murine models of AD recapitulate these motor deficits and neurodegeneration, including 5xFAD mice. In the 5xFAD mouse model, neurodegeneration of layer V corticospinal neurons (CSNs) occurs and may be contributing to the motor deficits. To investigate whether mTOR activation could prevent or delay motor deficits in a mouse model of AD, we created a new transgenic model by crossing 5xFAD, $Rosa^{tdT}$ and $PTEN^{flox/flox(f/f)}$ mice. The $5xFAD^{+/-}/PTEN^{f/f}/Rosa^{tdT}$ model allows for permanent Cre-dependent expression of tdT in the cell bodies, dendrites and axons of the neurons in which PTEN has been deleted. Here, we assessed whether deletion of PTEN, which leads to activation of mTOR, prevents or delays age-dependent progression of motor deficits in 5xFAD mice. At 2-3 months of age, $5xFAD^{+/-}/PTEN^{f/f}/Rosa^{tdT}$ mice received intra-spinal cord injections of AAV-retrograde (rg)/Cre at cervical level 5 (C5). The AAV-rg/Cre transduced neurons retrogradely and resulted in permanent labeling of corticospinal neurons (CSNs) in layer V of the sensorimotor cortex and simultaneous deletion of PTEN in those same neurons. Controls were $5xFAD^{+/-}/Rosa^{tdT}$ and $Rosa^{tdT}$ mice in which AAV-rg/Cre injections led only to induction of tdT in CSNs (PTEN expression intact) and $PTEN^{f/f}/Rosa^{tdT}$ mice (no 5xFAD but PTEN-deleted). Motor function of $5xFAD^{+/-}/PTEN^{f/f}/Rosa^{tdT}$, $5xFAD^{+/-}/Rosa^{tdT}$, $PTEN^{f/f}/Rosa^{tdT}$ and $Rosa^{tdT}$ mice was assessed

monthly from 2-3 months to 12-15 months of age on the Rotarod®, grip strength meter (GSM) and balance beam. 5xFAD$^{+/-}$/Rosa^{tdT} (PTEN intact) displayed motor deficits on the rotarod task beginning at 10 months of age, while 5xFAD$^{+/-}$/PTEN$^{f/f}$/Rosa^{tdT} remained indistinguishable from non-5xFAD controls (PTEN$^{f/f}$/Rosa^{tdT} and Rosa^{tdT}). On the balance beam task, 5xFAD$^{+/-}$/PTEN$^{f/f}$/Rosa^{tdT} had significantly fewer foot slips than 5xFAD$^{+/-}$/Rosa^{tdT} mice but their speed was comparable. On the GSM task, there were no significant differences between strains. Our results indicate that PTEN deletion prevents motor coordination deficits on rotarod and balance beam but age-related impairments in grip strength persist in 5xFAD$^{+/-}$/PTEN$^{f/f}$/Rosa^{tdT} by mTOR activation in CSNs.

Introduction

An estimated 7.4 million Americans aged 65 and older are living with Alzheimer's disease (AD), making it one of the most prevalent neurodegenerative diseases (2026 Alzheimer's disease facts and figures). In AD, neuropathology is primarily characterized by progressive accumulation of extracellular amyloid beta (Aβ) plaques and intraneuronal neurofibrillary tangles (Terry, 1963). As the disease advances, cognitive decline becomes clinically detectable. It has been reported that motor impairments also appear in AD and may even precede cognitive decline (Albers et al., 2015). Tremors and other extrapyramidal signs have been reported to predict worse outcomes of AD (Scarmeas et al., 2005).

Mouse models are widely used to study AD, but most murine models do not exhibit significant neurodegeneration. One model that does exhibit extensive neurodegeneration is the 5xFAD transgenic strain. 5xFAD mice express two mutant human genes, amyloid precursor protein

(APP) and presenilin 1 (PSEN1), carrying five familial AD mutations (three in APP, two in PSEN1). The two transgenes inserted into a single locus and are driven by the neuron-specific elements of the mouse Thy-1 promoter, which restricts expression to select forebrain neuron populations (Oakley et al., 2006).

5xFAD mice display robust amyloid plaque accumulation and neurodegeneration in layer V of the cerebral cortex (Oakley et al., 2006; Eimer and Vassar, 2013; Bhatt et al., 2014). Our lab has recently established that corticospinal neurons (CSNs) are a subset of the layer V neurons that degenerate in the 5xFAD mouse model (Gallardo and Steward, 2026). Important to this study, 5xFAD mice also develop motor deficits beginning at approximately 9 months of age (O'Leary et al., 2018). Thus, the extensive neurodegeneration of CSNs in cortical layer V is of particular interest, as these neurons are the cells of origin of the corticospinal tract. Having a defined population of neurons that degenerate in the 5xFAD model, CSNs (Gallardo and Steward, 2026), provides a functionally defined and targetable population in which to study the progression of motor deficits. Retrograde adeno-associated virus carrying Cre (AAV-rg/Cre), combined with a Cre-dependent tdTomato (tdT) reporter (Madisen et al., 2010; Tervo et al., 2016), enables specific transduction and labeling of CSNs when injected into the spinal cord (Steward et al., 2021; Gallardo and Steward, 2026).

Our CSN targeting platform (Gallardo and Steward, 2026) allows us to test whether activating an intrinsic growth signaling pathway in CSNs can protect 5xFAD mice from developing motor deficits. Deletion of phosphatase and tensin homolog (PTEN), a negative regulator of the mammalian target of rapamycin (mTOR) pathway, has been shown to promote growth across multiple mouse models (Park et al., 2008; Liu et al., 2010; Gallent and Steward, 2018; Yonan

and Steward, 2023). Our lab has reported that mTOR activation in adult cortical neurons induces *de novo* cell growth, an increase in dendrite branching complexity and length (Gallent and Steward, 2018). Notably, our lab has also shown that PTEN deletion and Cre-dependent tdT labeling can be driven within the same CSNs (Metcalfe and Steward, 2023), and cervical level 5 (C5) retrograde injections reliably label CSNs originating in the sensorimotor cortex (Steward et al., 2021). This provides a platform in which mTOR can be activated selectively and permanently in labeled CSNs.

Methods

2.1 Experimental Animals

All procedures involving animals were approved by the Institutional Animal Care and use Committee (IACUC) at the University of California, Irvine (UCI) in accordance with the National Institute of Health (NIH) guidelines. Mice had *ad lib* access to food and water and were housed at 25°C with a 12h light/dark cycle.

Breeding strategy: To produce the transgenic mice for these studies, hemizygous 5xFAD (B6SJL-Tg (APPSwFlLon, PSEN1*M146L*L286V) 6799Vas/Mmjax; Strain #: 34840-JAXRRID:MMRRC_034840-JAX) mice were crossed with $PTEN^{f/f}/Rosa^{tdT}$ mice developed in our lab (reported in Gallent and Steward, 2018). Homozygous $PTEN^{f/f}/Rosa^{tdT}$ had been maintained in our breeding colony over multiple generations before being crossed with 5xFAD mice. The $PTEN^{f/f}/Rosa^{tdT}$ were developed by crossing $Rosa^{tdT}$ (B6;129S6-Gt (ROSA)26Sortm9(CAG-tdTomato)Hze/J, Strain #:007905, RRID:IMSR_JAX:007905) mice and $PTEN^{f/f}$ (B6.129S4-Ptentm1Hwu/J, Strain #:006440, RRID:IMSR_JAX:006440) mice.

All mice of the F1 generation from the 5xFAD$^{+/-}$ x PTEN$^{f/f}$/Rosa$^{tdT\ +/+}$ cross were hemizygous at both PTEN$^{f/f}$/Rosa^{tdT} loci and approximately 50% of the mice were hemizygous for 5xFAD. Genotypes were determined by real time PCR with probes designed for hAPP and hPSEN1 (Transnetyx, Cordova, TN). When sufficient numbers of 5xFAD$^{+/-}$/PTEN$^{f/f}$/Rosa$^{tdT\ +/+}$ were obtained, breeding pairs were created with 5xFAD$^{+/-}$/PTEN$^{f/f}$/Rosa$^{tdT\ +/+}$ crossed with PTEN$^{f/f}$/Rosa$^{tdT\ +/+}$ to generate 5xFAD$^{+/-}$/PTEN$^{f/f}$/Rosa$^{tdT\ +/+}$ and 5xFAD$^{-/-}$/PTEN$^{f/f}$/Rosa$^{tdT\ +/+}$ controls. Another colony of 5xFAD$^{+/-}$/Rosa$^{tdT\ +/+}$ and Rosa$^{tdT\ +/+}$ controls. Similarly, all mice of the F1 generation from the 5xFAD$^{+/-}$ x Rosa$^{tdT\ +/+}$ cross were hemizygous at the Rosa^{tdT} locus and approximately 50% of the mice were hemizygous for 5xFAD. When enough 5xFAD $^{+/-}$/Rosa$^{tdT\ +/+}$ were obtained, breeding pairs were created with Rosa$^{tdT\ +/+}$/5xFAD $^{+/-}$ crossed with Rosa$^{tdT\ +/+}$ to generate Rosa$^{tdT\ +/+}$/ 5xFAD$^{+/-}$ and Rosa$^{tdT\ +/+}$/5xFAD $^{-/-}$ controls. Genotyping of progeny of these breeders was done with PCR probes designed according to the protocol provided by Jackson lab (protocol ID = 22421) with confirmation of presence, or absence of hAPP by IF against hAPP protein using the clone 1D1 primary antibody (RRID:AB_3665093).

Note: The mice in the present study are the same mice used for the study of whether mTOR activation via PTEN deletion prevented or delayed age-related neurodegeneration of CSNs (Chapter 3). In this regard, some mice were harvested at predefined ages leading to diminishing members of mice in the different groups over age (see Table 1). Paragraphs describing surgical procedures and post-operative care are repeated here in anticipation of the possibility that this chapter and chapter 3 may be submitted as separate papers.

Table 4.1 Experimental animals

Months post AAV-rg/Cre injection	5xFAD$^{+/-}$/PTEN$^{f/f}$/Rosa^{tdT}	5xFAD$^{+/-}$/Rosa^{tdT}	PTEN$^{f/f}$/Rosa^{tdT}	Rosa^{tdT}	Attrition
0-3	n = 5 (2M, 3 F)	n = 6 (5F, 1M)	n = 5 (3M, 2F)	n = 2 (2F)	-
4-5	n = 4 (1M, 3F)	n = 6 (5F, 1M)	n = 4 (2M, 2F)	n = 2 (2F)	n = 1 (1M) 5xFAD$^{+/-}$/PTEN$^{f/f}$/Rosa^{tdT} and n = 1 (1M) PTEN$^{f/f}$/Rosa^{tdT}
6-7	n = 2 (1M, 1F)	n = 6 (5F, 1M)	n = 4 (2M, 2F)	n = 2 (2F)	n = 2 (2F) 5xFAD$^{+/-}$/PTEN$^{f/f}$/Rosa^{tdT}
8-10	n = 2 (1M, 1F)	n = 6 (5F, 1M)	n = 4 (2M, 2F)	n = 2 (2F)	-
All injected between 2-3 months of age					

All mice were injected with AAV-rg/Cre within a day of each other and were all tested at the same time. The same cohort of mice was carried on throughout the behavioral testing period, but mice were perfused at predetermined timepoints that were relevant for immunohistology, or if there was a decline in their condition (e.g. scratching pathology as reported in Metcalfe and Steward, 2023).

2.2 Surgical procedures

For 5xFAD$^{+/-}$/PTEN$^{f/f}$/Rosa^{tdT}, 5xFAD$^{+/-}$/Rosa^{tdT}, PTEN$^{f/f}$/Rosa^{tdT} and Rosa^{tdT} studies, surgical methods are as reported in Gallardo and Steward 2025 and are described in detail below. Mice received unilateral intra-spinal cord injections of AAV-retrograde(rg)/Cre (Addgene viral prep #24593-AAVrg) at cervical level 5 (C5). Injections were unilateral in order to transduce neurons on the contralateral side of the brain leaving most neurons on the ipsilateral side as non-

transduced control. For surgery, mice were anesthetized with continuous Isoflurane (2-2.5%) administration, their eyes were swabbed with Vaseline to prevent drying, and the scalp was shaved and cleaned with Betadine®. A laminectomy was performed at C5 to expose the spinal cord and AAV-rg/Cre was injected 0.5 mm left of the midline and 0.5 mm deep (3E9 viral genome copies (GC) per mouse) using a Hamilton microsyringe fitted with a pulled glass micropipette. The needle was kept in place for 1 minute after completing the injection. Following injection, the muscle layers were sutured, and the skin was closed by wound clips.

2.3 Post-operative care

After surgery, mice were immediately placed in cages with Alpha-Dri bedding with half of the cage placed on a circulating water warming pad set to 37ºC. Placing the cage partially on top of warming pads allows mice to remove themselves from the heat source, if desired. Mice were kept on the warming pad for 3 days post-surgery and received lactated Ringer's solution once a day (1ml/20g, subcutaneously), enrofloxacin once a day (Baytril® 2.5mg/kg, subcutaneously) and buprenorphine twice a day (0.01mg/kg, subcutaneously). Mice were monitored twice daily for 3 days post-surgery for general health and signs of distress. If bladders of mice were full, indicating difficulty to urinate due to surgery, the bladders were manually expressed twice daily. Bladder expression was required for a small number of animals and for a maximum of 3 days post-surgery. After 3 days, the cages were removed from the warming pads and were transferred back to the mouse housing room set at 25°C. Once in the housing room, mice were routinely monitored by vivarium staff and research staff.

2.4 Behavioral testing

Rotarod

Rotarod testing was done to assess motor coordination and motor learning. The testing paradigm was done as reported in Gallent and Steward 2018. The mice were tested for four consecutive days with two test trials and three regular trials per day. During the first two days, the Rotarod was set to an initial speed of 4 rotations per minute (RPM) and an acceleration of 0.1 RPM/s. On the next two days, days 3 and 4, the Rotarod was set to an initial speed of 6 RPM and an acceleration of 0.2 RPM/s. Each trial had a maximum time of 2 minutes with a 20 second rest in between each trial. If a mouse fell before 2 minutes, the trial ended for that mouse. Four mice were tested at a time. Cage and mouse order was randomized. Performance (final speed) was measured by ((latency to fall $*$ acceleration) + starting speed). The average of each trial per group was recorded and compared to other groups. In this paradigm, basic motor coordination is reflected by performance in initial trials. Learning is reflected by improved performance across trials and days.

Balance Beam

Mice were tested on a flat, rectangular, metal narrow beam measuring 2.5 cm in width, 100 cm in length and raised 3 inches with lines drawn every centimeter. A bright light was placed at the start of the beam and a black box measuring 12H x 7W inches, baited with Froot Loops® cereal and dirty bedding from their respective cage, was placed on the opposite end of the beam. The mice were trained for two consecutive days and tested on the third day. Each day, mice completed three trials with a maximum time of 120 seconds or until the mice fell. The distance traveled and the time to fall, or reach the end of the beam, was recorded. The average movement

speed was calculated for each trial. Each day mice completed three trials with a maximum time of 120 seconds or until the mice fell. The distance traveled and the time to fall, or reach the end of the beam, was recorded. The average movement speed was calculated for each trial. If the mice fell, it was counted as a foot slip on both hind paws (left and right). The distance at which the mouse fell was recorded. The full beam measured 90 cm and the speed at which the mice crossed the beam was calculated by: [(distance (cm)/100)/sec].

Grip Strength Meter (GSM)

The GSM measures forelimb grip strength by recording the maximal force (grams) while a mouse grips a thin metal bar as it's being gently pulled away. The mice were handled for 2 weeks prior to testing and were allowed four days of training on the GSM before being tested. Individual forelimbs were tested by taping the forelimb opposite to the one being tested with non-stick surgical tape (Danilov and Steward, 2015). The mice were held by the tail and suspended 2-3 inches above the plate of the GSM. The mice were then gradually brought toward the bar to allow them to reach out and grip the bar. Once grip was established, the mice were gently pulled away until the grip was released. This process was repeated 4 times (repetitions) to make up one testing session. Maximal force was recorded separately for each forelimb and averaged across each session.

We assessed motor function of all four genotypes on GSM, balance beam and rotarod task.

Results

3.1 Preservation of motor coordination in rotarod task in mice with PTEN deletion

5xFAD mice have been reported to exhibit motor impairments by 9-10 months of age on a task assessing motor coordination, the Rotarod® task (O'Leary et al., 2018). To assess whether motor coordination deficits on the rotarod task were altered by PTEN deletion and mTOR activation in corticospinal neurons (CSNs), we tested 4 strains: 1) $5xFAD^{+/-}/PTEN^{f/f}/Rosa^{tdT}$; 2) $5xFAD^{+/-}/Rosa^{tdT}$ (PTEN expression intact); 3) $PTEN^{f/f}/Rosa^{tdT}$ (no 5xFAD but PTEN deleted) and $Rosa^{tdT}$ mice (no 5xFAD, PTEN expression intact). The mice were tested over four consecutive days each month. Days 1-2 were done at a lower acceleration and considered "easy trials", while days 3-4 were done at a higher acceleration and considered "challenge trials".

Figure 4.1 illustrates comparisons between genotypes at representative ages. At 4 months of age, scores across genotypes were similar. As shown in **Figure 4.1A**, all genotypes ($5xFAD^{+/-}/PTEN^{f/f}/Rosa^{tdT}$ (n = 5), $5xFAD^{+/-}/Rosa^{tdT}$ (n = 6), $PTEN^{f/f}/Rosa^{tdT}$ (n = 5) and $Rosa^{tdT}$ (n = 2)) mice displayed capability of being able to reach the maximum speed allowed, per the protocol (16RPM easy trials, 30RPM challenge trials). Qualitatively, we observed slight dips in performance across the four days of trials, amongst all genotypes, but most of the dips happened in the first two test trials of each day and they remained close to the maximum attainable speed in those trials (**Fig. 4.1A**). Note that while all genotypes increased performance with the increase in acceleration, mice had been pre-trained on the Rotarod® so improvement between easy and challenging trials could not be interpreted as learning. Overall, the data at 4 months of age indicated that all genotypes performed at or near the maximum attainable speed on both the easy and challenge trials. Next, we ran a mixed-effects model (Residual Maximum Likelihood, REML) analysis on data from $5xFAD^{+/-}/PTEN^{f/f}/Rosa^{tdT}$ and $5xFAD^{+/-}/Rosa^{tdT}$ revealed a

significant effect of trial (F (2.581, 25.34) = 66.05, $p < 0.0001$) at 4 months of age, since there was a change in acceleration from Days 2 and 3 to Days 3 and 4. There was not a significant main effect of genotype (F (1, 108) = 0.3501, p = 0.5553) and no genotype and trial interaction (F (11, 108) = 0.8863, p = 0.5561) at 4 months of age (**Fig. 4.1A**). The mixed-effects ANOVA (REML) analysis only included 5xFAD$^{+/-}$/PTEN$^{f/f}$/Rosa^{tdT} and 5xFAD$^{+/-}$/Rosa^{tdT}, since we are assessing the effect of PTEN deletion in 5xFAD mice. The controls, PTEN$^{f/f}$/Rosa^{tdT} and Rosa^{tdT} are shown on the graph for reference (**Fig. 4.1A**). These results indicate that no motor deficits were present in any of the genotypes at 4 months of age and provide the baseline motor performance prior to the onset of age-related neurodegeneration. Importantly, it indicates that there are no significant differences in performance at 4 months between 5xFAD$^{+/-}$/PTEN$^{f/f}$/Rosa^{tdT} and 5xFAD$^{+/-}$/Rosa^{tdT} mice.

At 10 months of age, 5xFAD$^{+/-}$/Rosa^{tdT} (n = 6) mice failed to reach the maximum attainable speed during the easy and challenge trials, falling off the Rotarod® at an average of 11 RPM in Days 1 and 2 (**Fig. 4.1B**). 5xFAD$^{+/-}$/Rosa^{tdT} showed slight improvement in performance in Day 3 and even more so in Day 4, but they still failed to reach the maximum attainable speed in any of the trials. Most importantly, the experimental mice with PTEN deletion (5xFAD$^{+/-}$/PTEN$^{f/f}$/Rosa^{tdT}, n = 2) reached the maximum attainable speed in almost all the trials and showed improvement between easy and challenge trials (**Fig. 4.1B**). The controls, PTEN$^{f/f}$/Rosa^{tdT} (n = 4) and Rosa^{tdT} (n = 2) mice, continued to reach the maximum attainable speed on most trials (easy and challenge trials, **Fig. 4.1B**). However, in Day 3, the Rosa^{tdT} mice performed the worst out of all the genotypes, averaging at 6 RPM. This may have been due to an inability to adjust to the faster start and steeper acceleration, rather than due to motor deficits.

Performance greatly improved on Day 4 for the $Rosa^{tdT}$ mice (**Fig. 4.1B)**. A mixed-effects ANOVA revealed a significant main effect of genotype ($F (1, 6) = 15.69$, $p = 0.0074$) but no significant main effect of trials ($F (1.880, 11.28) = 3.023$, $p = 0.0911$) and no significant trial and genotype interaction ($F (11, 66) = 0.7107$, $p = 0.7240$). These results reveal that 5xFAD mice with PTEN deletion in CSNs ($5xFAD^{+/-}/PTEN^{f/f}/Rosa^{tdT}$) did not exhibit the motor deficits seen in $5xFAD^{+/-}/Rosa^{tdT}$ mice, suggesting that PTEN deletion did delay or prevent deficits in motor function.

Differences were even more apparent at 12 months of age. $5xFAD^{+/-}/Rosa^{tdT}$ ($n = 5$) mice did not reach the maximum attainable speed and instead fell off the Rotarod® at an average of 7 RPM on both easy and challenge trials. Their failure to reach the attainable speed indicated that they had motor deficits severe enough to not be able to complete the easy trials. The rest of the genotypes, $5xFAD^{+/-}/PTEN^{f/f}/Rosa^{tdT}$ ($n = 2$), $PTEN^{f/f}/Rosa^{tdT}$ ($n = 4$) and $Rosa^{tdT}$ ($n = 2$) mice were still able to reach the maximum attainable speed on most trials, both easy and challenge (**Fig. 4.1C**). Although the performance of $PTEN^{f/f}/Rosa^{tdT}$ and $Rosa^{tdT}$ varied more than previous months, with larger dips in speed attainment, the overall trend remained consistent. Mixed-effects ANOVA revealed a significant main effect of genotype ($F (1, 5) = 38.06$, $p = 0.0016$), no significant main effect of trial ($F (2.654, 13.27) = 2.341$, $p = 0.1247$) and no significant interaction ($F (11, 55) = 0.7644$, $p = 0.6729$) (**Fig. 4.1C**). Our data reveals that motor deficits in $5xFAD^{+/-}/Rosa^{tdT}$ mice worsened by 12 months of age while performance in $5xFAD^{+/-}/PTEN^{f/f}/Rosa^{tdT}$, $PTEN^{f/f}/Rosa^{tdT}$ and $Rosa^{tdT}$ remained largely unchanged, further suggesting that PTEN deletion did delay or prevent deficits in motor function.

Together, our results show that young mice, of all genotypes, performed well on the rotarod task and motor deficits were apparent by 10 months of age in 5xFAD$^{+/-}$/Rosa^{tdT} while 5xFAD$^{+/-}$/PTEN$^{f/f}$/Rosa^{tdT} continued to perform well even at 12 months of age. These data suggest that PTEN deletion prevented or delayed the age-related decline that occurs in 5xFAD mice.

3.2. PTEN deletion/mTOR activation in CSNs does not prevent or delay age-related decreases in grip strength

To assess whether PTEN deletion prevented or delayed age-related changes in grip strength, we measured maximal forelimb force monthly on the grip strength meter (GSM). As described in Methods, GSM measurements were taken for both forelimbs individually by placing a small piece of tape on the forelimb that was not being tested. Then, we allowed the mouse to reach for the GSM bar and gently pulled the mouse back. Maximal force was recorded once the mouse released its grip while being pulled back.

We first assessed whether there were differences between the forelimbs. Since we injected AAV-rg/Cre into the left side of the spinal cord, the neurons that projected to the left side of the spinal cord were transduced and thus affected the left forelimb. Thus, we wanted to determine if PTEN deletion/mTOR activation led to a prevention or delay of functional force deterioration in the left forelimb. In the 5xFAD$^{+/-}$/Rosa^{tdT} mice, the force exerted by the left forelimb was less than that of the right across all ages, with the biggest differences seen past 11 months of age (**Fig. 4.2A**). It's important to note that the maximal force recorded from the left forelimb was less than the right forelimb even before injection of AAV-rg/Cre, at 3 months of age, indicating that the

disparity in forelimb strength was preexisting. A mixed-effects ANOVA revealed significant differences between forelimbs (right stronger than left) ($F (1, 122) = 20.90$, $p < 0.0001$) and significant decrease in grip strength with age ($F (12, 122) = 4.853$, $p < 0.0001$) and a non-significant interaction ($F (12, 122) = 0.6104$, $p = 0.8300$). In the $5xFAD^{+/-}/PTEN^{f/f}/Rosa^{tdT}$ mice, the left forelimb was also weaker than the right forelimb, but the differences were more apparent past 12 months of age (**Fig. 4.2B**). In $5xFAD^{+/-}/PTEN^{f/f}/Rosa^{tdT}$ mice, the left forelimb was also weaker than the right prior to injection revealing the strength difference was present without intervention. A mixed-effects ANOVA showed significant differences between forelimbs (right stronger than left) ($F (1, 71) = 13.88$, $p = 0.0004$) and significant decrease in grip strength with age ($F (13, 71) = 2.426$, $p = 0.0090$) and a non-significant interaction ($F (13, 71) = 0.9969$, $p = 0.4636$). In non-5xFAD mice ($PTEN^{f/f}/Rosa^{tdT}$), the force recorded from the left and right forelimbs were similar before the injection (2 months of age) and at approximately a month post-injection (3 months of age) (**Fig. 4.2C**). However, in the following months the right forelimb appeared to perform better than the left forelimb, except for at months 8, 9 and 13 (**Fig. 4.2C**). A mixed-effects ANOVA revealed significant differences between forelimbs (right stronger than left) ($F (1, 94) = 4.163$, $p = 0.0441$) and significant decrease in grip strength with age ($F (13, 94) = 6.389$, $p < 0.0001$) and no significant interaction ($F (13, 94) = 1.340$, $p = 0.2045$). Lastly, in $Rosa^{tdT}$ mice the right limb exerted more force than the left forelimb across all ages, except at 9 months of age (**Fig. 4.2D**). The differences between the right and the left forelimb were present even before injection, at 3 months of age (**Fig. 4.2D**). A mixed-effects ANOVA showed significant differences between forelimbs (right stronger than left) ($F (1, 26) = 20.97$, $p = 0.0001$) and no significant decrease in grip strength with age ($F (12, 26) = 1.802$, $p = 0.1015$) and no interaction between forelimbs and age ($F (12, 26) = 0.5822$, $p = 0.8365$). Thus, the asymmetry in

forelimb strength (right stronger than left) appeared to be present in all genotypes, with the left forelimb being weaker than the right. However, the left forelimb was weaker before the injection in all genotypes except for PTEN$^{f/f}$/Rosa^{tdT} mice.

Our hypothesis is that PTEN deletion delays or prevents age-related motor deficits in 5xFAD mice. By comparing the right and left forelimbs, the right forelimb served as an intra-animal control. Our results have revealed that the right forelimb is significantly stronger than the left forelimb in all genotypes, even without PTEN deletion (Rosa^{tdT}, **Fig. 4.2D**) and without the presence of transgenes (Rosa^{tdT}, **Fig. 4.2D** and PTEN$^{f/f}$/Rosa^{tdT}, **Fig. 4.2C**). In addition, the right forelimb was stronger across age even when there wasn't a preexisting difference in strength (PTEN$^{f/f}$/Rosa^{tdT}, **Fig. 4.2C**). The data comparing left and right forelimbs in 5xFAD$^{+/-}$/Rosa^{tdT} (**Fig. 4.2A**) and Rosa^{tdT} (**Fig. 4.2D**) mice suggest that PTEN deletion does not appear to result in a delay or prevention of age-related motor deficits in 5xFAD mice as hypothesized. However, it is not clear whether the injection into the cervical spinal cord impairs grip strength, to an extent, since the left forelimb was weaker even in non-PTEN deleted genotypes (5xFAD$^{+/-}$/Rosa^{tdT}, **Fig. 4.2A** and Rosa^{tdT}, **Fig. 4.2D)**.

To determine whether PTEN deletion prevented or delayed loss of grip strength in 5xFAD mice, we compared the data from the GSM task for both right and left forelimbs in 5xFAD$^{+/-}$/PTEN$^{f/f}$/Rosa^{tdT} and 5xFAD$^{+/-}$/Rosa^{tdT} mice. In 5xFAD$^{+/-}$/Rosa^{tdT} mice, the maximal force recorded from both forelimbs appeared to be similar to that of 5xFAD$^{+/-}$/PTEN$^{f/f}$/Rosa^{tdT} mice before 11 months of age (**Fig. 4.2E**). Past 11 months of age, the strength recorded from both genotypes appeared to diverge. The right forelimb of 5xFAD$^{+/-}$/PTEN$^{f/f}$/Rosa^{tdT} exerted greater

force than the left forelimb of 5xFAD$^{+/-}$/PTEN$^{f/f}$/Rosa^{tdT} mice and both forelimbs of 5xFAD$^{+/-}$/Rosa^{tdT} mice. These data suggest that the difference in grip strength force between the two genotypes is being driven by the right forelimb data from 5xFAD$^{+/-}$/PTEN$^{f/f}$/Rosa^{tdT} mice (non-transduced forelimb). However, the left forelimb of 5xFAD$^{+/-}$/PTEN$^{f/f}$/Rosa^{tdT} mice exerted a similar force to the left forelimb of 5xFAD$^{+/-}$/Rosa^{tdT} mice, and greater force than the right forelimb of 5xFAD$^{+/-}$/Rosa^{tdT} mice. Thus, the data may be confounded by the possible injury caused by the injection into the spinal cord. However, these data combined do not convinsingly suggest that there is a delay or prevention in grip strength decline due to PTEN deletion.

Because we determined grip strength differed between the right and left forelimbs in all genotypes, likely due to a combination of pre-existing forelimb differences and minor injury due to injection, we did not combine left and right forelimb data. Measurements from the left forelimb are separately reported below, as the left forelimb is ipsilateral to the injection.

To assess whether PTEN deletion prevented or delayed motor deficits in 5xFAD mice, we looked at the force exerted by the left forelimb on GSM in 5xFAD$^{+/-}$/PTEN$^{f/f}$/Rosa^{tdT} vs 5xFAD$^{+/-}$/Rosa^{tdT} mice. We observed that maximal grip force increased across all genotypes until approximately 8 months of age and then began to decline (**Fig. 4.2F**). However, the 5xFAD$^{+/-}$/PTEN$^{f/f}$/Rosa^{tdT} mice appeared to decline at a slower rate and exerted greater force than 5xFAD$^{+/-}$/Rosa^{tdT} mice past 11 months of age (**Fig. 4.2F**). These data suggest that there is a delay in the progression of grip strength loss, with PTEN deletion. Mixed-effects ANOVA (REML) analysis on only the left forelimb measurements from 5xFAD$^{+/-}$/Rosa^{tdT} vs. 5xFAD$^{+/-}$/PTEN$^{f/f}$/Rosa^{tdT} mice revealed no significant difference in GSM values by genotype ($F(3, 14) =$

1.537, p = 0.2487) with significant effect of age (F (5.598, 74.92) = 6.353, p < 0.0001) (**Fig. 4.2F**). These results show that age related grip strength deficits may be delayed by PTEN deletion but not prevented.

3.3 PTEN-deleted 5xFAD mice make fewer foot slips at all ages without altering speed on balance beam task

To determine whether motor coordination and balance deficits were prevented or delayed by PTEN deletion, we tested the mice on the balance beam. We allowed the mice to cross from one end of the beam to the other and reach a small black box with their cage bedding and Froot Loops®. During the balance beam task, the number of hindlimb foot slips and speed was recorded. Foot slips were recorded for both right and left hindlimbs as the mouse traversed across the balance beam. However, the left hindlimb is ipsilateral to the injection and is the most relevant to our study.

To first determine whether there were differences between the left and the right hindlimb, we compared the number of slips from each hindlimb within each genotype. Across the entire testing period, both right and left hindlimbs had similar counts of slips within each genotype, suggesting both hindlimbs were performing equally (**Fig. 4.3A-D**). There were no clear differences between the left and right foot slips even before injection, indicating that there were no preexisting asymmetrical differences (**Fig. 4.3A-D**). A mixed-effects ANOVA (REML) between right and left hindlimb data within each genotype, revealed that the number of slips from each hindlimb did not differ in 5xFAD$^{+/-}$/Rosa^{tdT} (F (1, 10) = 0.6393, p = 0.4425), 5xFAD$^{+/-}$

/PTEN$^{f/f}$/Rosa^{tdT} (F (1, 63) = 0.8352, p = 0.3643), PTEN$^{f/f}$/Rosa^{tdT} (F (1, 86) = 2.270, p = 0.1355) and Rosa^{tdT} (F (1, 2) = 0.2588, p = 0.6615). In most genotypes, the number of foot slips from both hindlimbs was about the same across age (**Fig. 4.3B-D**), except for 5xFAD$^{+/-}$/Rosa^{tdT} (**Fig. 4.3A**). In the 5xFAD$^{+/-}$/Rosa^{tdT} mice, the number of foot slips appeared to increase past 10 months of age (**Fig. 4.3A**). This suggests that the motor deficits in 5xFAD$^{+/-}$/Rosa^{tdT} mice appear past 10 months of age on the balance beam, while the deficits do not appear in any of the other genotypes, including 5xFAD mice with PTEN deletion (5xFAD$^{+/-}$/PTEN$^{f/f}$/Rosa^{tdT}). However, mixed-effects ANOVA (REML) between right and left hindlimb data within each genotype, revealed that foot slips did not differ across age in 5xFAD$^{+/-}$/Rosa^{tdT} (F (2.572, 24.32) = 1.862, p = 0.1688), 5xFAD$^{+/-}$/PTEN$^{f/f}$/Rosa^{tdT} (F (3.273, 17.18) = 1.514, p = 0.2454), PTEN$^{f/f}$/Rosa^{tdT} (F (3.256, 23.34) = 2.154, p = 0.1165) and Rosa^{tdT} (F (1.523, 3.046) = 1.593, p = 0.3216). Along with this, there was no significant age x hindlimb interaction in 5xFAD$^{+/-}$/Rosa^{tdT} (F (11, 104) = 0.3267, p = 0.9783), 5xFAD$^{+/-}$/PTEN$^{f/f}$/Rosa^{tdT} (F (12, 63) = 1.629, p = 0.1063), PTEN$^{f/f}$/Rosa^{tdT} (F (12, 86) = 0.9267, p = 0.5244) and Rosa^{tdT} (F (11, 22) = 0.9025, p = 0.5532) mice, indicating the number of times the hindlimbs slipped off the balance beam did not differ across age between the right and left.

Since the foot slips for right and left were recorded at the same time and there were no significant differences, we combined the two data sets. After combining the data, we wanted to assess whether PTEN deletion delayed or prevented the motor deficits seen during the balance beam task. Our results showed that across all ages tested, 5xFAD$^{+/-}$/PTEN$^{f/f}$/Rosa^{tdT} mice had fewer foot slips than 5xFAD$^{+/-}$/Rosa^{tdT} (**Fig. 4.3E**). Interestingly, the PTEN$^{f/f}$/Rosa^{tdT} and Rosa^{tdT} mice also had a high number of foot slips, comparable to the number of foot slips in 5xFAD$^{+/-}$

/Rosa^{tdT} mice (**Fig. 4.3E**). We ran a mixed-effects ANOVA (REML) analysis on foot slips between 5xFAD$^{+/-}$/PTEN$^{f/f}$/Rosa^{tdT} and 5xFAD$^{+/-}$/Rosa^{tdT}. We found that foot slips did not differ significantly by age ($F(12, 91) = 1.217$, $p = 0.2837$) but did differ significantly by genotype ($F(1, 9) = 11.59$, $p = 0.0078$) (**Fig. 4.3E**). Our results suggest that PTEN deletion may be ameliorating motor coordination deficits shown by reduced foot slips compared to 5xFAD$^{+/-}$/Rosa^{tdT} mice.

Next, we wanted to assess whether PTEN deletion prevented or delayed the speed deficits seen in 5xFAD mice (O'Leary et al., 2018). Our results show that the speed at which the mice crossed the beam declined with age in all genotypes (**Fig 4.3F**). However, PTEN$^{f/f}$/Rosa^{tdT} mice and 5xFAD$^{+/-}$/PTEN$^{f/f}$/Rosa^{tdT} mice performed better than non-PTEN deleted mice past 8 months of age. We did a mixed-effects ANOVA (REML) on the recorded speed from 5xFAD$^{+/-}$/PTEN$^{f/f}$/Rosa^{tdT} and 5xFAD$^{+/-}$/Rosa^{tdT} on the balance beam task. We found that they differed significantly by age ($F(1.515, 12.50) = 4.167$, $p = 0.0499$) but they did not differ significantly by genotype ($F(1, 99) = 3.714$, $p= 0.0568$) (**Fig. 4.3F**). This suggests that speed was affected by age, but these age-related changes to speed were not affected by PTEN deletion.

Discussion

4.1 Motor behavior preservation on Rotarod in the absence of CSN rescue

We have previously found that PTEN deletion does not appear to reduce or delay neurodegeneration in the 5xFAD$^{+/-}$/PTEN$^{f/f}$/Rosa^{tdT} model (Chapter 3). Despite the lack of effect PTEN deletion had on neuronal survival, 5xFAD$^{+/-}$/PTEN$^{f/f}$/Rosa^{tdT} mice did not develop the

rotarod deficits that were seen in 5xFAD$^{+/-}$/Rosa^{tdT} mice. This reveals our key point – the 5xFAD$^{+/-}$/PTEN$^{f/f}$/Rosa^{tdT} mice performed well on a task that depends on motor coordination yet the neurons responsible for motor function were degenerating. This dissociation suggests that PTEN deletion/mTOR activation may support motor function through mechanisms other than neuronal survival. Complementary work from our lab (Yonan and Steward, 2023; Gallent and Steward, 2018) has shown that PTEN deletion increases dendritic complexity and branching in CSNs and hippocampal neurons. Rather than simply preventing neuronal death, PTEN-deletion-mediated mTOR activation may instead improve the structural and functional capacity of the surviving neuronal population. For example, by increasing dendritic arborization complexity and synaptic connectivity, it could support circuit functionality that is sufficient to improve motor coordination even as CSNs degenerate.

It's important to note that the 5xFAD$^{+/-}$/PTEN$^{f/f}$/Rosa^{tdT} and Rosa^{tdT} mice performed close to the maximum attainable speed on nearly every trial. This result tells us that our protocol did not permit assessment of improved motor performance since there was a "ceiling." It's possible that 5xFAD$^{+/-}$/PTEN$^{f/f}$/Rosa^{tdT} could have performed better than all the other genotypes. Our finding is therefore that PTEN deletion prevents the decline of motor coordination in 5xFAD$^{+/-}$/PTEN$^{f/f}$/Rosa^{tdT} on the rotarod task. A different, more challenging, protocol would be required to determine whether PTEN deletion in 5xFAD$^{+/-}$/PTEN$^{f/f}$/Rosa^{tdT} mice led to improved motor coordination on the rotarod task.

4.2 Task differences

The three tasks used in this study gave distinct results. First, rotarod performance showed a large and age-related difference between genotypes. Second, the foot slips on the balance beam were a smaller yet significant difference. It could be hypothesized that the 5xFAD$^{+/-}$/PTEN$^{f/f}$/Rosa^{tdT} mice had less foot slips than 5xafd controls because they crossed the beam faster, but there were no significant differences ($p = 0.0568$) in speed between the genotypes. Third, there was no difference in forelimb grip strength between genotypes. We saw a significant difference between right and left forelimbs with the left forelimb being weaker than the right, suggesting a possibility that injection caused a small injury and a decrease in motor strength on the left forelimb. We did however see age-decline in grip strength on both the right and left forelimbs.

The differences in tasks are informative in hypothesizing what PTEN deletion could be doing to result in prevention of motor deficits in some tasks but not others. For the rotarod, it's assessing full body motor coordination. Mice need to keep moving and use all four limbs to stay on the rotating cylinder. The mice that are unable to achieve all of these movements, end up falling faster. If they can't coordinate between moving their forelimbs and hindlimbs in sync, they will not stay on the rotating cylinder. The rotarod task is the most unforgiving and revealing out of the three tasks (rotarod, balance beam and GSM). It has a discrete form of measurement. The mouse either falls or reaches the maximum attainable speed. Thus, differences in motor coordination are more noticeable. In addition, the mice are more motivated to stay on the cylinder since the alternative is falling off the cylinder and onto the platform. PTEN deletion may be more involved in potentially improved synaptic connectivity which allows the motor system to function.

In the balance beam task, the differences in motor coordination aren't as apparent but can be determined by counting foot slips and determining speed. A caveat is that the non-5xFAD control genotypes had as many or more foot slips than 5xfad mice at several ages. This indicated that the beam did not properly detect the AD-related phenotype in this cohort of mice, which may limit the strength of the findings. The decrease in the foot slips in PTEN deleted mice suggest that 5xFAD$^{+/-}$/PTEN$^{f/f}$/Rosa^{tdT} mice were better at motor coordination. The non-significant difference in speed indicated that motor coordination was preserved at the same speed as controls. This test indicated that the 5xFAD$^{+/-}$/PTEN$^{f/f}$/Rosa^{tdT} are preserving balance and limb placement compared to 5xFAD$^{+/-}$/Rosa^{tdT} (non-PTEN deleted mice).

The grip strength meter results are the weakest since there is an important caveat of injection affecting grip strength of the left forelimb. However, taking this into account and only comparing the left forelimb we found no significant differences amongst genotypes. This indicated the PTEN deletion did not have an effect on grip strength.

All these three results indicate that PTEN deletion may help with motor coordination but not as much with individual functionality of forelimbs (grip strength).

4.3 Rubrospinal tract

Our platform selectively transduced CSNs but it wasn't exclusive to them. Neurons that form part of the rubrospinal tract also project to C5 of the spinal cord, which resulted in them being transduced (Metcalfe et al., 2022). Therefore, PTEN was also deleted in neurons of the rubrospinal tract and motor behavior can't be attributed to only mTOR activation in CSNs. The

rubrospinal tract, along with the corticospinal tract, also contributes to coordination of limb movement. Thus, the rubrospinal tract may be involved in preserving motor coordination as seen in the rotarod task and balance beam. We have, however, found that neurons in the red nucleus, which contains neurons that form the rubrospinal tract, degenerate in 5xFAD mice (Gallardo and Steward, 2026). Because both populations of neurons degenerate and were transduced, CSNs and rubrospinal tract neurons, the preservation may reflect outcomes from both or either, but the model doesn't allow us to distinguish which population of neurons is responsible. To distinguish between the two neuronal populations, we could use an intersectional approach to restrict deletion of PTEN to CSNs.

4.4 Activation of mTOR does not accelerate functional decline

Numerous studies have found that mTOR is overactivated in AD brains (An et al., 2003; Li et al., 2005; Tramutola et al., 2015), predicting that mTOR overactivation results in negative consequences for neuropathology. The mTOR pathway is a negative regulator of autophagy and it's suggested that it's overactivation is expected to impair clearance of aggregated proteins (Perluigi et al., 2015). There are also reports that show that reducing mTOR activation genetically or pharmacologically improves AD pathology and cognition (Caccamo et al., 2014; Spilman et al., 2010).

Our results on motor behavior studies do not support this hypothesis. We did not see a worsening in motor performance on any of the three motor behavior tasks and it's important to mention that we did not see an increase in neurodegeneration in $5xFAD^{+/-}/PTEN^{f/f}/Rosa^{tdT}$ mice in chapter 3 (Gallardo and Steward, 2026). This is a key finding as most studies have shown that decreasing

mTOR activation is beneficial, but it had not been established that intentional and sustained overactivation of mTOR did not increase motor deficits nor neurodegeneration.

4.5 Limitations

The largest limitation of this Chapter are the sample sizes. The 5xFAD$^{+/-}$/PTEN$^{f/f}$/Rosa^{tdT} cohort had to be reduced from n = 5 to n = 2 by 8 months of age due to development of a scratching pathology associated with PTEN deletion (Metcalfe and Steward, 2023). The scratching pathology did not appear to be interacting with their performance. Thus, we did not inadvertently remove the lower performing mice. The Rosa^{tdT} mice also had a small sample size throughout all timepoints n=2. Given the small sample sizes, it's important to take this into account when interpreting findings and they should be regarded as pending replication in a larger cohort.

4.6 Conclusions and future directions

Selective and permanent deletion of PTEN in CSNs preserved motor coordination in 5xFAD$^{+/-}$/PTEN$^{f/f}$/Rosa^{tdT} mice but we reported in Chapter 3 that it did not result in preservation of CSN count. The difference in findings suggests that functional outcomes of PTEN deletion may be separate from survival of neurons. Thus, interventions that fail to prevent neuronal loss may still maintain motor function, so neuronal survival may not predict functional outcome. Because of this, PTEN deletion is affecting CSNs in a different way other than promoting neuronal survival. It's possible that there is an increase in dendritic growth, an increase in the number of synapses, a functional increase in synaptic connectivity or even all three. To determine this, morphological and electrophysiological analysis of surviving CSNs would have to be done.

Figures

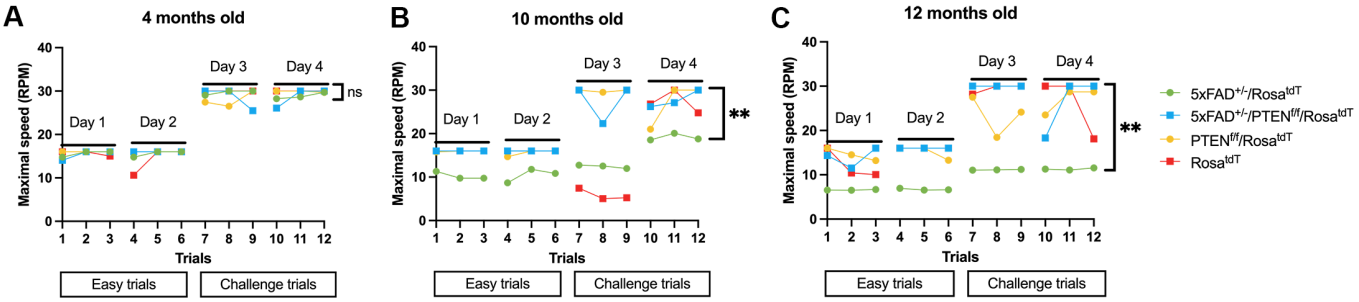


Figure 4.1 PTEN deletion ameliorated motor deficits in 5xFAD$^{+/-}$/PTEN$^{f/f}$/Rosa^{tdT} mice on the rotarod task

Mice were tested on an accelerating rotarod over 4 consecutive days (3 trials each day, 12 trials total) each month. Days 1-2 were "easy trials," done at a starting speed of 4 RPM and an acceleration of 0.1 RPM/sec. Days 3-4 were "challenge trials," done at a starting speed of 6 RPM and an acceleration of 0.2 RPM/sec. Average maximal speed is shown at **(A)** 4 months of age, **(B)** 10 months of age and **(C)** at 12 months of age.

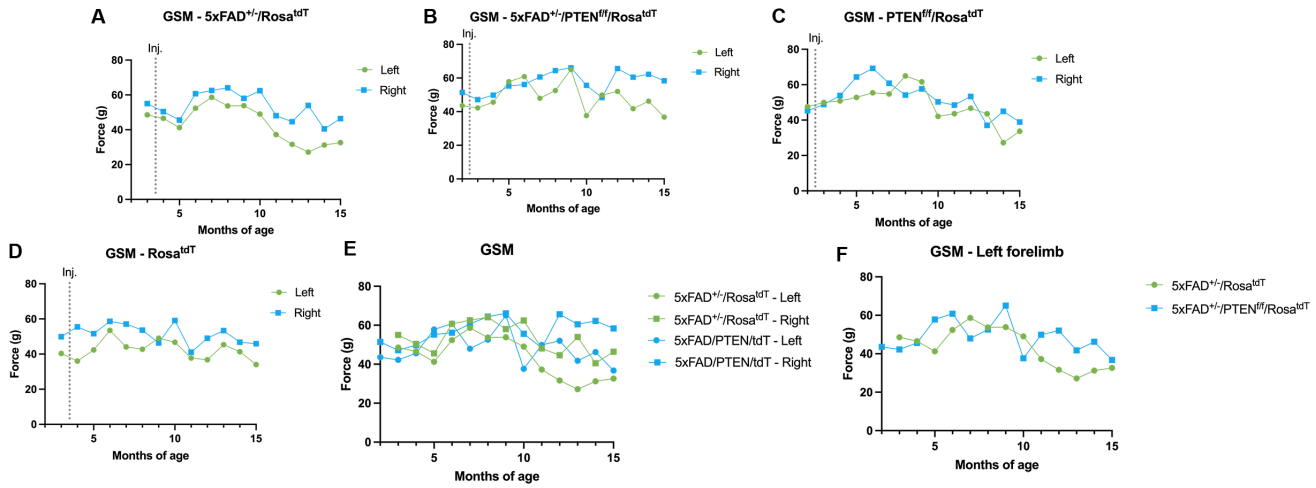


Figure 4.2 Forelimb grip strength declines with age independently of genotype.

Maximal recorded force (g) was measured monthly from 2 to 15 months of age from left and right forelimbs in **(A)** 5xFAD$^{+/-}$/Rosa^{tdT}, **(B)** 5xFAD$^{+/-}$/PTEN$^{f/f}$/Rosa^{tdT}, **(C)** PTEN$^{f/f}$/Rosa^{tdT} and **(D)** Rosa^{tdT}. **(E)** Maximal force recorded in both right and left forelimbs of both 5xFAD$^{+/-}$/Rosa^{tdT} and 5xFAD$^{+/-}$/PTEN$^{f/f}$/Rosa^{tdT}. **(F)** Left forelimb force from both 5xFAD$^{+/-}$/Rosa^{tdT} and 5xFAD$^{+/-}$/PTEN$^{f/f}$/Rosa^{tdT}. A mixed-model (REML) analysis on 5xFAD$^{+/-}$/PTEN$^{f/f}$/Rosa^{tdT} and 5xFAD$^{+/-}$/Rosa^{tdT} mice revealed a significant main effect of age ($p < 0.0001$) but no effect of genotype ($p = 0.2487$).

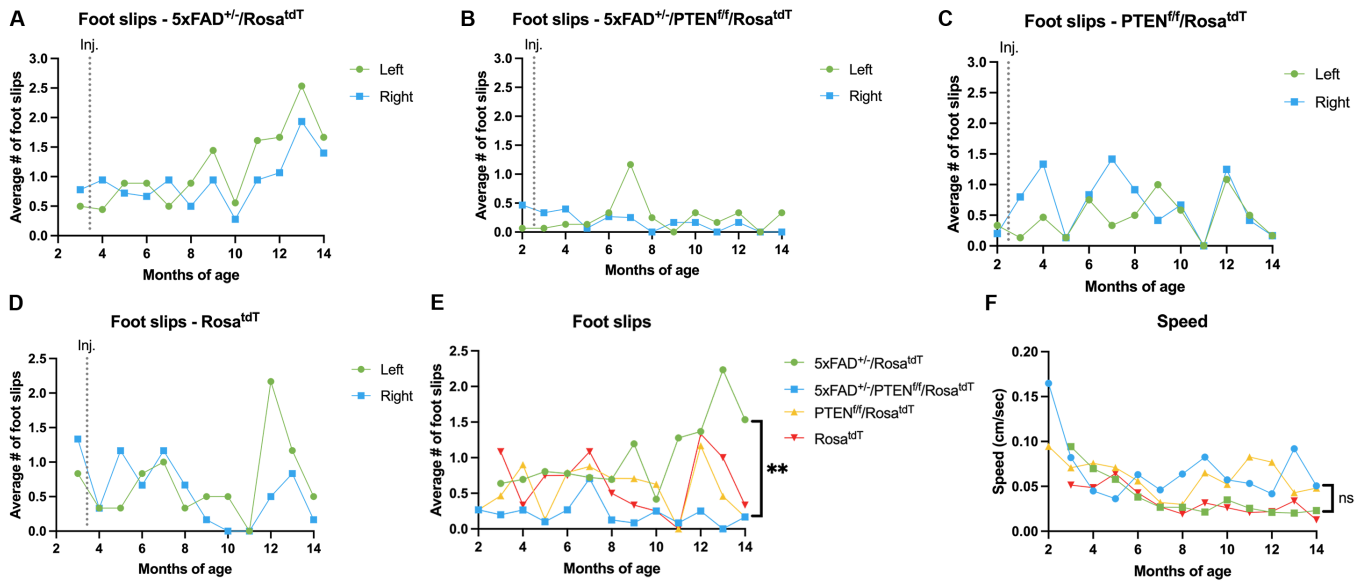


Figure 4.3 PTEN deletion decreases foot slips without affecting speed on balance beam task.

Mice were tested on a 90cm beam monthly from 2 to 14 months of age. There were three trials per session. The average number of left and right hindlimb foot slips per crossing in **(A)** 5xFAD$^{+/-}$/Rosa^{tdT}, **(B)** 5xFAD$^{+/-}$/PTEN$^{f/f}$/Rosa^{tdT}, **(C)** PTEN$^{f/f}$/Rosa^{tdT} and **(D)** Rosa^{tdT}. **(E)** The average number of foot slips from combined hindlimbs (left and right) per crossing. A mixed-model (REML) analysis on 5xFAD$^{+/-}$/PTEN$^{f/f}$/Rosa^{tdT} and 5xFAD$^{+/-}$/Rosa^{tdT} mice revealed a significant main effect of genotype on foot slips ($p = 0.0078$) and no significant effect of age. **(F)** The speed at which the mice crossed the balance beam. A mixed-model (REML) analysis on 5xFAD$^{+/-}$/PTEN$^{f/f}$/Rosa^{tdT} and 5xFAD$^{+/-}$/Rosa^{tdT} mice revealed a non-significant main effect of genotype ($p = 0.0568$) and a significant effect of age ($p = 0.0499$). PTEN$^{f/f}$/Rosa^{tdT} and Rosa^{tdT} mice are shown for reference. The legend in **(E)** applies to **(F)**.

References

1. Tramutola, A. et al. Alteration of mTOR signaling occurs early in the progression of Alzheimer disease (AD): analysis of brain from subjects with pre-clinical AD, amnestic mild cognitive impairment and late-stage AD. Journal of Neurochemistry 133, 739–749 (2015).
2. Oakley, H. et al. Intraneuronal beta-amyloid aggregates, neurodegeneration, and neuron loss in transgenic mice with five familial Alzheimer's disease mutations: potential factors in amyloid plaque formation. J Neurosci 26, 10129–10140 (2006).
3. Gallent, E. A. & Steward, O. Neuronal PTEN deletion in adult cortical neurons triggers progressive growth of cell bodies, dendrites, and axons. Exp Neurol 303, 12–28 (2018).
4. Eimer, W. A. & Vassar, R. Neuron loss in the 5XFAD mouse model of Alzheimer's disease correlates with intraneuronal Aβ42 accumulation and Caspase-3 activation. Molecular Neurodegeneration 8, 2 (2013).
5. Oakley, H. et al. Intraneuronal beta-amyloid aggregates, neurodegeneration, and neuron loss in transgenic mice with five familial Alzheimer's disease mutations: potential factors in amyloid plaque formation. J Neurosci 26, 10129–10140 (2006).
6. Metcalfe, M. et al. Harnessing rAAV-retro for gene manipulations in multiple pathways that are interrupted after spinal cord injury. Exp Neurol 350, 113965 (2022).
7. Tervo, D. G. R. et al. A Designer AAV Variant Permits Efficient Retrograde Access to Projection Neurons. Neuron 92, 372–382 (2016).
8. O'Leary, T. P., Robertson, A., Chipman, P. H., Rafuse, V. F. & Brown, R. E. Motor function deficits in the 12 month-old female 5xFAD mouse model of Alzheimer's disease. Behavioural Brain Research 337, 256–263 (2018).

9. Caccamo, A. et al. Necroptosis activation in Alzheimer's disease. Nat Neurosci 20, 1236–1246 (2017).
10. Steward, O. et al. Rostro-Caudal Specificity of Corticospinal Tract Projections in Mice. Cereb Cortex 31, 2322–2344 (2021).
11. Gallardo, D. & Steward, O. Development and characterization of a novel transgenic strain to selectively label neurons that degenerate in 5xFAD mice. Experimental Neurology 405, 115914 (2026).
12. Li, X., Alafuzoff, I., Soininen, H., Winblad, B. & Pei, J. Levels of mTOR and its downstream targets 4E-BP1, eEF2, and eEF2 kinase in relationships with tau in Alzheimer's disease brain. The FEBS Journal 272, 4211–4220 (2005).
13. O'Leary, T. P., Mantolino, H. M., Stover, K. R. & Brown, R. E. Age-related deterioration of motor function in male and female 5xFAD mice from 3 to 16 months of age. Genes Brain and Behavior 19, e12538 (2020).
14. Scarmeas, N. et al. Motor signs predict poor outcomes in Alzheimer disease. Neurology 64, 1696–1703 (2005).
15. Terry, R. D. THE FINE STRUCTURE OF NEUROFIBRILLARY TANGLES IN ALZHEIMER'S DISEASE: Journal of Neuropathology and Experimental Neurology 22, 629–642 (1963).
16. Albers, M. W. et al. At the interface of sensory and motor dysfunctions and Alzheimer's disease. Alzheimers Dement 11, 70–98 (2015).
17. Madisen, L. et al. A robust and high-throughput Cre reporting and characterization system for the whole mouse brain. Nat Neurosci 13, 133–140 (2010).

18. Steward, O. et al. Rostro-Caudal Specificity of Corticospinal Tract Projections in Mice. Cereb Cortex 31, 2322–2344 (2021).
19. Yonan, J. M. & Steward, O. Vector-mediated PTEN deletion in the adult dentate gyrus initiates new growth of granule cell bodies and dendrites and expansion of mossy fiber terminal fields that continues for months. Neurobiol Dis 184, 106190 (2023).
20. Park, K. K. et al. Promoting axon regeneration in the adult CNS by modulation of the PTEN/mTOR pathway. Science 322, 963–966 (2008).
21. Spilman, P. et al. Inhibition of mTOR by rapamycin abolishes cognitive deficits and reduces amyloid-beta levels in a mouse model of Alzheimer's disease. PLoS One 5, e9979 (2010).
22. Metcalfe, M. & Steward, O. PTEN deletion in spinal pathways via retrograde transduction with AAV-rg enhances forelimb motor recovery after cervical spinal cord injury; sex differences and late-onset pathophysiologies. Preprint at https://doi.org/10.1101/2023.03.20.533502 (2023).

Chapter 5 - Summary and Conclusions

Overall summary

Neurodegeneration is a major feature of late-stage Alzheimer's disease (AD), yet the mechanisms driving it remain poorly understood. The only disease modifying interventions that have reached patients are targeting amyloid pathology rather than neuronal loss. The most defining symptom of AD is cognitive decline, and the therapies targeting amyloid only provide mild short-term improvement. Thus, it may be beneficial to focus on other aspects of the disease, such as neuronal loss. This dissertation aimed to reveal the mechanisms underlying neurodegeneration in AD by determining whether a defined, vulnerable population of neurons could be tracked across the lifespan of a mouse and protected by activation of an intrinsic growth pathway.

We focused on neurodegeneration in the corticospinal pathway since it was a vulnerable and easily traceable population of neurons. The commonly used murine model of AD, 5xFAD mice, display neurodegeneration in cortical layer V, and corticospinal neurons (CSNs) form a part of that layer. CSNs can be identified and easily selected by where they project to rather than having to rely on a molecular marker. We injected AAV-retrograde (rg)/Cre into the cervical spinal cord of 5xFAD mice carrying a Cre-dependent tdTomato (tdT) reporter gene ($5xFAD^{+/-}/Rosa^{tdT}$), to label the cell bodies, dendrites and axons of CSNs. Along with this model, we also used $5xFAD^{+/-}/Rosa^{tdT}$ combined with mice carrying flox sites flanking exon 5 of the *PTEN* gene,

5xFAD$^{+/-}$/PTEN$^{flox/flox(f/f)}$/Rosa^{tdT}, which allowed us to activate the mTOR pathway and label those same neurons with tdT.

The three chapters used the 5xFAD$^{+/-}$/Rosa^{tdT} and 5xFAD$^{+/-}$/PTEN$^{f/f}$/Rosa^{tdT} models to ask: what does CSN degeneration look like in 5xFAD mice (*Chapter 2*), does mTOR activation alter it (*chapter 3)*, and does mTOR activation alter motor deficits that accompany it (*chapter 4*).

The primary finding is that *PTEN* deletion did not preserve CSNs, yet it prevented the decline in motor coordination that occurs in 5xFAD mice. Importantly, mTOR activation did not accelerate degeneration as the AD literature would predict.

Chapter 2 summary: CSN labeling reveals previously undescribed features of degeneration

Delivering AAV-rg/Cre into the spinal cord of 5xFAD$^{+/-}$/Rosa^{tdT} mice resulted in permanent labeling of CSNs in layer V. Quantitative assessment across age confirmed progressive degeneration of layer V CSNs and established features of 5xFAD pathology that had not been described before.

We showed that transgene expression of human APP (hAPP) was present at high levels in neuronal populations that are known to degenerate in 5xFAD mice, such as in cortical layer V and subiculum. However, we also found that hAPP was also found in high levels in populations of neurons that were not previously known to degenerate in 5xFAD mice, such as neurons in the red nucleus. Extensive age-related degeneration of neurons in the red nucleus was a key finding

in this chapter. We also found moderately high expression levels of hAPP in neuronal populations that did not appear to degenerate, such as the basolateral amygdala. Notably, neurons of the entorhinal cortex that projects to dentate gyrus and hippocampus did not express the transgene at all, which reveals differences in this model relating to the hippocampal circuit degeneration that is central to human AD.

The most unexpected observation was the presence of hAPP-positive granules. The granules usually formed a rosette or petal-shaped cluster. As mice aged, hAPP labeling, visualized by immunofluorescence (IF), shifted from neuronal cell bodies to extracellular granules. The granules were not only prominent in regions containing hAPP-expressing cell bodies but also in regions containing their axons and synaptic terminals. The areas included the pons where no hAPP-expressing neurons are present.

A key aspect of the hAPP-labeled clusters is that tdT labeled clusters also accumulated in these granules. Both tdT labeled clusters and hAPP labeled clusters co-localized with Aβ containing plaques. Since tdT-positive clusters accumulated as tdT-positive neurons were lost, these accumulations provided a second measure by which degeneration of a defined population could be tracked in 5xFAD mice.

Importantly, this chapter revealed degeneration of CSNs, revealing a population of neurons in layer V that had not specifically been identified to degenerate in 5xFAD mice.

Chapter 3 summary: PTEN deletion does not appear to alter CSN degeneration in our model

Our transgenic 5xFAD$^{+/-}$/PTEN$^{f/f}$/Rosa^{tdT} model received AAV-rg/Cre at 2-4 months of age, and tissue was collected at 2-4, 6-10 and 11-17 months of age. The model was created to test whether mTOR activation, via *PTEN*-deletion altered neurodegeneration. Before we tested the effect of mTOR activation on neuronal survival, we performed three control experiments: 1. *PTEN* was deleted in tdT-labeled CSNs, as confirmed by "ghost cells" which we characterize for lacking PTEN immunostaining within the tdT-labeled neurons; 2. Expression of hAPP transgene is maintained rather than diminished by mTOR activation as seen by IF levels of hAPP in PTEN-deleted neurons; 3. Activation of mTOR was present at one month and sustained at four months post-deletion of PTEN, as assessed by phosphorylation of ribosomal protein S6 (pS6).

Having validated our model, we quantified neurodegeneration of CSNs across age. We found that tdT-labeled CSN counts declined with age in 5xFAD$^{+/-}$/Rosa^{tdT} and 5xFAD$^{+/-}$/PTEN$^{f/f}$/Rosa^{tdT} but did not find significant differences between PTEN-deleted and non-PTEN deleted 5xFAD mice at any age. In parallel, tdT-positive clusters increased with age but did not significantly differ in PTEN-deleted and non-deleted mice. Importantly, PTEN deletion in non-5xFAD mice did not alter CSN count across age.

Chapter 3 also piloted a longitudinal *in vivo* tracking system using AAV-rg-fLuc and an *in vivo* bioluminescent imaging system (IVIS). The bioluminescent signal was successfully localized to layer V and the descending corticospinal trajectory. However, in our control CAMKIIa mice in which no degeneration was expected, the signal declined sharply after 11-12 days. The decline

likely reveals a loss of viral expression rather than neuronal loss, making this platform not suitable for tracking neurodegeneration over months.

Chapter 4 summary: Aspects of motor coordination may be preserved by PTEN deletion

A group of the same cohort of mice used in chapter 3 were assessed monthly from 2 to 12-15 months of age on three motor tasks. On the rotarod task, the 5xFAD$^{+/-}$/Rosa^{tdT} mice developed motor deficits from 10 months of age, consistent with reports of motor deficits appearing around 9 months of age in 5xFAD mice. Importantly, the 5xFAD$^{+/-}$/PTEN$^{f/f}$/Rosa^{tdT} mice did not display motor deficits on the rotarod since they performed at the maximal attainable speed that the protocol permitted and were indistinguishable from non-5xFAD controls.

On the balance beam, PTEN-deleted 5xFAD mice had fewer hindlimb foot slips than non-deleted 5xFAD mice. The speed at which the mice crossed the balance beam declined with age in all genotypes and did not differ significantly by genotype ($p = 0.0568$). On the grip strength meter task (GSM), grip strength peaked at approximately 8 months of age and declined after 8 months in all genotypes, indicating that PTEN deletion did not have an effect on grip strength.

Discussion: Dissociation between neuronal survival and motor function

Activation of mTOR did not appear to reduce CSN degeneration, yet it preserved motor function as shown by the rotarod task and foot slip counts on the balance beam task. We had predicted that mTOR activation would reduce neurodegeneration as this would've indicated

neuroprotection. However, our results on motor coordination preservation indicate that mTOR activation can still preserve function of CSNs. Thus, an intervention that doesn't result in neuronal survival can still preserve function.

Prior work in the lab reports that PTEN deletion results in a perpetual increase in soma size, dendritic complexity and branching in adult cortical neurons (Gallent and Steward, 2018). Thus, the most likely mechanism is that PTEN deletion increases dendritic complexity and branching which may allow for an increase in functional synapses. The expanded dendritic arborization and synaptic connectivity could compensate for the reduction in neurons and result in sustained motor coordination. This has yet to be tested but is described under future directions below.

Discussion: differences between three behavioral tasks

The three behavioral tasks had distinct results: a large age-dependent difference in performance on the rotarod between PTEN deleted and non-PTEN deleted 5xFAD mice; a small difference in foot slips and no difference in speed on the balance beam task; and no difference in grip strength on GSM. These results indicate that mTOR activation results in maintaining coordination-dependent measures but not strength-dependent ones. Although, it's possible that the GSM task was tested at ages where grip strength deficits were not yet prominent. It's been reported that 5xFAD mice have deficits on GSM starting around 12 to 16 months of age (Pechlivanidou et al., 2022).

On the rotarod task, we determined that 5xFAD$^{+/-}$/PTEN$^{f/f}$/Rosa^{tdT} mice preserved motor function since the typical motor deficits seen in 5xFAD mice were not seen in 5xFAD mice with PTEN deletion. However, since our protocol had a time limit on how long the mice stayed on the rotarod, we could not determine whether the 5xFAD$^{+/-}$/PTEN$^{f/f}$/Rosa^{tdT} mice performed better than non-5xFAD controls. A greater increase in acceleration or a longer period of time on the cylinder would have allowed us to determine if there were differences in non-5xFAD and 5xFAD$^{+/-}$/PTEN$^{f/f}$/Rosa^{tdT} mice.

Future directions

Determine whether surviving neurons have differences in morphology due to PTEN deletion in 5xFAD mice. The dissociation between CSN survival and function leads us to predict that PTEN-deleted CSNs would show greater soma size, dendritic complexity and density than non-PTEN-deleted CSNs. Sholl analysis on tdT-labeled neurons in aged 5xFAD$^{+/-}$/PTEN$^{f/f}$/Rosa^{tdT} mice and 5xFAD$^{+/-}$/Rosa^{tdT} would reveal differences. Electrophysiological recordings of corticospinal transmission would determine how well the structural changes, due to PTEN deletion, translate into preserved circuit output.

Determine whether tdT-labeled clusters are "mitochondrial plaques." A paper published recently reports finding "mitochondrial plaques" that are separate from amyloid-beta plaques, with only a 7.3% overlap (Dan et al., 2026). In some of the mitochondrial plaques, they show amyloid-beta at the core, similar to what we report in chapter 2. It is likely that what the authors have termed mitochondrial plaques are equivalent to what we're seeing as tdT-positive clusters.

The mitochondrial plaques were reported to be surprisingly large (up to 13,320.64μm^2) and were determined to be bundles of neuronal processes. Our model may provide a platform to label these potential mitochondrial plaques, determine when they first appear and further study their composition. To determine whether our tdT-labeled clusters are mitochondrial plaques we could further our immunofluorescence studies on tdT-clusters and Lysosomal-associated membrane protein 1 (LAMP-1), along with voltage-dependent anion channel (VDAC), to determine overlap.